*UNIVERSITÀ DEGLI STUDI DI NAPOLI "FEDERICO II"*

*in consorzio con*
*SECONDA UNIVERSITÀ DI NAPOLI*
*UNIVERSITÀ "PARTHENOPE" NAPOLI*
*in convenzione con*
*ISTITUTO PER L'AMBIENTE MARINO COSTIERO – C.N.R.*
*STAZIONE ZOOLOGICA "ANTON DOHRN"*

Dottorato in Scienze ed Ingegneria del Mare
XX ciclo

Tesi di Dottorato

# Spectral analysis of wave transmission behind submerged breakwaters

Candidato: Ing. Vincenzo Ferrante

Tutor: Prof. Diego Vicinanza

Il Coordinatore del Dottorato: Prof. Bruno D'Argenio

**ANNO 2007**

**Abstract**

The coastal zone is a delicate and dynamic area in which the majority of a water body's kinetic energy is dissipated through wave breaking, run-up and bed friction. The most significant result of these processes is the erosion and subsequent transport of the shore and beach materials. This littoral zone is very important to the public for economic and social reasons and to wildlife for habitat and food supply purposes. It is therefore very important that the coastal zone be protected and maintained so that these considerations are addressed in a compatible and effective fashion. In recent years, increased attention has been given to a class of breakwaters collectively termed submerged breakwaters. As indicated by the name, these structures are constructed below a specified design water level. Some studies have put in evidence that for the submerged barriers realized in various parts of the world only a small percentage have a positive effect on the coastal zone. Such result is probably due to a lack of knowledge of the complex phenomena that develop in the interaction of the barrier with the wave motion. The purpose of this thesis is to contribute through the high order analysis a to a best knowledge of the nonlinear phenomena that develops in the interaction of the waves with the submerged barriers.

**Sommario**

Le zone costiere sono delle aree delicate e dinamiche nelle quali la maggior parte dell'energia del moto ondoso viene dissipata attraverso il frangimento e gli attriti sul fondo. Talvolta questi processi possono portare all'erosione delle coste ed al trasporto di materiale fuori dell'unità fisiografica. Le zone costiere sono molto importanti sia dal punto di vista economico che sociale e rappresentano l'habitat per molte specie animali e vegetali. È quindi importante che le zone costiere siano protette dall'erosione e vengano rispettati gli ecosistemi esistenti. Tra gli interventi di protezioni dei litorali negli ultimi anni si è diffuso l'uso delle barriere sommerse. Come indicato dal nome si tratta di barriere costruite sotto il livello medio del mare. Dei recenti studi effettuati su un vasto campione di barriere hanno evidenziato che solo una piccola percentuale di tali opere effettivamente producono degli effetti positivi per la stabilizzazione della linea di riva. Probabilmente questo è dovuto alla scarsa conoscenza in merito ai fenomeni complessi che intervengono nell'interazione tra il moto ondoso e la barriera. Lo scopo di questo lavoro di tesi è quello di approfondire l'aspetto che riguarda le interazioni non lineari tra il moto ondoso e le barriere sommerse attraverso l'uso di analisi spettrali di ordine superiore.

# CHAPTER 1
# INTRODUZIONE

The coastal zone is a delicate and dynamic area in which the majority of a water body's kinetic energy is dissipated through wave breaking, run-up and bed friction. The most significant result of these processes is the erosion and subsequent transport of the shore and beach materials. This littoral zone is very important to the public for economic and social reasons and to wildlife for habitat and food supply purposes. It is therefore very important that the coastal zone be protected and maintained so that these considerations are addressed in a compatible and effective fashion. Engineered shoreline protection measures have taken many forms in the past; some have met with certain degrees of success while others have been obvious failures. Although the most evident failures are those related to structural integrity, there are many more subtle failures. The effects of which are often not discovered for a number of years. These subtle failures are often directly related to the disruption or destruction of natural habitats and processes. Therefore the focus of shoreline protection design has been expanding to include features which protect against and compensate for any loss of natural habitat areas. Conventional emerged breakwaters are typically designed to totally eliminate wave energy in their lee for a particular design wave condition. Often, this design wave condition is relatively severe and as a result, the structure must be very large. Where a minor degree of overtopping is permissible, the physical requirements of the breakwater are only slightly reduced. As such, these structures must be massive to withstand the impact forces of breaking waves, and often they all but eliminate water circulation in the protected area.

Although this calm condition developed in the lee of the breakwater protects the shoreline and can provide for good mooring conditions, under certain circumstances, the hydrodynamics developed at emerged breakwaters and the associated shoreline response can degrade water quality and natural habitat (CEM; 2004).

In recent years, increased attention has been given to a class of breakwaters collectively termed submerged breakwaters. As indicated by the name, these structures are constructed below a specified design water level. In comparison to emerged breakwaters, submerged structures permit the passage of some wave energy and in turn allow for circulation along the shoreline zone at the cost of a reduced level of protection. In addition to providing environmental benefits these structures have also found applications as preliminary defence measures in extreme wave climates where they reduce the wave forces on the primary defence structures (Cornett et al., 1994). This approach can be particularly beneficial in areas where a primary defence structure has sustained some damage or in areas where there is a projected long-term relative increase in sea levels and wave heights. The class of submerged breakwaters includes numerous specific types including active submerged, flexible membrane, fixed wave barriers, reef breakwaters or conventional rubble mound submerged breakwaters. Although there has been a considerable amount of research performed on these various structures, the physical processes are very complex and there are still several outstanding questions, especially with respect to practical design guidelines and procedures. In fact the insufficiency of these information has been underlined in some studies lead on sites (Seiji, Uda and Tanaka, 1987 and Brigand et al., 2002), where it emerges that only the 60% of the analyzed structures had produced shoreline, while in the 40% of the cases the protection has not gotten any meaningful effect and in some cases (Dean, Chen and Browder, 1997) a drastic withdrawal of the line of coast is recorded with the loss of huge quantities of sand.

This thesis deals with nonlinear transformation of wave spectra behind submerged breakwaters, in particular those due to nonlinear triad interactions. The study aims at increasing the knowledge and the physical insight in the mechanism of these processes.

**Thesis outline**

In *chapter I* the various types of breakwaters have been analyzed putting in evidence the advantage of the use of the submerged barriers. It has been introduced besides the physical phenomena that concern the transformation of the waves in the coastal zones, such as refraction, diffraction, reflection and breaking.

In *chapter II* are analyzed hydraulic performances of submerged barriers. Next, both experimental and analytical studies are analyzed on the phenomena that concern the barriers as the wave transmission, the setup, shoreline response, wave roller.

In *chapter III* theoretical models of interaction between submerged barriers and wave motion are analyzed. Particularly the solution of Massel (1984) is introduced. Subsequently are presented previous studies on wave barrier interaction performed by van der Meer (2000), Yamashiro et al (1999) and Black and Oumeraci (2001).

In *chapter IV* the experimental study performed at GWK (Hannover, Germany) is described.

In *chapter V* GWK data are analyzed using bispectral analysis. High order analysis allows to put in evidence phase coupling between frequencies and non linear triad interaction. A parametrical analysis has been carried out to understand the rules of barrier and wave behaviour in non linear

phenomena. Also the Hilbert Huang Transform (HHT) analysis has been carried out to perform time-frequency investigation. HHT results have been compared to bispectral results in order to evaluate HHT capabilities in water wave analysis.

## 1.1 Types of Rubble Mound Breakwaters

Conventional rubble mound breakwaters are commonly used to provide sheltered areas for marinas, erosion protection, beach formation and recreational activities. Their design consists of a large volume of rock that pierces the water surface, thus blocking the incoming waves and providing shelter in their lee. Conventional rubble mound breakwaters do an excellent job of reducing wave heights. However, there are some disadvantages using conventional surface piercing structures including:

- reducing the water circulation resulting in water quality issues
- reducing the biologic activity or diversity in the area
- navigational problems
- deface the natural landscape of the sea
- large amounts of wave reflection causing increased incident wave heights

Submerged breakwaters were introduced over the past few decades as a means of solving some of the specific problems that surface piercing breakwaters could not. As indicated by their name, submerged breakwaters consist of a rubble mound structure with a crest set at some desired depth below the surface. The offshore waves approach this structure and are reduced by a number of energy dissipation mechanisms, including wave breaking and frictional dissipation. There are still many uncertainties associated with the submerged breakwater due to the complex physical processes and relatively less information available to a designer than for the surface piercing breakwater. A submerged breakwater does have some advantages over their surface piercing counterpart including:

- being invisible from the shoreline thus maintaining natural landscape
- improving navigational issues
- because they are submerged they do not cease the circulation of water thus
- improving water quality
- Allowing for aquatic life to bypass the structure relatively unimpeded.

However, there are some drawbacks to the submerged breakwaters, mainly:

- they do not provide an impermeable barrier to the wave action thus blocking only a portion of the incoming wave energy
- there are difficulties using them in areas of large water level fluctuations design guidelines are relatively sparse, thus their implementation is without
- the same confidence level as emerged structures.
- large offshore (rip) currents are usually experienced on the edges of the breakwater and in the gap between barriers

The rubble mound breakwater is the most commonly applied type of breakwater. A rubble mound breakwater dissipates the main part of the incoming wave energy by wave breaking on the slope and partly by porous flow in the mound. The remaining energy is partly reflected back to the sea and partly transmitted into the protected area by wave penetration and wave overtopping. Various kinds of rubble mound breakwaters have been constructed depending on the purpose of the breakwater, cf. Fig. 1.1. The most simple rubble mound breakwater consist only of a mound of stones (Fig. 1.1 a). However, this type of structure is very permeable and will cause heavy penetration of waves and sediment. Moreover, large stones are expensive because most quarries yield a lot of finer material and relatively few large stones. Figure 1.1-b and 1.1-c are the two most common types of rubble mound breakwaters and are known as conventional rubble mound breakwaters with and without a superstructure. Even though the two types of structures appear different the structures have several points of

resemblance. Both breakwaters consists of a core of fine material covered by layers of larger units preventing the fine core material from being washed out. The outer seaward layer, the armour layer, consist of units of rock or concrete, large and heavy enough to remain in their position during design wave conditions. The inclination of the front slope is one of the parameters that determines the required mass of the armour unit. Concrete armour units are typically more expensive than rock, but in some cases large enough rock is not available nearby, unless a very flat front slope of the breakwater is applied. Using a flat front slope increases the needed volume of material, and hence the construction costs, dramatically. The maximum size of rocks that quarries can yield and handle is at the moment 10-20 tons. For rock typical front slope inclinations are in the range 1:1.5 to 1:4 depending on the available rock and the soil conditions. In case of concrete armour units a steep front slope is for most types of units used, as the weight of the above lying units has a stabilizing effect. Typically 1:1 to 1:2 is used for concrete units depending on the interlocking of the units. Unless the breakwater is located on a rock bottom, a toe is constructed to provide a safe base for the armour layer. On the rear side an armour layer is constructed to protect the breakwater against overtopping waves and waves in the harbour basin. Figure 1.1-b shows a structure primary used in relatively shallow water, where berthing along the breakwater and access on the breakwater is not required. In these cases relatively large amounts of wave overtopping are typically allowed. In Figure 1.1-c is shown a breakwater with a concrete superstructure, which works as a shelter for the overtopping waves and an access road for repairment and traffic to and from the breakwater. For similar overtopping conditions a structure with a crown wall needs significant smaller volume of material. Since the 1980'ties a design based on natural reshaping of the front rock armour during wave action has gained more attention (Fig. 1.1-d). This type of breakwater is known as berm breakwaters or reshaping breakwaters. The main advantage of this structure is that simpler construction methods can be applied. In most cases this type of

structure is built with no superstructure as shown in Fig. 1.1. Furthermore, the berm breakwater is considered as a more durable structure with much easier and cheaper repair methods as compared to the conventional rubble mound breakwater. The berm breakwater is typically built with a very steep front slope and with relatively smaller armour units. The profile self-adjusts to the wave climate leading to a profile stable for the given climate. Lately also non-reshaping berm breakwaters have been considered, often with several stone classes to maximize the total stability and quarry utilization, as indicated in Fig. 1.1-e. Especially in Iceland this structure is widely used, and is therefore also known as the Icelandic type of berm breakwater. Structures constructed with an S-shaped profile are typically used in large water depths to reduce the volume of material, but construction costs are in most cases significantly larger than for the reshaping berm breakwater, resulting in approximately the same profile. Fig. 1.1-g shows a reef breakwater which is a submerged breakwater mainly use for protecting beaches.

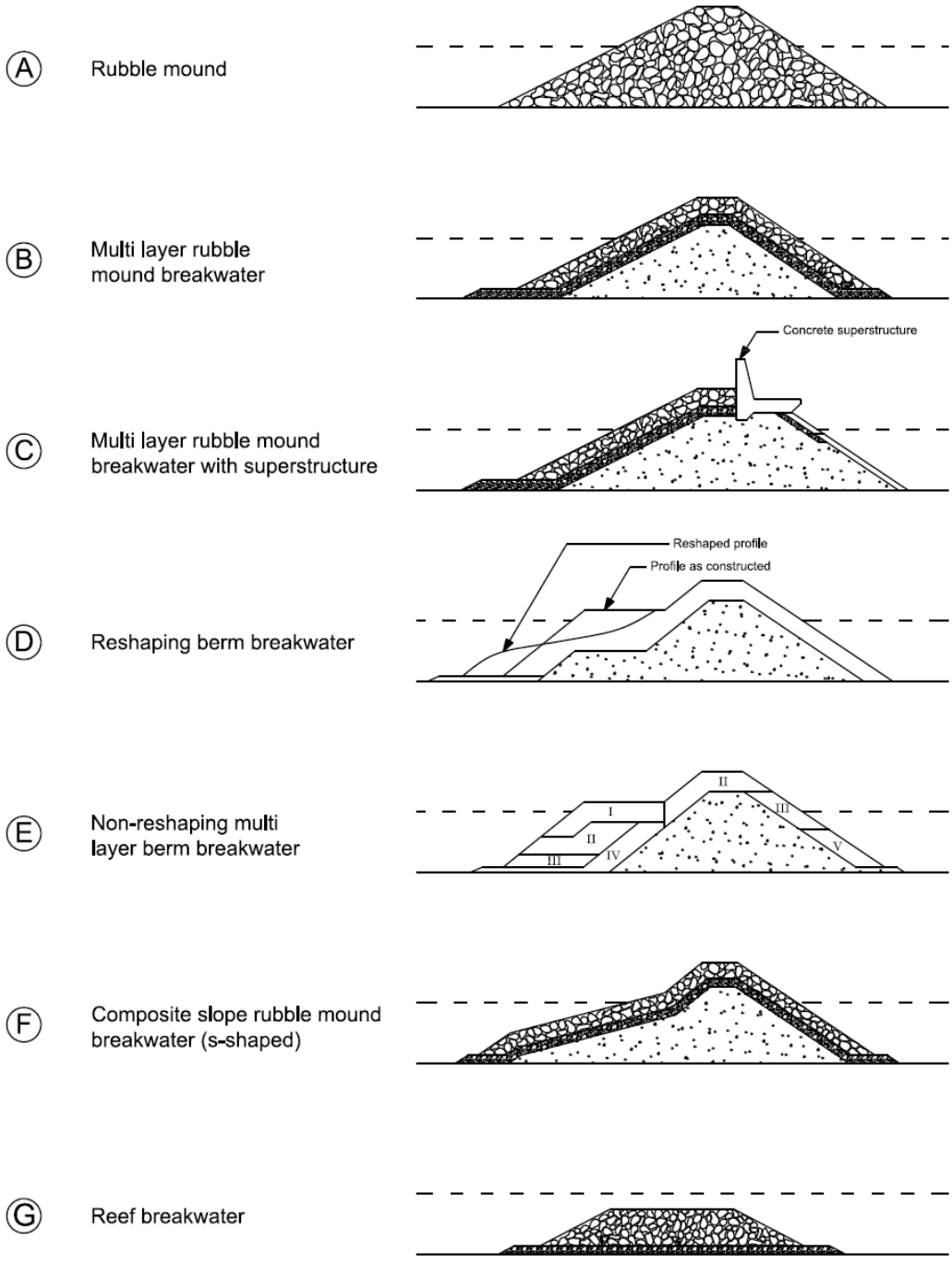


**Figure 1.1 – Types of breakwaters**

## 1.2 Wave transformation phenomena

Shallow water wave theory and past studies on submerged breakwaters indicate that these structures alter the wave climate by the following transformation mechanisms:

- wave shoaling
- wave refraction
- wave diffraction
- wave reflection
- wave breaking

altering the fundamental wave frequency (or period) to higher harmonic frequencies.

Longitudinal submerged breakwaters also use these physics processes to transform the waves although the interaction of the transformation mechanisms is very complex and unique to the wave characteristics and also the geometry of the longitudinal submerged breakwater system. Identifying the geometric properties of these longitudinal structures that most affect the transmitted wave must come from an understanding of the physical wave transformations taking place.

### 1.2.1 Shoaling

Shoaling describes wave transformations as the waves approach the shoreline perpendicularly. It is extended from the integration of the conservation of energy flux

equation:

$$\nabla\left(EC_g\right) = 0 \qquad [1.1]$$

where

$\nabla$ = differential vector operator

$E$ = wave energy ( $1/8\,\rho g H^2$ )

$\rho$ = density of water

$g$ = gravitational acceleration

$H$ = wave height

$C_g$ = wave group celerity (speed)

Shoaling theory is based on the assumption that the wave energy and group celerity product $(EC_g)$ is constant since the energy flux is conserved. That is, waves at any two depths cm be elated by their height and celerity. As waves enter shallow water, interference with the sea floor causes the p u p celerity to decrease. Therefore, the energy (wave height) must increase. However, shoaling theory must be used in accordance with wave refraction, diffraction and breaking, since shoaling theory alone would predict infinitely high wave heights as the wave group celerity approached zero. in actuality, the wave can only retain a certain form beyond which increased wave heights would cause instability in the wave form and energy loss through diffraction and/or breaking.

### 1.2.2 Wave refraction

Wave refraction describes wave transformations as the wave arrives at an angle to the bottom contours. During refraction, wave crests align themselves with the bottom contours (see Figure 1.2). Wave celerity is dependent on water depth. Thus, the section of wave crest in deeper water will travel faster than the section in shallow water and the

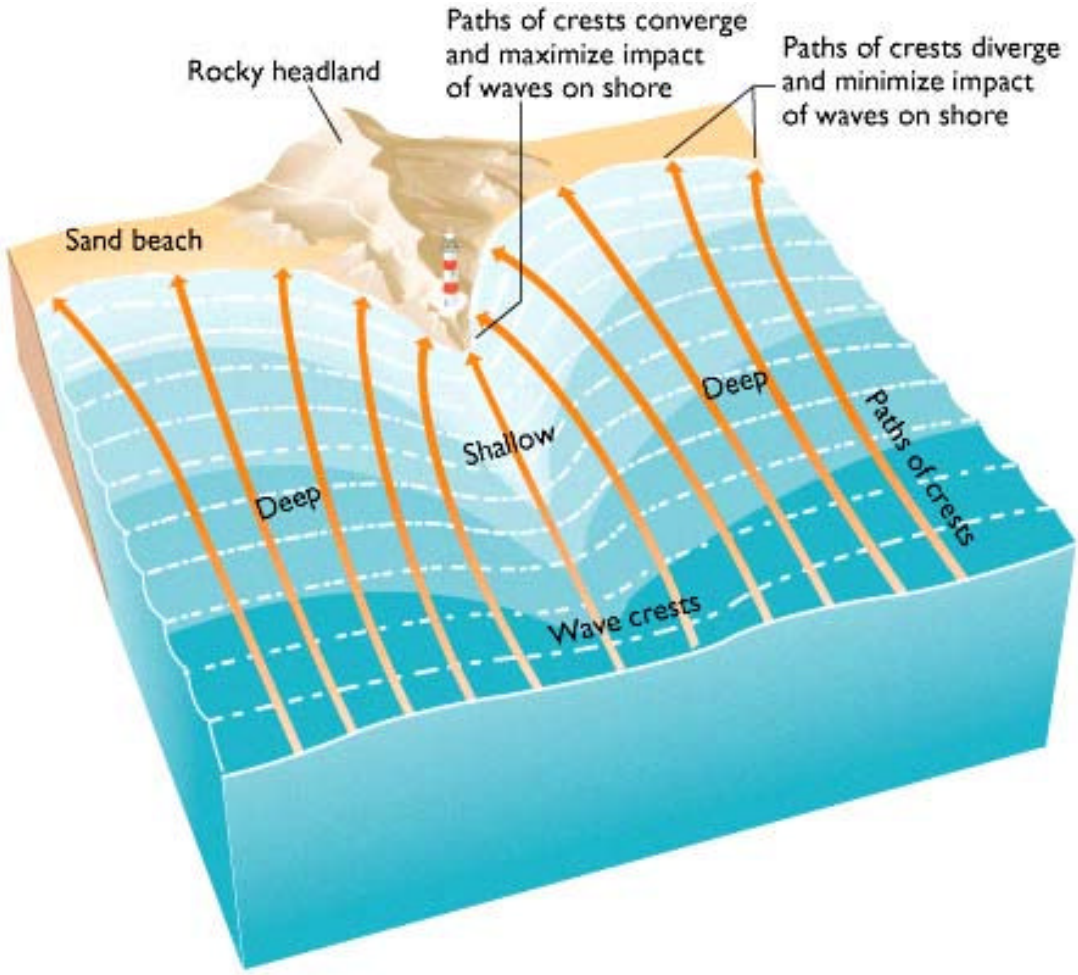


**Figure 1.2 – Wave refraction.**

wave crest will bend itself to align with the bottom contours. The conservation of energy flux between the wave rays is used to analyze refraction effects and leads to the application of Snell's Law which is:

$$\frac{C}{\sin \alpha} = c \qquad [1.2]$$

Where

$C$ = the wave celerity (or speed)

$\alpha$ = the incident angle between the wave crest and the bottom contour

$c$ =constant

However, Snell's Law can only be used for "relatively" straight bottom contours that are "relatively" parallel. This assumption is valid for many problems in coastal engineering, but not for longitudinal submerged breakwaters where the bottom contours that influence refraction are in fact the breakwater contours and are distinctly not parallel. Also, looking strictly at refraction (pure refraction), irregularities in bottom contours cm cause wave rays to cross (caustics), and since the energy density between rays is constant, this would indicate an infinite wave height. As was the case for pure shoaling, pure refraction does not allow diffraction or breaking in which the wave energy would spi11 across the wave ray and dissipate, thus reducing the wave heights and negating these caustics.

### 1.2.3 Wave reflection

Like sound waves, surface waves can be bent (refracted) or bounced back (reflected) by solid objects. Waves do not propagate in a strict line but tend to spread outward while becoming smaller. Where a wave front is large, such spreading cancels out and the parallel wave fronts are seen travelling in the same direction. Where a lee shore exists, such as inside a harbour or behind an island, waves can be seen to bend towards where no waves are. In the lee of islands, waves can create an area where they interfere, causing steep and hazardous seas. When approaching a gently sloping shore, waves are slowed down and bent towards the shore. When approaching a steep rocky shore, waves are bounced back, creating a 'confused sea' of interfering waves with twice the height and steepness. Such places may become hazardous to shipping in otherwise acceptable sea conditions.

### 1.2.4 Wave diffraction

Wave diffraction is concerned with the spilling of wave energy across wave rays or the propagation of energy along the wave crest. In reality, diffraction, refraction and shoaling al1 occur simultaneously. When waves encounter an obstruction, or a sudden change in bathymetry, some of the

wave energy will be forced to dissipate across the wave ray (or along the wave crest). The most simple example is wave crests corning in contact with an obstruction that causes a "shadow zone" behind the obstruction (Fig. 1.3). The wave energy leaks into the shadow zone and creates a diffraction

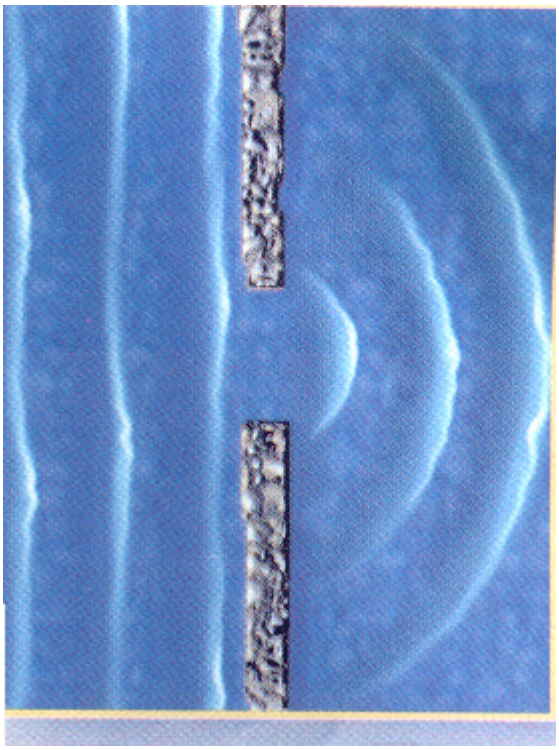

**Figure 1.3 – Wave diffraction.**

pattern. Figure 2-4 shows a diffraction pattern for the single obstacle case described above and an idealized diffraction pattern for a double obstacle, such as a longitudinal submerged breakwater. Obviously, the multiple obstruction case has a very confused sea state seaward of the structures which is almost beyond description. Attempts have been made to numeric model the wave transformations occurring at submerged breakwaters by applying equations of non-linear wave theory that are versatile enough to describe the complete wave transformation process in shallow water, including shoaling, refraction and diffraction. Boussinesq equations are for long waves of moderate amplitude over a slowly varying bed, and despite these simplifying assumptions have been used to model wave transformations over a submerged breakwater (Cruz, Isobe, & Watanabe,

1994). Their model seems to describe the wave well over the crest of the structure, but is inaccurate in modelling the wave field leeward of the breakwater. The Mild Slope equation can also be used to describe refraction and diffraction

simultaneously, but due to the high number of variables and the large variances in the contours of the longitudinal submerged breakwater system, many simplifications and assumptions would need to be postulated in any numerical models using the Boussinesq or Mild Slope equations, thus clouding the results.

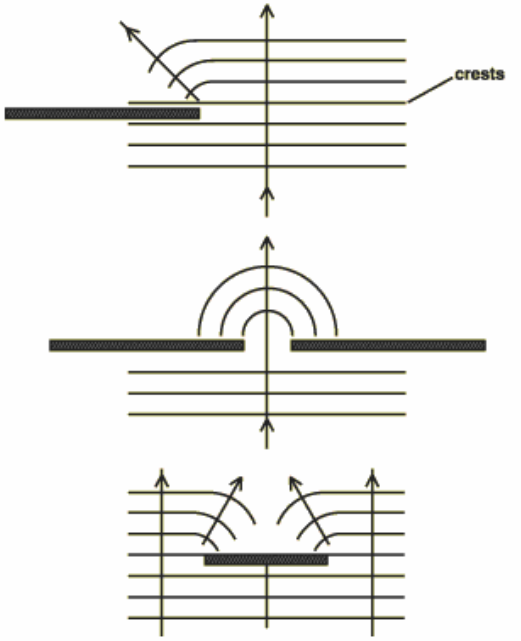


**Figure 1.3 – Diffraction pattern for the single obstacle and an idealized diffraction pattern for a double obstacle**

### 1.2.5 Wave breaking

Although shoaling, refraction and diffraction theory may predict a wave of a certain height, there is a physical limit to the steepness of a wave (steepness is defined as wave height, H, divided by the wavelength, L or the steepness of the front face of the wave. Beyond this steepness, the wave can no longer retain its form, and will break, dissipating a large portion of its energy. Miche

(1944) described wave breaking once this limiting steepness is exceeded. McCowan (1894) and later Munk (1949) described the depth of water that causes waves of limiting steepness using Solitary Wave Theory. The slope of the sea floor also effects wave breaking, particularly the shape of the wave at breaking, and Kamphuis (1991) expanded on the theories of McCowan, Munk and Miche to incorporate the beach slope. The effect of wave breaking on reducing the transmitted wave energy for longitudinal submerged breakwaters is thought to be more efficient than for submerged breakwaters mainly due to wave refraction (Goda 1996). Refraction through the valleys between the structures and over the side slopes cause increased wave heights over the crests of the submerged longitudinal breakwaters and thus increased amounts of wave breaking and subsequently energy dissipation.

# CHAPTER 2

## 2.1 Wave Phenomena at Submerged Breakwaters

The physical processes involved in the wave-structure interaction at submerged breakwaters are very complex. The complexities arise from two distinct sources: the extreme variability of the local wave climate and the numerous physical processes associated with the interaction of any specific wave climate with the unique characteristics of a given submerged breakwater configuration. It is this interaction which dictates the degree and rate of wave transformation at a submerged structure and thereby defines the resulting wave transmission, reflection and energy dissipation. The energy dissipation at the structure, defines the forces which will influence the stability of the breakwater. Basic physical processes at a submerged breakwater can generally be separated into three regions. These regions are shown in Fig. 2.1 for a typical submerged breakwater configuration with the notation for physical variables used throughout this study. The three regions are described briefly in the following paragraphs. Region 1 is located over the seaward slope of the structure. In this region the incident wave field is complex and irregular in nature, varying spatially and temporally at any given location. incident waves may exhibit varying degrees of non linearities due to the complex forces which have generated them and they may be transmitted on a water surface which fluctuates with a much longer period due to tidal or surge effects. Shoaling and refraction by the local bathymetric conditions offshore of the breakwater increase the non-linearity of the wave field.

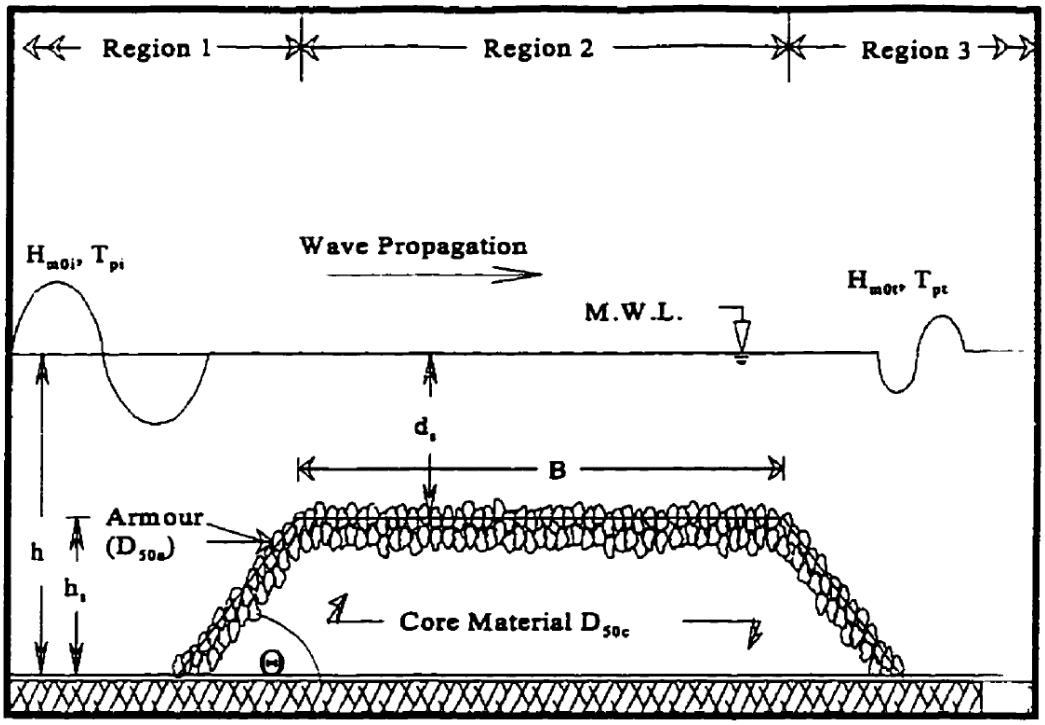


**Figure 2.1 – Typical submerged breakwater configuration with the notation for physical variables used throughout this study**

in Region 1, the incident wave encounters the rising face of the submerged breakwater and begins to shoal. As a result of this shoaling, bound harmonic waves are generated (Beji and Batjes, 1993). Some of the incident wave energy is reflected and this reflection has been found to be strongly dependent on the depth of submergence (Ahrens, 1987; Van der Meer, 1991) and somewhat dependent on the slope of the structure Dattatri et al., 1979). Wave breaking characteristics at bars and artificial reefs are largely influenced by the slope of the forward face of the structure and the depth of submergence as well as the offshore velocity across the breakwater crest (Smith and Kraus, 1990). Other phenomena found to occur in this region in laboratory tests include the build-up of low-frequency wave heights, thought to be the result of interaction between incident bond long waves, and an offshore current developed by a set-up of water level behind the breakwater (Petti and Ruol, 1991 and 1993; Liberatore and Petti, 1993).

Region 2 is located on the crest of the breakwater. In this region, energy from the fundamental wave frequency is transferred to higher harmonic

frequencies (Driscoll, Darlymple and Grilli, 1993). Beji and Battjes (1993) demise this phenomenon (for long waves propagating over a bar) as a rapid flow of energy from the primary wave to higher harmonics, generating "dispersive wave tails" which appear to travel with nearly the same celerity as the primary waves. For the case of submerged breakwater, where the incident wave transformations will be more abrupt, the process may be affected to some degree by the influence of reflected waves and wave breaking onto the crest of the structure. As the waveform passes over the breakwater crest energy is also dissipated through frictional resistance. Because the breakwater is permeable, laminar and turbulent flows within the structure also result in some energy dissipation.

Region 3, located beyond the shoreward limits of the breakwater crest is a transition to deeper water where the higher frequency wave components developed in Regions 1 and 2 separate from the fundamental components and travel with their own celerity (Beji and Battjes, 1993). This process generally results in a broad energy spectrum in the lee of the breakwater with a decreased characteristic wave height ($H_{m0}$) and reduced peak wave period ($T_p$). Again, this process has been observed in investigations involving spectral analysis of wave transformations at submerged breakwaters (Petti and Ruol, 1993; Cornett, Mansard and Funke, 1994). Studies of velocity fields at submerged breakwaters show the development of eddies, indicating flow separation and subsequent energy losses immediately shoreward of the breakwater crest (Ting and Kim, 1994). Other general phenomena that may occur in the vicinity of submerged breakwaters include a local setup of water levels in the lee of the breakwater due to a net mass flux of water over the breakwater crest, and wave current interactions as an offshore current (return flow) is developed in the surface region over the breakwater (Petti and Ruol, 1991 ) or in gaps between segmented breakwater structures (Fulford 1985). It is therefore evident that there are numerous factors associated with the incident wave field. The breakwater geometry and the local bathymetry which can affect the wave transformation and the resulting

energy transmission, reflection and dissipation at a submerged breakwater. Previous physical and numerical investigations have been performed in an effort to concisely define the effects of these various factors.

Laboratory experimental testing, numerical modelling approaches and field studies continue to be developed for improved understanding of hydrodynamic and morphodynamic effects of this kind of structure in the coastal zone. The previous laboratory experimental research on submerged breakwaters is summarized in Table 2.1. The table clearly indicates test conditions (wave climate, breakwater type and geometry, water depth, wave flume/basin dimensions, etc) of previous laboratory studies. This chapter presents historical investigations and research of hydrodynamic studies on submerged breakwaters including wave transformation/transformation, wave-induced set-up and current across submerged breakwaters or reefs.

**Wave Transmission**

Various experiment laboratory studies and numerical models have been developed for predicting wave transmission passing across low-crested breakwaters.

## 2.2 Experimental Studies

**Goda et al. (1979)** carried out a series of laboratory experiments in a wave channel with regular waves on vertical and composite overtopping breakwaters. Results shown that the transmission coefficient is linked to submergence ratio ($h_s/H_i$) on the other hand the dimensionless wave characteristics such as $H/L_0$ and $H_i/h$ did not influence the relation between submergence ratio and wave transmission coefficient. Goda et al. (1967) also observed that for large crest width of the breakwater, transmission coefficient decrease. The following empirical formula was proposed by Goda et al. (1967) for calculating transmission coefficient "$Kt$":

$$K_t = 0.5\left[1 - \sin\frac{\pi}{2\alpha}\left(\beta - \frac{h_s}{H_i}\right)\right] \qquad [2.1]$$

in which $h_s$ is distance of still water lever from breakwater crest, $\alpha$ and $\beta$ are variables $\alpha$=2.0 and $\beta$ has the value of 0.1, 0.3 and 0.5 for high, medium and low mound breakwaters respectively.

**Seeling (1980)** carried out a series of laboratory tests with a smooth and impermeable overtopping breakwater using both regular and irregular waves. He revealed, according to Goda (1969), that submergence ratio ($h_s/H_i$) is the parameter that mostly influence the transmission coefficient. The author also shows, that the formula proposed by Goda (1969) is also approximately valid for the irregular waves.

**Abdul Khader and Rai (1980)** performed a series of 2D laboratory tests on smooth and impermeable submerged breakwaters with different shape and geometry. Authors shown that energy dissipation the is very dependent on relative crest height ($d/h$). Abdul Khader and Rai (1980) have shown that the amount of energy dissipated is greater for larger values of the wave steepness, both in the case of rectangular and of trapezoidal breakwaters. However, trapezoidal breakwaters are effective even for low range of $d/h$ due to the shoaling impacts caused by sloping sides of the breakwater.

**Allsop (1983)** in order to study the stability of the structure, number of waves overtopping and transmission coefficient carried out a series of experiments on low-crest rock armoured breakwaters. The tests were carried out using random wave field with different climate (height and period ). He modified Goda' s empirical model (Goda, 1969) for wave transmission coefficient by substituting "$K_t - 0.5$" instead of $K_t$ and introduced $R^*$ parameter instead of $h_s/H_i$ to fit the model to measured data:

$$K_t = 0.5\left[1 - \sin\frac{\pi}{2\alpha}\left(\beta - R^*\right)\right] \qquad [2.2]$$

where

$$R^* = \frac{h_s}{H_s}\left(\frac{s}{2\pi}\right)^{1/2} \qquad [2.3]$$

in which $H_s$ is significant wave height at breakwater location in absence of the structure and s is the wave steepness ($H/L_0$). Powell and Allsop (1985) provided empirical curves (as design guidelines) for estimating wave transmission coefficient over low-crested permeable breakwater with 40% porosity (Figure 2.2).

| References | Water depth | Flume/Basin dimension | Wave condition | | | Breakwater type | Breakwater dimension | | |
|---|---|---|---|---|---|---|---|---|---|
| | ***h*** **(cm)** | **(m)** | **r/ir** | ***H*** $_i$ **(cm)** | ***Tp*** **(sec)** | | ***B*** **(cm)** | ***d*** **(cm)** | **tan □** |
| Johnson et al. (1951) | - | 0.33 | R | | - | plywood | 10,22,33 | - | 0 |
| Goda et al. (1967) | 50,35 | 20x30 | | 3-30 | 0.8-2.76 | wall | 40,90 | 20-70 | ... |
| Diskin et al. (1970) | 18 | 1.4x0.6x26 | R | 10.6-16.1 | 1.22-1.62 | rubble | 12-14 | 15,21 | - |
| Seeling (1980) | 125=-21 to 42 | - | Ir-r | 0.08-0.177 | 0.91-3.46 | rubble | 30,40 | 33,66,75 | var |
| Abdul Khader & Rai (1980) | - | 0.9x0.9x30 | R | 4.7-13.1 | - | plywood | 12-36 | 0.15-0.97(d/h) | 0-1:2 |
| Allsop (1983) | Var. | 1.5x3x42 | Ir | 5.5-19.4 | 0.4-1.71 | rubble | 13.9 | 16.6-22.2 | 1:2 |
| Aminti et al. (1983) | - | 0.8x1.5x20 | R | 6.25-15.6 | 1.0,1.5,2.0 | var | var | 6.25,9.4,12.5 | 1:1-var |
| Powell & Allsop (1985) | $h_i$ = -7.9 to **18.6** | | Ir | 9-22.9 | 1.39-2.3 | rubble | 14-30 | 25-66 | var |
| Adams & Choule (1986) | Var. | 24x37 | Ir | 3.8-8.2 | - | rubble | 22-48 | h-d=3.6-(-3.6) | 1:2 |
| Ahrens (1987) | 25-30 | 1.2(0.61)x46x42.7 | Ir | 2.25-18.2 | 1.45&3.6 | rubble | 5.6-9.0 | 17-35 | 1:1.5 |
| van der Meer (1988) | 40 | - | Ir | 7.5-19.2 | 1.96-2.6 | rubble | 30 | -12.8 to 9.4 | 1:2 |
| Gómez and Valdés (1990) | $h_i$=6- 13 | - | R | - | 1.5-3.5 | rubble | 0.8-1.2 | - | |
| Daemen (1991) | $h_i$=-19.6 to 57 | 1.2x1.0x50 | Ir | 0.049-0.148 | 0.99-2.88 | rubble | 0.34 | 0.4 | 1:1.5 |
| Petti & Roul (1992) | h5 =6 | 0.8x0.8x50 | Ir | 8.6-14.1 | 1.2-1.53 | impermeable | 24 | 14 | 1:3.5,1:1.5 |
| Chiaia et al. (1992) | 30 | 1.2x1.0x45 | Ir | 1.58-2.63 | - | rubble | 60 | 25 | 1:1.5 |
| Davies & Kriebel (1992) | $h_i$ =5.1,0,-5.1 | Basin(0.61x16.61) | r-ir | 0.9-1.81 | - | PVC-rubble | 15.2 | 10.2,15.2,20.3 | |
| De Later (1996) | h5 =10 | 0.6x14x28 | R | 8,10,12 | 1.55 | rubble | 16 | 30 | 0.67 |
| Gourlay (1996a) | 32,37,42 | 6(3)x30 | R | 2.8-20.4 | 0.9-2.2 | mortar | 15 | 32 | 1:6 |
| Groenewoud et al. (1996) | 40 | 1.0x0.8x32 | r-ir | 10,13.3,6.7 | 1.29-2.07 | rubble | 16 | 30 | 0.67 |
| Seabrook (1997) | $h_i$ =0,5,10,15,20<br>$h_5$=3.2,6.3,12.6 | 1.2x1.0x47<br>1.2x25x30 | r-ir | 5,10,15,20<br>3.2,6.3,9.5 | 1.2,1.5,2.0<br>0.95-1.98 | Rubble<br>rubble | 30,250<br>19,38,95 | - | var |
| Rivero et al. (1997) | h5 =38 | 5x3x100 | r-ir | 25,37.5,50 | 2.5,3,3.5,4 | rubble | 61 | 112 | 1:2 |
| Loveless et al. (1998) | 400-650<br>29.7,32,368 | 1.1x1.5x15<br>36x23 | r-ir | 50-200<br>5,6.6,7.35 | 4.5-11.2<br>0.83,1.1,1.7 | rubble | 20-80<br>0.14,35 | 35,50<br>21.5,12.5 | 1:2 |
| Drei & Lamberti (1999) | 40 | 0.8x0.8x48 | r-ir | 4,8,16 | 0.92-2.5 | plywood | - | 40,41,43.45.5 | |

**Table 2.1 - Test conditions of previous laboratory experimental research on submerged breakwater.**

| References | Water depth | Flume/Basin dimension | Wave condition | | | Breakwater | Breakwater dimension | | |
|---|---|---|---|---|---|---|---|---|---|
| | *h* (cm) | (m) | r/ir | *Hi (cm)* | *Tp* (sec) | | *B (cm)* | *d* (cm) | tan □ |
| Bleck & Oumeraci (2001) | 70 | 2.0x100 | r-ir | 8-12-16-20 | 1.1-6.0 | plywood | 50,100 | 40,50,60 | 0 |
| Vidal et al. (2001) | $h_s$ =-0.05,0,0.05 | 0.8x0.6x24 | r-ir | 5, 10, 15 | 1.6,2.4,3.2 | rubble | 25,100 | 30,35,40 | 1:2 |
| Schlurmann et al. (2002) | 62,72,82 | 2.0x100 | r-ir | 8-20 | 1.0-5.0 | plywood | 100 | 52 | 0 |
| Roul & Faedo (2002) | 10,15,20 | 1.2x1.0x36 | Ir | 2.4-15.5 | 1.1-2.33 | rubble | 20 | 10,15,20,25,30 | 1:2 |
| Calabrese et al. (2002,2003) | 100-170 | 7.0x5.0x300 | - | 60-100 | 3.5,4.5,6.5 | rubble | 100 | 130 | 1:2 |
| Gironella et al. (2002) | - | 1.5x3.0x35 | Ir | - | - | rubble | 122.5 | 158.5 | 1:2 |
| Melito and Melby (2002) | 20,50,70 | 2x3(0.9)x74.6 | Ir | 3.5-22.4 | 1.12,1.88,2.62 | Core-loc | 24.3 | 40,80 | 1:1.5 |
| Zanuttigh & Lamberti (2003) | $h_s$ =0,7,-3 | 1x12x18 | r/ir | 4-12.1 | 0.7-1.97 | rubble | 20,60 | 20 | 0.5 |
| Garcia et al. (2004) | 30,35,40 | 0.8x0.6x24.05 | r/ir | 5,10,15 | 1.6,2.4,3.2 | rubble | 25,100 | 24 | 0.5 |

**Table 2.1(continued) - Test conditions of previous laboratory experimental research on submerged breakwater.**

Notes: Wave conditions tested being "r" regular or "ir" irregular waves

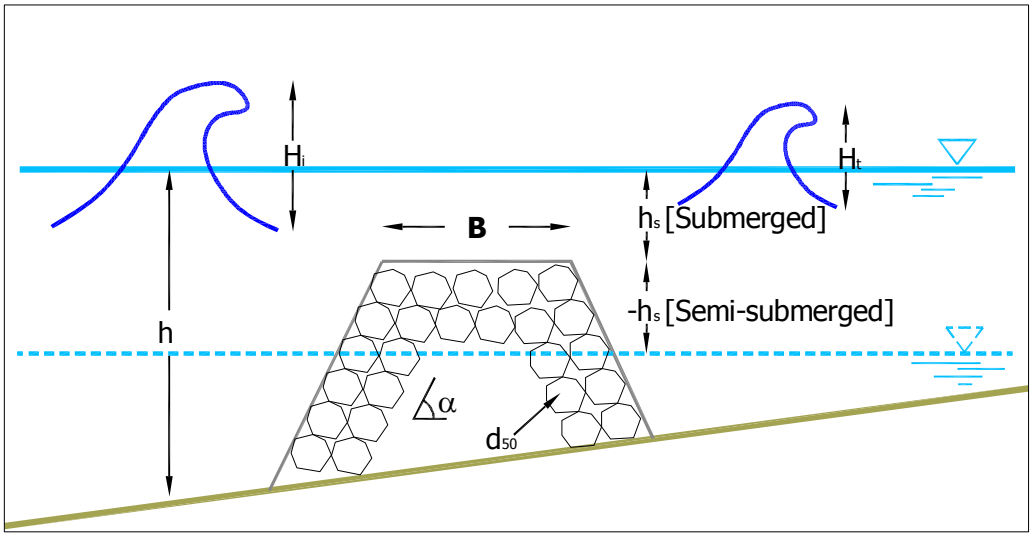


**Figure 2.2 – Definition of submerged (semi-submerged) breakwater parameters and wave transmission.**

**Ahren (1987)** investigated the performance of low-crested breakwaters by conducting a wide series of experimental tests (Table 2.1) at the US Army Engineer Waterways Experiment Station's Coastal Engineering Research Centre. The aim of the laboratory tests was to study stability of rouble-mound reef-type breakwaters and their effects on wave transmission and reflection. He proposed the following expression for wave transmission coefficient $K_t$:

$$K_t = \frac{1.0}{1.0 + \left( \frac{H_s A_r}{L_p d_{50}^2} \right)^{0.592}} \quad \text{for} \quad \frac{h_s}{H_s} < -1 \qquad [2.4]$$

$$K_t = \frac{1.0}{1.0 + \left( \frac{d}{h} \right)^{C1} \left( \frac{A_r}{hL_p} \right)^{C2} \exp\left[ C3 \left( \frac{h_s}{H_s} \right) + C4 \left( \frac{A_r^{3/2}}{d_{50}^2 L_p} \right) \right]} \quad \text{for} \quad \frac{h_s}{H_s} > -1 \qquad [2.5]$$

where the constant *C1=1.188*, *C2=0.261*, *C3=-0.592* and *C4=0.00551*. The parameters $H_s$ indicates the significant wave height, $A_t$ is area of breakwater cross section, $d_{50}$ is dimension of stone, $L_P$ is wave length corresponding to peak wave period, $d$ is reef crest height, $h$ is stili water level and $h_s$ is the distance between water surface and the crest reef (positive above the crest reef). Ahren (1987) found that the reflection coefficient is not much dependent on dimensionless submergence ($h_s/H_s$) and can be calculated by the following equation:

$$K_r = \exp\left[C1\left(\frac{h}{L_p}\right) + C2\left(\frac{d}{h}\right)^{-1} + C3\left(\frac{A_t}{d^2}\right) + C4\left(\frac{-h_s}{H_s}\right)\right] \qquad [2.6]$$

where *C1= -0.6774*, *C2= -0.293*, *C3= -0.0860* and *C4= 0.0833.*

**Gómez Pina and Valdés (1990)** analyzing the data of laboratory experiments have suggested that the wave transmission coefficient shows a oscillatory trend according to relative crest width ($B/L_0$). They also shown that for both breaking and non-breaking wave conditions, the transmission coefficient is related to the Iribarren parameter $\xi$ ($B/h_s$)as shown in Figure 2.3 gives reasonable results for predicting transmission coefficient. Iribarren number can be calculated by knowing the onshore face slope of breakwater $\alpha$ and incident wave steepness:

$$\xi = \frac{\tan\alpha}{\sqrt{H_i / L_0}} \qquad [2.7]$$

in which $H_i$ is incident wave height and $L_0$ is incident wave length in deepwater.

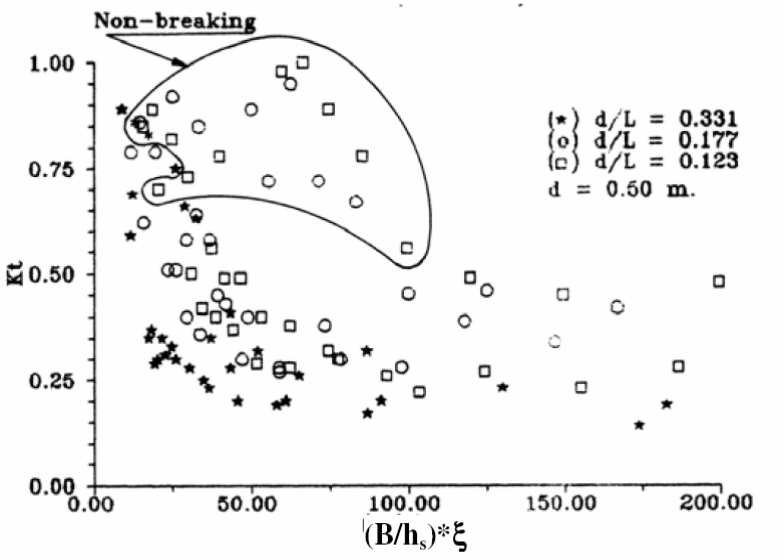


**Figure 2.3 – Influence of braking conditions on wave transmission coefficient by Gómez Pina and Valdés (1990)**

**van der Meer (1988, 1990 and 1991)** using previous laboratory data found a new formula for wave transmission coefficient. This empirical formula is based on relative freeboard values (Figure 2.4):

$$\begin{aligned} K_t &= 0.8 && \text{for} \quad 1.13 < h_s/H_i < 2.0 \\ K_t &= 0.46 + 0.3\, h_s/H_i && \text{for} \quad 0.2 < h_s/H_i < 1.13 \\ K_t &= 0.1 && \text{for} \quad -2.0 < h_s/H_i < -1.2 \end{aligned} \qquad [2.8]$$

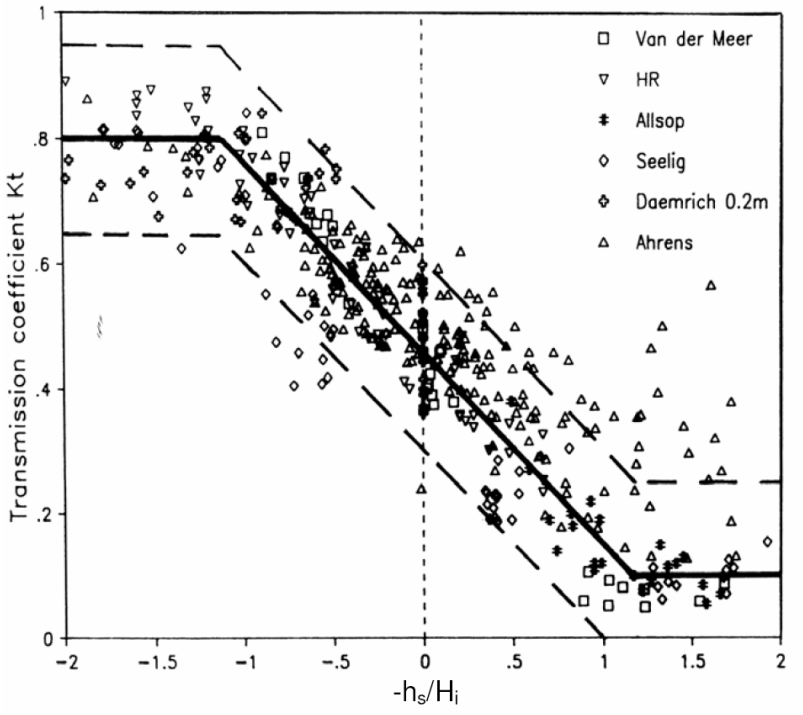


**Figure 2.4 – Proposed wave transmission coefficient by van der Meer (1990)**

**Daemen (1991)** carried out 2D tests in a wave flume at Delft Hydraulics in random wave conditions. van der Meer (1991) and van der Meer and Daemen (1994) proposed an empirical formula for low-crested breakwaters related to crest width and height, wave steepness and incident wave height. They found a linear relationship between the wave transmission coefficient $K_t$ and relative crest height $h_s/d_{50}$:

$$K_t = a\frac{-h_s}{d_{50}} + b \qquad [2.9]$$

where

$$a = 0.031\left(H_i / d_{50}\right) - 0.24 \qquad [2.10]$$

and the coefficient $b$ is defined by:

$$b = -5.42\left(H_i / L_0\right) + 0.0323(H_i / d_{50}) - 0.0017(B / d_{50})^{1.84} + 0.51 \qquad [2.11]$$

and for reef type (gradually deforming) breakwaters:

$$b = -2.6\left(H_i / L_0\right) - 0.05(H_i / d_{50}) + 0.85 \qquad [2.12]$$

in which $h_s$ is water depth over the breakwater $d_{50}$ is nominal diameter of armour rock, $H_i$ is significant incident wave height and $L_0$ is wave length of the incident wave height in deep water. This empirical formula is valid within the dimensionless parameters used in tests. The range of variation of transmission coefficient Kt in the test for conventional breakwaters is 0.075 < $K_t$ < 0.75 and for reef type breakwaters is 0.15 < $K_t$ < 0.6.

**Davies and Kriebel (1992)** performed a series of experimental tests on solid and rubblemound breakwater models using both regular and random wave field. They proposed a new dimensionless parameter of freeboard ratio $(h_s+R_u)/H_i$ They proposed a new parameter to predict the transmission coefficient past a reef breakwater at all values of freeboard where is the potential run-up as proposed by Ahrens and McCartney (1975) This new parameter is function of Iribarren number defined above:

$$\frac{R_u}{H_i} = \frac{a\xi}{1 + b\xi} \qquad [2.13]$$

in which a and b are empirical coefficients which have the values of $a=0.775$ and $b=0.361$, as proposed by Gunbak (1979) for rubble mound breakwaters.

**Davies and Kriebel (1992)** carried out a large number of 2D tests in a wave using two types of breakwater (rubble-mound and solid) and imposing both regular and irregular waves. They found that transmission coefficient does not significantly differ between the solid and rubble-mound breakwater in the case of submerged breakwater. The tests also indicated that the Bulk Number ($B = A_t/d^2_{50}$) does not appear to affect much wave transmission for submerged breakwater and small difference in transmission coefficient were

observed between the rubblemound and solid (smooth) breakwater, particularly for low steepness waves (Figure 2.5).

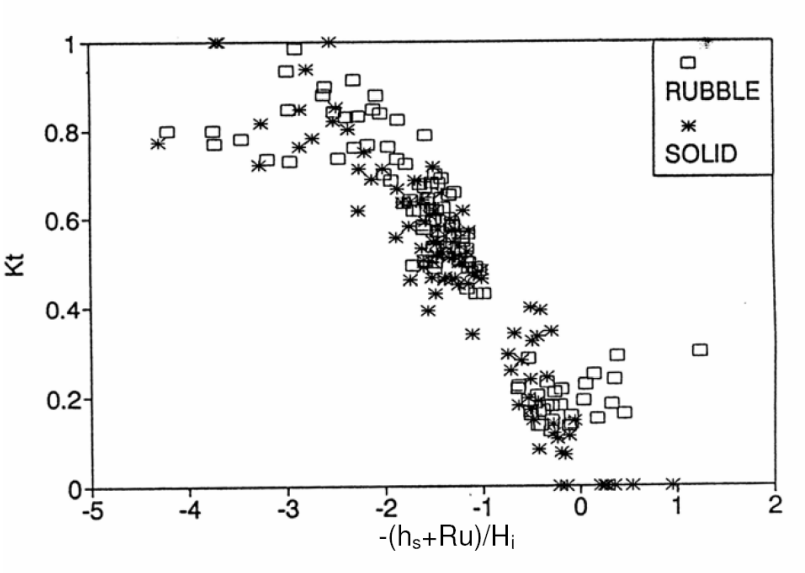


**Figure 2.5 – Transmission coefficient over submerged breakwater by Davies and Kriebel (1992)**

**d'Angremond et al. (1996)** reanalysed data sets collected from other experimental test (Seeling, 1980; Allsop, 1983; Daemrich and Kahle, 1985; Powel and Allsop, 1985; van der Meer, 1988; Daemen, 1991) in order to find a better formulation for transmitted wave height passing over permeable and impermeable submerged breakwaters:

$$K_t = 0.4\frac{h_s}{H_i} + \left(\frac{B}{H_i}\right)^{-0.31} \times a\left(1 - e^{-0.5\xi}\right) \qquad [2.14]$$

where *a=0.64* and *0.8* for permeable and impermeable breakwaters respectively with limits *0.075< $K_t$ < 0.80* for both conditions and is the Iribarren parameter that was defined in Equation 2.8.

**Seabrook and Hall (1997, 1998)** performed 2D and 3D laboratory tests with irregular waves to investigate transmitted wave height passing over submerged rubble mound breakwaters. They shown that the formula provided by Ahrens (1987) and van der Meer (1991) are not suitable to forecast $K_t$ when crest width is large. Seabrook and Hall (1998) observed

that the relative submergence and crest width are most important in determining transmission coefficient. They suggested a new design formula for transmission coefficient $K_t$ taking in count the effect of crest width:

$$K_t = 1 - \left( e^{-0.56\left(\frac{h_s}{H_i}\right)-1.09\left(\frac{H_i}{B}\right)} + 0.047\left(\frac{B}{L_0}\cdot\frac{h_s}{d_{50}}\right) - 0.67\left(\frac{h_s}{B}\cdot\frac{H_i}{d_{50}}\right)\right) \qquad [2.15]$$

The following ranges were recommended for applying the proposed equation:

$$0 \le \frac{B}{L_0}\cdot\frac{h_s}{d_{50}} \le 7.08$$
$$0 \le \frac{h_s}{B}\cdot\frac{H_i}{d_{50}} \le 2.14 \qquad [2.16]$$

Seabrook and Hall (1997) also found that the $d_{50}$ has modest effect on wave transmission (Figure 2.6) and the effect of crest width on transmission coefficient is evidenced in the energy transfer to higher harmonic frequencies of spectra behind submerged breakwaters (Figure 2.7).

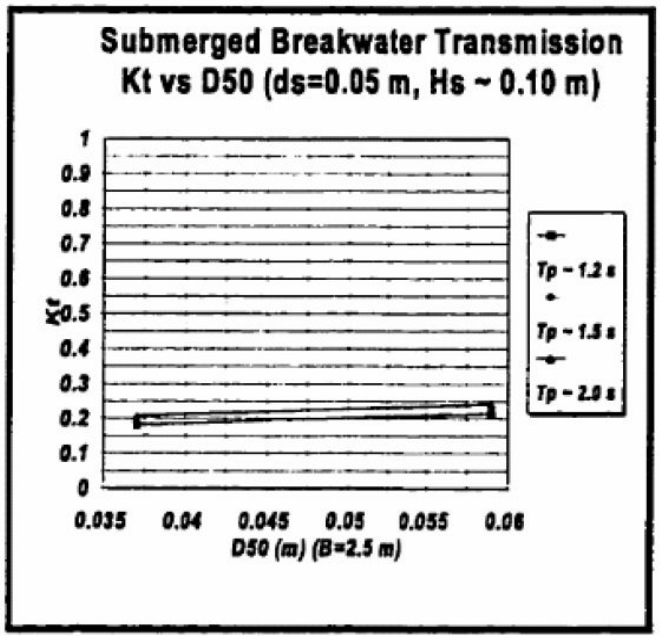


**Figure 2.6 – The effect of armour rock size on transmission coefficient by Seabrook (1997)**

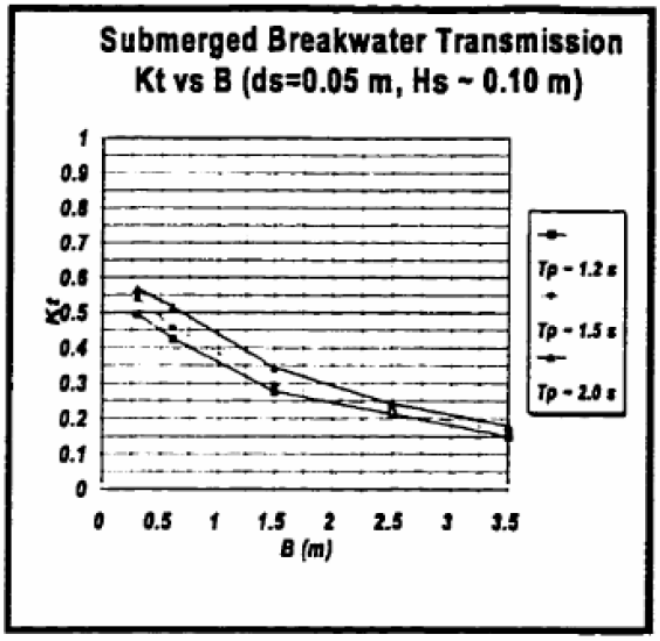


**Figure 2.7 – Variation of transmission against breakwater width by Seabrook (1997)**

**Gironella and Sanchez-Arcilla (1999)** reanalysing some data sets, elaborated a wave transmission and reflection coefficient model for submerged breakwater. These expressions is based on ratio of $h_i/L_0$ (submergence over deepwater wavelength) and Iribarren number as expressed in Equation 2.8. The authors applied a multilinear regression and found:

$$K_t = C_1\left(\xi \frac{h_s}{L_0}\right) + C_2 \frac{h_s}{L_0} + C_3 \qquad [2.17]$$

where the empirical coefficient of $C_1$, $C_2$ and $C_3$ were determined as *6.43*, *14.63* and *0.52*, respectively, which leads to a level of correlation of $R^2=0.98$. The proposed equation is valid in the range of experimental test values, which were:

$$3.2 \le \xi \le 5.5; \qquad 0 \le \frac{h_s}{L_0} \le 0.04; \qquad 0.015 \le \frac{H_i}{L_0} \le 0.04$$

**Roul and Faedo (2002)** performed some experimental tests in wave flume at IMAGE Department of University of Padova, Italy, in order to better understand the hydraulic performance of rubble-mound submerged

breakwaters under breaking waves conditions. They developed an empirical expression for wave transmission coefficient using the dimensionless freeboard $(h_s+R_u)/H_i$ as proposed by Davies and Kriebel (1992):

$$K_t = -0.0928\left(\frac{h_s + R_u}{H_s}\right)^2 + 0.1862\left(\frac{h_s + R_u}{H_s}\right) + 0.1176 \qquad [2.18]$$

**Calabrese et al., (2002 and 2003)** carried out a series of large-scale laboratory model tests on rubble mound submerged breakwaters at "Grosser WellenKanal" of Hannover, Germany. The tests were performed under random wave field conditions in order to verify, at large scale, the accuracy of existing formula . Calabrese et al. (2002) used $h_s/B$ ratio as adimensional parameter instead of incident wave height. Results shown that d'Angremond et al. (1996) equation (Equation 2.15) was more accurate than other for estimating wave transmission coefficient. Authors using data obtained from the large-scale experimental tests developed a new expression for transmission coefficient

$$K_t = a \cdot \frac{h_s}{B} + b \qquad [2.19]$$

in which the intercept $b$ is expressed by an exponential formula:

$$b = \alpha \cdot e^{-0.0845\frac{B}{H_i}} \qquad [2.20]$$

where

$$\alpha = 1 - 0.562 \cdot e^{-0.0507\,\xi} \qquad [2.21]$$

and the angular coefficient $a$ was expressed as a function of relative crest width $B/H_i$:

$$a = \beta \cdot e^{0.2568\frac{B}{H_i}} \qquad [2.22]$$

in which is a scale parameter where water depth has been included:

$$\beta = 0.6957\,\frac{H_i}{h} - 0.7021 \qquad [2.23]$$

Calabrese et al. (2002) formula was calibrated in the test range of:

$$-0.3 \le h_s / B \le 0.4$$
$$1.06 \le B / H_i \le 8.13$$
$$0.31 \le H_i / h \le 0.61$$
$$3.0 \le \xi \le 5.20$$

**van der Meer et al. (2004)** in order to improve the formula provided by van der Meer (1991) and d'Angremond et al. (1996) analyzed previous collected data, considering the value of crest width ratio $B/H_i$. van der Meer et al. (2004) found that equation provided by d'Angremond et al. (1996) are suitable for rubble mound structures with $B/Hi < 10$ and for $B/H_i > 10$, a little modification of [2.18] (d'Angremond et al., 1996) provides more realistic results. They proposed the following modified equation for low crested rubblemound breakwater in case of $B/H_i > 10$:

$$K_t = 0.35 \frac{h_s}{H_i} + 0.51 \left( \frac{B}{H_i} \right)^{-0.65} \cdot \left( 1 - e^{-0.41\xi} \right) \qquad [2.24]$$

The authors set a maximum value of $K_{tu}$ in function of ratio of $B/H_i$ (as proposed by d'Angremond et al., 1996) For $K_t$ values higher than $K_{tu}$ formula may give inaccurate results:

$$K_{tu} = -0.006\, B / H_i + 0.93 \qquad [2.25]$$

The lower limit of transmission coefficient $K_t$ was kept constant as proposed by d'Angremond et al. (1996).

They also studied the influence of wave angle $\Theta$ on transmission coefficient and found that, in case of rubble mound structures, transmission coefficient is not sensitive to incident wave angle.

## 2.2 Analytical/Numerical Modelling of Wave Transmission

The phenomena of waves transmission behind submerged barriers was also studied using numerical models.

**Kobayashi and Wurjanto (1988)** developed a numerical model to predict wave reflection and transmission over an impermeable submerged breakwater in case of monochromatic wave. The model provided quite good prediction of transmission coefficient over submerged impermeable breakwaters in comparison with the limited data measured in laboratory by the authors.

**Rojanakamthorn et al. (1990)** developed a mathematical model for the estimation of wave transformation over a permeable submerged breakwater. Model are based on equation of waves on a porous layer as a two-dimensional elliptic equation analogous to the mild slope equation. Results shown a good agreement with 2D experiments conducted by Rojanakamthorn et al. (1990). However, the calculated transmitted wave height was slightly smaller than the measured one.

**Shen et al. (2004)** developed a VOF (Volume Of Fluid) type model in order to simulate the propagation of cnoidal waves over a submerged bar (breakwater). The calculated water surface elevation around a breakwater was compared with the 2D experimental data collected by Ohyama et al. (1995). The results of numerical model were relatively in good agreement with measured water surface even if some differences are observed due to to higher harmonics generation over the breakwater in the laboratory test.

**Garcia et al. (2004)** used a numerical model named COrnell BReaking waves And Structures (COBRAS Lin & Liu 1998; Liu et al. 1999) to calculate water surface elevation and circulation in the presence of permeable low-crested breakwaters for regular breaking waves. The COBRAS model solves the 2DV Reynolds Averaged Navier-Stokes (RANS) equation that was firstly provided by Lin and Liu (1998). "The model is based on the composition of

the instantaneous velocity and pressure fields into mean and turbulent components", Garcia et al. (2004). The results of surface elevation around the breakwater, the pressure field inside the rubble and the flow field were compared with data collected from 2D experimental tests carried out by Vidal et al. (2001) showing a good agreement.

**Johnson (2006)** used MIKE 21 PMS ( developed by DHI water & environment) to model wave field in the presence of submerged breakwaters. MIKE 21 PMS is based on parabolic mild slope equations. The results put in evidence that using dissipation model of Battjes and Janssen (1978) MIKE 21 PMS predict higher energy dissipation than experimental data (Zanuttigh and Lamberti, 2003) over a submerged breakwater. The breaker parameter in the Battjes and Janssen' s dissipation model was used to calibrate the model by Johnson (2006) .

**Wave set-up**

Breaking waves passing over a submerged breakwater causes water to flow into the protected area (onshore) of the breakwater. On the other hand, the difference in mean water level inside and outside of the protected zone results in water flowing out of this area. Piling-up will occur when a quasi-equilibrium between inflow and out-flow is reached. Few experimental, theoretical or numerical studies have been undertaken that provide a good understanding of set-up and the behaviour of longshore current behind submerged breakwaters.

For a submerged breakwater, where no breaking is considered, an analytical solution for set-up, $\delta$, has been given by Longuet-Higgins (1967). His approach applies vertical momentum flux balance above the still water level and yields the following expression:

$$\delta = \frac{\left(H_i^2 + H_r^2\right) k_i}{8 \sinh 2k_i h_1} - \frac{H_t^2 k_t}{8 \sinh 2k_i h_2} \qquad [2.26]$$

in which $H_t$ is the transmitted wave height; $H_t^2$ is the sum squared of incident and reflected wave heights; $\delta$ is the water depth; k is the wave number; the numerical subscripts denote parameters values before and behind the breakwater. Eq. 2.40 basically represents the difference between the "set down" (Longuet-Higgins and Stewart, 1964) expected respectively at rear and in front of the barrier. Measurements of 2D laboratory measurements by Dick (1968) showed that the equation provided by Longuet-Higgins (1967) greatly underestimates the mean sea level difference $\delta$.

Dick (1968) measured the set-up for an impermeable rectangular breakwater and found out that Eq. 2.40 greatly underestimated experimental values. Subsequently, Diskin (1970) performed a study on a two dimensional physical model of a trapezoidal breakwater with an homogeneous cross section. Using regular waves, the Author developed an empirical relationship between set-up, incident wave height, Hi and depth of submergence, Rc: breakwaters:

$$\frac{\delta}{H_i} = 0.6 \exp\left(-\left(0.7 + \frac{h_s}{H_i}\right)^2\right) \qquad [2.27]$$

The equation is valid in the range of the tested values of submergence ratio *(-2.0<$h_s/H_i$<1.5)*. It should be noted the test conditions were such that the piled-up water behind the breakwater could return offshore only by passing over and through the structure. In this case no longshore current can develop behind the breakwater. Eq. 2.41 indicates that set up increases with Hi and that, for a given wave height, it attains a maximum when the water level is just below the crest, Rc = 0.7 Hi. For water levels above and below this value, set-up lowers and tends to zero. In the Diskin's formula neither crest extent, B, or period, T, influences have been considered. Since only one size of rock was tested, Diskin was unable including permeability of the barrier in the formula.

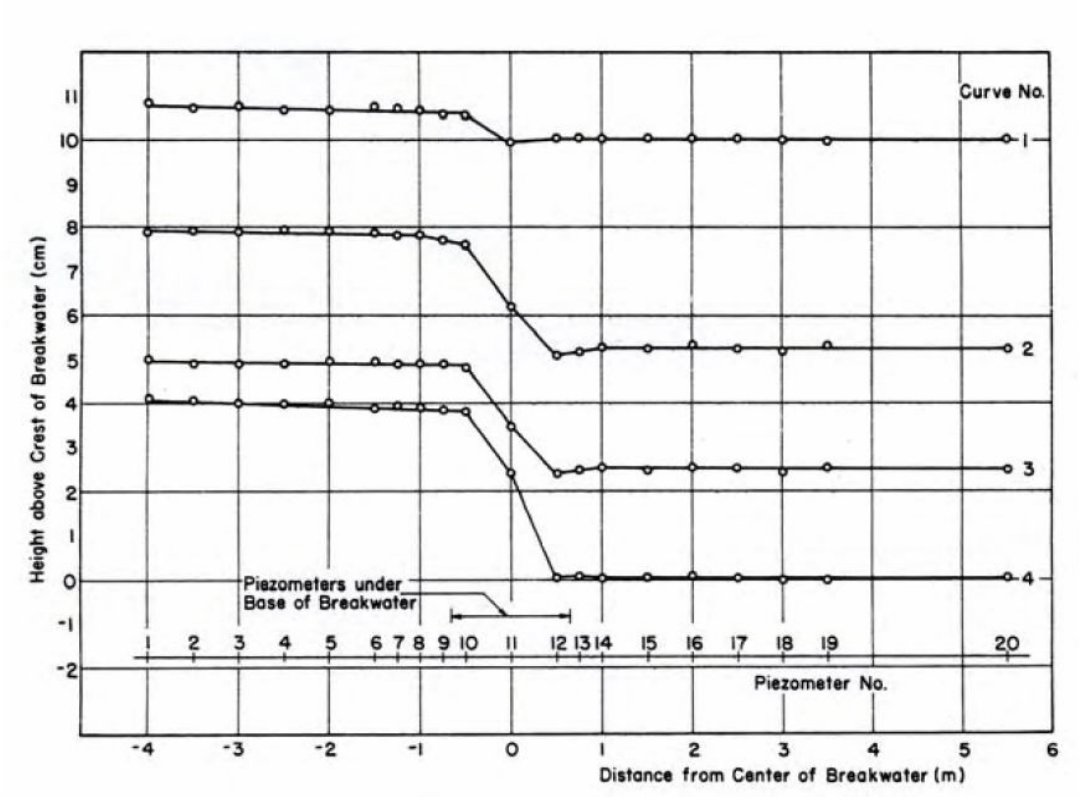


**Figure 2.9 – Examples of mean water surfaces curves under wave action by Diskin at al. (1970)**

A more extensive program of experiments have been carried out by Loveless et al. (1998) in the random wave flume at the Hydraulics Laboratory of University of Bristol's Civil Engineering Department. On the whole, eight different models have been tested including variations in crest width, front slope angle and rock size. All the models were homogeneous rubble mound structures, made up on rock of narrow grading. Most of experiments were conducted with regular waves; some irregular wave trains have been also run in order to study how information obtained under monochromatic waves should be transferred to spectral ones. First the Authors noted that Diskin's formula predicted with some accuracy the values of set-up for submerged breakwaters (Rc < 0), while it largely overestimated experimental data for emerged or "no freeboard" ones (Rc ³ 0). This was attributed to permeability (Diskin's model had median diameter, D50, of 40% less than the smallest of the Loveless models), which is expected to have no influence for submerged

breakwaters, but to greatly affect the behaviour of emerged ones. Moreover the Authors found out that to adapt monochromatic waves results to irregular waves, the average wave height should be used instead of significant one. Finally following expression has been proposed: breakwaters:

$$\delta = 0.125 \frac{H_i}{T} \cdot \frac{L_0}{h} \cdot \exp\left(-20\left(h_s/d\right)^2\right) \qquad [2.28]$$

where $H_i$ is incident wave height, $T$ is wave period, $L_0$ is wave length in deepwater, $h$ is water depth at the offshore toe of the breakwater and $d$ is the breakwater crest height.

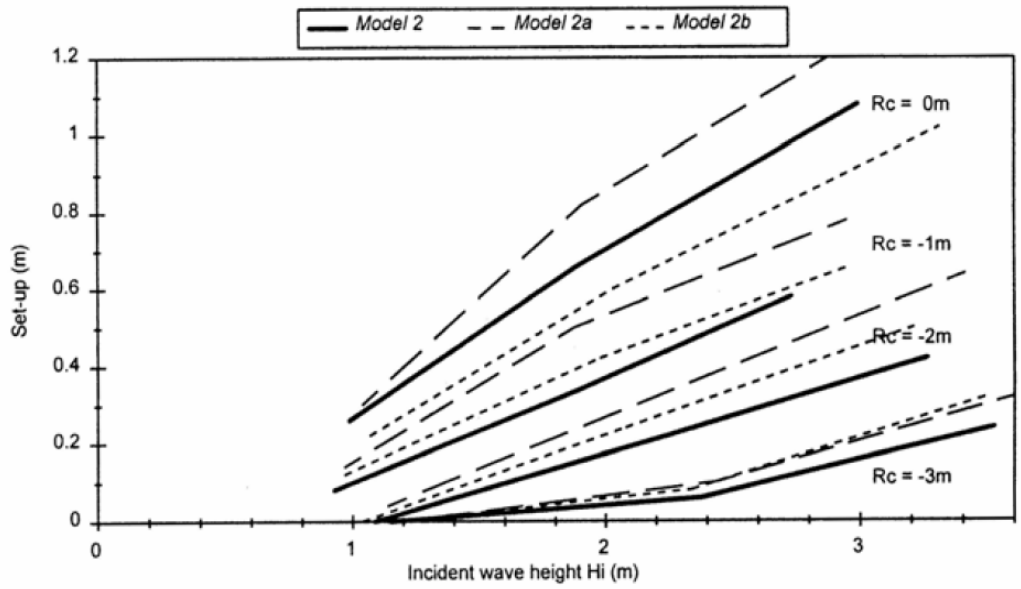


**Figure 2.10 – The influence of crest width on set-up by Loveless and Debsky (1997)**

The experiments also demonstrated that set-up is significantly influenced by the porosity (influenced by the rock size $d_{50}$) and the crest width $B$ of the breakwater. Loveless et al. (1998) improved the original Equation 2.42 by linear regression analysis and provided the following expression for calculating set-up behind a permeable submerged breakwater:

$$\frac{\delta}{B} = \frac{\left(H_i L_0 / hT\right)^2}{8gd_{50}} \cdot \exp\left[20\left(h_s / d\right)\right] \qquad [2.29]$$

Calabrese et al. (2003) developed a model based on hypothesis that wave set-up is dominated by the amount of momentum released by the breaking waves on the breakwater $\delta_m$ plus a further contribution called "continuity set-up" $\delta_s$:

$$\delta = \delta_m + \delta_s \qquad [2.30]$$

Applying the momentum equation and assuming that the surf zone extends from the breaker point on the sea-face slope to the inshore toe of the breakwater (linear increasing of set-up), Calabrese et al. (2003) provided the following equation for the momentum set-up $\delta_m$ :

$$\delta_m = 0.5\left[-b + \left(b^2 + 4c\right)\right]^{0.5} \qquad [2.31]$$

where

$$b = \left(2h - A\right) \qquad [2.32]$$

$$A = \left[\left(1 + \frac{x_b + B}{L_s}\right) \cdot d - \frac{h_b + h_s}{L_s} \cdot x_b\right] \qquad [2.33]$$

$$c = \frac{3}{8} H_i^2 \left(1 - K_t^2\right) \qquad [2.34]$$

in which $K_t$ is wave transmission coefficient, $h_b$ is wave breaker depth over the offshore slope, $h_s$ is submergence depth, $d$ is breakwater crest height and $L_s$ is the effective crest width of the breakwater (Figure 2.12).

The continuity set-up $\delta_s$ may be determined by assuming uniform return flow:

$$\delta_s = \frac{q^2}{f^2 \cdot \left|R_c\right|^{10/3}} \cdot B_{eq} \qquad [2.35]$$

where

$$q = \frac{1}{8} \cdot H_i^2 \cdot \sqrt{\frac{g}{h}} \qquad [2.36]$$

$$B_{eq} = B + d \cdot \cot g\alpha \qquad [2.37]$$

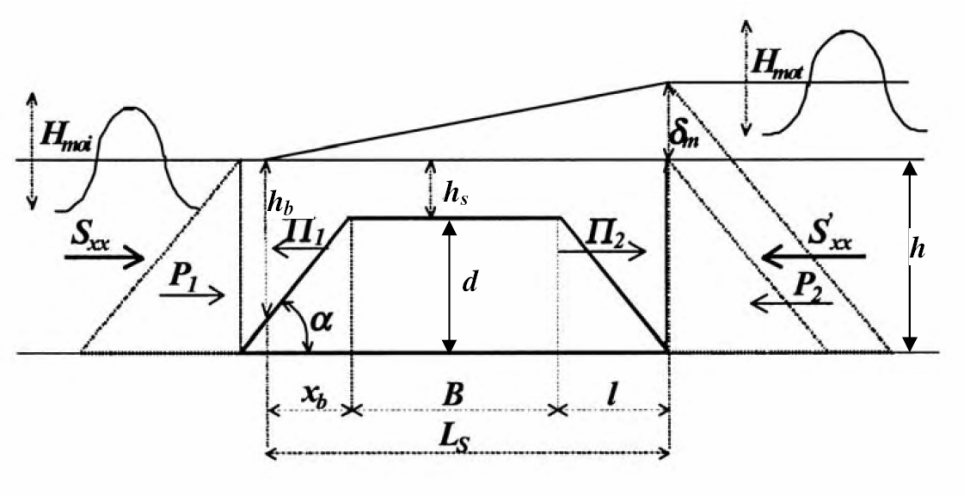


**Figure 2.11 – Definition of flux theory setup by Calabrese et al. (2003)**

**Summary**

The functional design knowledge of submerged breakwaters including their impacts on wave transmission, currents, sediment processes and shoreline response is stili developing.

Many numerical modelling and empirical approaches for estimating wave transmission over submerged breakwaters have been developed (Johnson et al., 1951; Adams and Sonu, 1986; Losada et al., 1996; d'Angremond et al., 1996; Seabrook and Hall, 1998; Schlurmann et al., 2002; van der Meer et al. 2005). Most of the previous experimental research on wave transmission over submerged breakwaters has been carried out as a subset of investigations into relatively narrow crested semi submerged breakwaters. The results of these previous experiments are limited to the tested ranges of breakwater crest width. As indicated in Chapter 1, narrow crested (fully) submerged breakwaters have been found to be ineffective in coastal protection in most field applications. Therefore more investigations are needed to extend the studies of wave transmission over submerged breakwaters with wide to broad crest width due to their improved efficiency in protection of coastal area.

The gradient of wave-induced set-up behind submerged breakwaters causes water to flow along the shoreline. Only a few experimental, theoretical or numerical studies have been undertaken that provide an understanding of set-up and the behaviour of longshore current behind submerged breakwaters (Longuet-Higgins, 1967; Diskin et al. ,1970; Debski and Loveless ,1997; Calabrese et al. ,2003).

# CHAPTER 3

# Interaction between wave and submerged barrier.

The study of the propagation of the wave on a varying topography constitutes one of the topic of greater interest in the field of the coastal engineering, in fact it is tightly connected to the problem of the description of the propagation of the waves from breadth toward shore. A synthesis of the principals developments of the subject can be found in Mei & Liu (1993) and Liu & Losada (2002). Coherently with the purposes of the present job, now the models of interaction between the wave motion and the submerged obstacles will be analyzed. In Figure 3.1 the geometry of the computational dominion are represented for the two schemes of obstacle, of endless length and of ended length. Both h the depth of the bottom to wide and, eventually, to back of the obstacle, and is $h_t$ the depth of the obstacle.

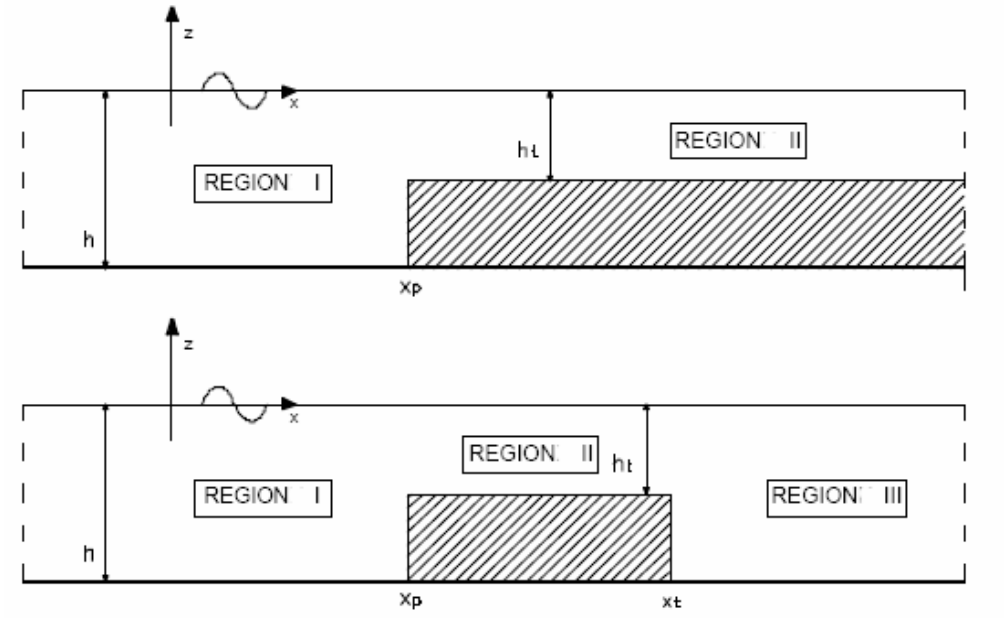


**Figure 3.1 – Geometry of computational domain**

The first studies on the argument have been conducted primarily using the linear theory; in the hypothesis of depth h, very small $h_t$ in comparison to the wavelength, the solution proposed by Lamb (1932), brought in numerous texts is:

$$R = \frac{1 - \sqrt{h_t/h}}{1 + \sqrt{h_t/h}} \quad \text{and} \quad \mathrm{T} = \frac{2}{1 + \sqrt{h_t/h}} \qquad [3.1]$$

In the formulas, R expresses the relationship between the height of reflected wave and the height of incidental wave (coefficient of reflection), while T is the relationship among the height of wave above the obstacle and the height of incidental wave (coefficient of transmission). In the case of very deep obstacle (ht/h=1) R=0, T=1, correspondent to the condition to the absence of obstacle, while, in the case of void depth on the threshold (ht/h=0), correspondent to the case of total reflection on a vertical wall, while the coefficient of transmission loses meaning.

Among the solutions, in the general case of wave of any period, in linear theory, Rey et al. (1992), have found the solution for an arbitrary bottom profile. The adopted procedure consists of schematizing the profile as a whole lines of constant depth, to seek the solution of the differential problem for every line and to impose the opportune conditions of congruence along the ideal surfaces that separate two lines adjacent at different depth. The solution described show that, on every line of bottom, are present two progressive waves , of which one is propagated in the positive verse of the axle of the abscissas, the other in the negative verse. The formulation of the differential problem and the relative solutions are not brought for brevity.

The hypothesis of linearity constitutes, for the examined problem, a very restrictive condition, especially above the obstacle, because the depth is normally small, and than is expected that the problem is strongly conditioned by nonlinear effects.

The development of non linear theories for the description of the interaction among the wave motion and a obstacle is relatively recent.

## 3.1 Massel solution

Massel (1983) gives the general formulation and the resolution of the differential problem for an impermeable step of ended or endless length , using second order Stokes theory. With reference to the geometric scheme of Fig. 3.1, $x_p$ is the abscissa offshore parameter of the step, and is $x_t$, in the case of obstacle of ended length, is the abscissa of the inshore parameter. Pedicis I, II, III indicate respectively the zones before, above and, eventually, to back of the step. The differential problem can be so formulated:

$$\nabla^2\Phi = 0 \qquad [3.2]$$

$$\frac{\partial\Phi}{\partial z} = \frac{\partial\eta}{\partial t} + \frac{\partial\Phi}{\partial x}\frac{\partial\eta}{\partial x} \qquad z=\eta \qquad [3.3]$$

$$\frac{\partial\Phi}{\partial t} + \frac{1}{2}\left[\left(\frac{\partial\Phi}{\partial x}\right)^2 + \left(\frac{\partial\Phi}{\partial z}\right)^2\right] + g\eta \qquad z=\eta \qquad [3.4]$$

$$\frac{\partial\Phi}{\partial z} = 0 \qquad z=-h \qquad z=-h_t \qquad [3.5]$$

To such conditions they are added those that define the incident wave motion at endless distance from the obstacle:

$$\eta = \eta_i^{(1)} + \eta_i^{(2)} = a\cos\left(kx-\omega t\right) + \frac{ka^2}{4}\frac{\cosh kh\left(2+\cosh 2kh\right)}{\sinh^3 kh}\cos 2\left(kx-\omega t\right) \qquad [3.6]$$

$$\Phi_i + \Phi_i^{(1)} + \Phi_i^{(2)} = \frac{ag}{\omega}\frac{\cosh k\left(h+z\right)}{\cosh kh}\sin\left(kx-\omega t\right) + \frac{3}{8}\omega a^2\frac{\cosh 2k\left(h+z\right)}{\sinh^4 kh}\sin 2\left(kx-\omega t\right) \qquad [3.7]$$

The conditions (3.2,3,4,5) must be verified in the whole dominion of integration. To them the followings conditions are added in correspondence of the contours of the regions I, II, III:

$$\Phi_I = \Phi_{II} \qquad x = x_p$$
$$\frac{\partial \Phi_I}{\partial x} = \begin{cases} \dfrac{\partial \Phi_{II}}{\partial x} & x = x_p \;\; z \in \left[-h_t, 0\right] \\ 0 & x = x_p \;\; z \in \left[-h, h_t\right] \end{cases} \qquad [3.8]$$

and, in the case of obstacle of ended length:

$$\Phi_{II} = \Phi_{III} \qquad x = x_p$$
$$\frac{\partial \Phi_{II}}{\partial x} = \begin{cases} \dfrac{\partial \Phi_{III}}{\partial x} & x = x_p \;\; z \in \left[-h_t, 0\right] \\ 0 & x = x_p \;\; z \in \left[-h, h_t\right] \end{cases} \qquad [3.9]$$

Illustrated conditions express the congruence among the solutions of the differential problems in the different regions.

Using the perturbation method of Stokes, the differential problem is divided in a problem at first order and a problem at second order, in which the unknown are $\Phi^{(1)}$ ed $\Phi^{(2)}$.

*First order problem*

In every of the three zones where the field of motion is divided, the solution of the problem includes a part that describes the waves that are propagated long x and endless evanescent modes that produce local oscillations around the surfaces of bonduary; they are pointed out with the apexes P and L,

respectively, the first one and the second type of so that (propagative and places). In the development of the theory, to the purpose to get more compact expressions the complex notation has been used.

In the region The the solution is the following:

$$\Phi_I^{(1)} + \Phi_I^{(1)P} + \Phi_I^{(1)L} \quad \text{con:}$$

$$\Phi_I^{(1)P} = \frac{ag}{\omega}\frac{\cosh k\left(h+z\right)}{\cosh kh}\sin\left(kx-\omega t\right) +$$

$$+\left|R_k^{(1)}\right|\frac{3}{8}\omega a^2\frac{\cosh 2k\left(h+z\right)}{\sinh^4 kh}\sin 2\left(kx-\omega t+\Psi^{(1)}\right) \qquad [3.10]$$

$$\Phi_I^{(1)L} = \frac{ag}{\omega}\,\mathrm{Im}\left[\sum_\alpha \left|R_\alpha^{(1)}\right| e^{\alpha\left(x-x_p\right)}\frac{\cos\alpha\left(h+z\right)}{\cos\alpha h}\sin\left(\varphi_{R_\alpha}-\omega t\right)\right]$$

In the (3.10) the first addendum represents the incidental wave, the second the wave reflected on vertical wall of the obstacle. The coefficient of reflection $R_k$ is a complex number whose modulus is the relationship between the amplitude of the reflected wave and that of the incidental wave, while the argument is function of the difference of phase among the two waves:

$$\Psi_I^{(1)} = \arg\left[R_k^{(1)}\right] + kx_P \qquad [3.11]$$

The wavenumber k is tied up to the frequency $\omega$ from linear dispersion relation:

$$\omega^2 = gk\tanh\left(kh\right) \qquad [3.12]$$

In the summation that appears in (3.10), every addendum corresponds to one of the infinite solutions of the equation:

$$\omega^2 = -g\alpha\tan\left(\alpha h\right) \qquad [3.13]$$

For every value of $\alpha$ a coefficient of reflection is gotten for the evanescent part, whose meaning is analogous to that for the propagation part; it results, therefore:

$$\varphi_{R_\alpha} = \arg\left[R_\alpha^{(1)}\right] \qquad [3.14]$$

In the region II, above the step, can be written, likewise observed for the region I:

[3.15]

$$
\begin{aligned}
&\Phi_{II}^{(1)} + \Phi_{II}^{(1)P} + \Phi_{II}^{(1)L} \quad \text{con:} \\
&\Phi_{II}^{(1)P} = \left|P_{K_t}^{(1)}\right| \frac{ag}{\omega} \frac{\cosh k_t\left(h_t + z\right)}{\cosh k_t h_t} \sin\left(k_t x - \omega t + \Psi_P\right) + \\
&-\left|Q_{k_t}^{(1)}\right| \frac{ag}{\omega} \frac{\cosh k_t\left(h_t + z\right)}{\cosh k_t h_t} \sin\left(k_t x - \omega t + \Psi_Q\right) \\
&\Phi_{II}^{(1)L} = \frac{ag}{\omega} \left\{ \sum_{\alpha_t} \left[ \begin{array}{l} \left|P_{\alpha_t}^{(1)}\right| e^{-\alpha_t\left(x - x_P\right)} \sin\left(\varphi_{P_{\alpha_t}} - \omega t\right) + \\ + \left|Q_{\alpha_t}^{(1)}\right| e^{\alpha_t\left(x - x_P\right)} \sin\left(\varphi_{Q_{\alpha_t}} - \omega t\right) \dfrac{\cos\alpha_t\left(z + h_t\right)}{\cos\alpha_t h_t} \end{array} \right] \right\}
\end{aligned}
\qquad [3.16]
$$

Can be observed that both propagative and evanescent terms are constituted by two part, the first represent the wave transmitted from region I to region II, the second represents the wave formed at bound between region II and region III. In case of step of endless lenght this term are null.

The coefficients $P_{kt}$ and $Q_{kt}$ are respectively the coefficient of transmission from region I to region II, and a coefficient of partial reflection at bound between region II and III. They can be expressed as:

$$
\begin{aligned}
\Psi_P^{(1)} &= \arctan\left[P_{k_t}^{(1)}\right] - k_t x_P \\
\Psi_Q^{(1)} &= \arctan\left[Q_{k_t}^{(1)}\right] - k_t x_t \\
\varphi_{P_{\alpha t}}^{(1)} &= \arctan\left[P_{\alpha_t}^{(1)}\right] \\
\varphi_{Q_{\alpha t}}^{(1)} &= \arctan\left[Q_{\alpha_t}^{(1)}\right]
\end{aligned}
\qquad [3.17]
$$

In the case in which the step has finite length, in the region III the potential can be expressed in the following form:

$$
\begin{aligned}
&\Phi_{III}^{(1)} + \Phi_{III}^{(1)P} + \Phi_{III}^{(1)L} \quad \text{con:} \\
&\Phi_{III}^{(1)P} = \left|T_k^{(1)}\right| \frac{ag}{\omega} \frac{\cosh k\left(h + z\right)}{\cosh kh} \sin\left(kx - \omega t + \Psi_T^{(1)}\right) \\
&\Phi_{III}^{(1)L} = \frac{ag}{\omega} \left[ \sum_{\alpha} \left|T_\alpha^{(1)}\right| e^{\alpha\left(x_t - x\right)} \frac{\cos\alpha\left(h + z\right)}{\cos\alpha h} \sin\left(\varphi_{T_\alpha} - \omega t\right) \right]
\end{aligned}
\qquad [3.18]
$$

Therefore wave motion in region III are constituted both for propagative and evanescent part from wave transmitted through region II. Transmission coefficient can be expresses as follows:

$$\begin{aligned} \Psi_t^{(1)} &= \arg\left[T_k^{(1)}\right] - kx_t \\ \varphi_{T_\alpha} &= \arctan\left[T_\alpha^{(1)}\right] \end{aligned} \qquad [3.19]$$

*Second order problem*

The second order solution is gotten gathering the terms that depend on the parameter perturbatinn (k · a); it can be so formulated:

$$\nabla^2\Phi^{(2)} = 0 \qquad [3.20]$$

$$\begin{aligned} &\frac{\partial^2\Phi^{(2)}}{\partial t^2} + g\frac{\partial\Phi^{(2)}}{\partial z} = -\frac{\partial}{\partial t}\overline{\left[\left(\frac{\partial\Phi^{(1)}}{\partial x}\right)^2 + \left(\frac{\partial\Phi^{(1)}}{\partial z}\right)^2\right]} + \\ &-\eta^{(1)}\frac{\partial}{\partial z}\left[\frac{\partial^2\Phi^{(1)}}{\partial t^2} + g\frac{\partial^2\overline{\Phi^{(1)}}}{\partial z}\right] = G'\left[\Phi^{(1)}\right] \end{aligned} \qquad [3.21]$$

$$\begin{aligned} &g\eta^{(2)} + \frac{\partial\Phi^{(2)}}{\partial t} = \frac{1}{2}\overline{\left[\left(\frac{\partial\Phi^{(1)}}{\partial x}\right)^2 + \left(\frac{\partial\Phi^{(1)}}{\partial z}\right)^2\right]} + \\ &-\eta^{(1)}\frac{\partial^2\Phi^{(1)}}{\partial z\partial t} = G''\left[\overline{\Phi^{(1)}}\right] \end{aligned} \qquad [3.22]$$

$$\frac{\partial\Phi^{(2)}}{\partial z} = 0 \qquad z = -h \qquad z = -h_t \qquad [3.23]$$

Matching condition can be expressed as follow

$$\begin{aligned} &\Phi_I^{(2)} = \Phi_{II}^{(2)} \qquad x = x_p \\ &\frac{\partial\Phi_I^{(2)}}{\partial x} = \begin{cases} \dfrac{\partial\Phi_{II}^{(2)}}{\partial x} & x = x_p \;\; z \in \left[-h_t, 0\right] \\ 0 & x = x_p \;\; z \in \left[-h, h_t\right] \end{cases} \end{aligned} \qquad [3.24]$$

$$\begin{aligned} &\Phi_{II}^{(2)} = \Phi_{II}^{(2)} \qquad x = x_p \\ &\frac{\partial\Phi_{II}^{(2)}}{\partial x} = \begin{cases} \dfrac{\partial\Phi_{III}^{(2)}}{\partial x} & x = x_p \;\; z \in \left[-h_t, 0\right] \\ 0 & x = x_p \;\; z \in \left[-h, h_t\right] \end{cases} \end{aligned} \qquad [3.25]$$

The differential problem is linear in the unknown $\square^{(2)}$ and $\square^{(2)}$, it is possible to express the solution in the following way:

$$\Phi^{(2)} = \tilde{\Phi}^{(2)} + \Phi^{(2)f} \qquad [3.26]$$

The first addendum of the (3.26) satisfies the non homogeneous equations (3.21,3.22) and represents the dependent terms of the second order from the solution to the first order. Therefore, it represents the bounds wave of pulsation $2\omega$, tied up to the principal harmonic of pulsation $\omega$.

The second addendum is the solution of the homogeneous form of the differential problem, comprehensive of the matchings condition (3.24,3.25) at the bound surface. Such term, insofar represents wave of pulsation $2\omega$that are propagated independently by the principal harmonic (free wave).

The solutions for second order are omitted for reasons for brevity. At the other hand such solution are available on many texts concerning this argument.

**Synthesis of solutions**

Neglecting the evanescent modes, whose amplitude exponentially weakens increasing distance from the obstacle, the presence of the following wave can be noticed:

FREE WAVES-REGION I

1. Incident principal harmonic, of amplitude a
2. Reflected principal harmonic, of amplitude $a\left|R_k^{(1)}\right|$
3. Reflected second harmonic, of amplitude $a\left|R_{k2}^{(2)}\right|$

BOUND WAVES-REGION I

1. Second harmonic tied to the incident principal harmonic (Stokes)
2. Second harmonic tied to the reflected principal harmonic (Stokes)

FREE WAVES-REGION II

1. Transmitted principal harmonic, of amplitude $a\left|P_{kt}^{(1)}\right|$
2. Reflected principal harmonic, of amplitude $a\left|Q_{kt}^{(1)}\right|$
3. Transmitted second harmonic, of amplitude $a\left|P_{k2t}^{(2)}\right|$
4. Reflected second harmonic, of amplitude $a\left|Q_{k2t}^{(2)}\right|$

BOUND WAVES-REGION II

1. Second harmonic tied to the transmitted principal harmonic (Stokes)
2. Second harmonic tied to the reflected principal harmonic (Stokes)

FREE WAVES-REGION III

1. Transmitted principal harmonic, of amplitude $a\left|T_{k}^{(1)}\right|$
2. Transmitted second harmonic, of amplitude $a\left|T_{k2}^{(2)}\right|$

BOUND WAVES-REGION III

1. Second harmonic tied to the transmitted principal harmonic (Stokes)

Free waves of second order propagated with smaller velocity respect to the corresponding bounds wave, the amplitude of the second harmonic, resultant from the interaction among the different components, is not constant long x, but it oscillates with spatial periodicity. The phenomenon is known in undulated mechanics as beat and it repeats in space according to a characteristic distance (beat length).

In the region I, the second reflected harmonic recurs according to the distance:

$$\lambda_{-}^{(2)} = \frac{2\pi}{k_{2} - 2k} \qquad [3.27]$$

while, for the incident progressive wave, it results:

$$\lambda_{+}^{(2)} = \frac{2\pi}{k_2 + 2k} \qquad [3.28]$$

In Fig. 3.2 are brought the amplitude of the first and the second harmonics, in the case of the obstacle of endless length, obtained arresting the solution to 20 evanescent modes. The incident wave has an amplitude a=2.3 cm and pulsation $\omega$=5 rad/s (f=0.796 Hz).

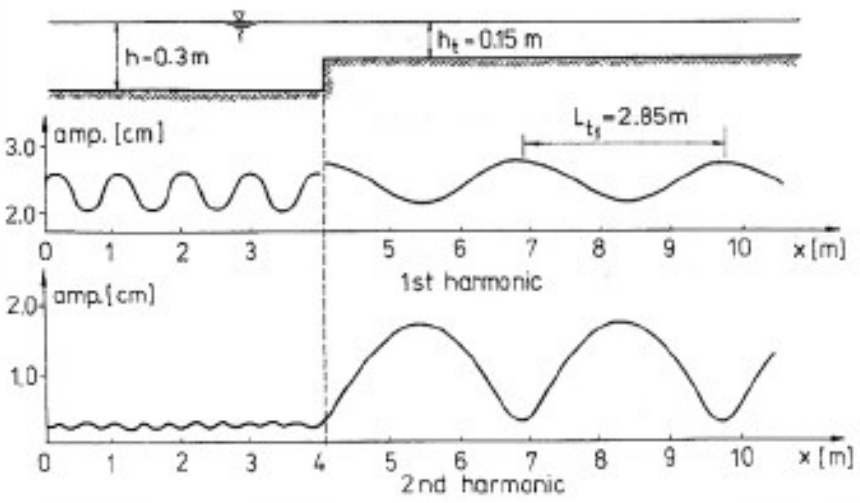


**Figure 3.2 – Wave amplitude of first and second harmonic. Massel solution (1993)**

## 3.2 Experimental study on wave/barrier interaction

The forecast of wave characteristics resultant from the interaction of the waves and a submerged barrier constitutes one of the argument of great application interest, testified by the number of jobs in literature.

From the theoretical point of view, the mechanism of interaction has been described in the previous chapter.

The introduced solutions, nevertheless, are not lent to an easy use, both for formal complexity, both for the consequential theoretical limitations. In fact the solutions are derived for a flat bottom and rectangular step.

Insofar, in the practical applications, for the evaluation of the characteristics of the wave motion in presence of a submerged barrier it is frequent the use of experimentation in the laboratory or the mathematical modelling of phenomena. From the theoretical point of view, a mathematical model able to describe with enough accuracy the interaction between wave motion and barrier should satisfy the followings conditions (Ohyama & Nadaoka, 1994):

2. Accurate description of the phenomenon of the dispersion, in presence of components of different frequency over an arbitrary depth;
3. Modeling of the effects of strong nonlinearity that can develop above of the barrier;
4. Description of the evolution of the wave motion on a bottom of elevated inclination;
5. Possibility to consider an irregular waves;

The comparison among the different mathematical formulations present in literature it underlines, that, besides the models based on the theory of Stokes, of which is discussed, are present three great typologies of models.

- The first type includes the models based on Boussinesq equations to the whose use. The use of this models are limited to cases of weak non linearity, in fact it is not possible to describe in correct way the generation of the free wave of superior order over the structure.
- The second typology of models are named BEM (Boundary Element Method), which found the solution, in the dominion of the time, of the integrated differential problem along the contour of the field of motion. Such approach seems to overcome the limitations shown by the formulations described in precedence, as shown in the comparison with experimental results.
- The third type of models are based on the direct solution of the equations of Navier-Stokes, in combination with opportune boundary conditions on the free surface. Such models, little used in past because of the great computational time, have known in times tightly tied up to the development of the computational tools.

Close to the mathematical models, in literature numerous jobs are based on experimental approach. The use of physical models, besides improving the knowledge of the qualitative and quantitative aspects of the studied phenomena, has allowed, through the comparison of the results, the validation of the proposed mathematical models.

In the present chapter are analyzed some work in literature on modelling of the interaction submerged wave-barrier. Coherently with the nature primarily experimental of the job of thesis, they are examined, particularly, the studies on physical models.

Yamashiro et al. (1999) have conducted some experimental studies in channel using regular waves of periods 1.20 sec, 1.43 sec, 1.79 sec and heights 2 cm, 4 cm and 6 cm. Further tests have been conducted with irregular waves, using the same values of regular waves as significant wave periods and wave heights

A scheme of the experimental installation is reported in Fig. 3.3

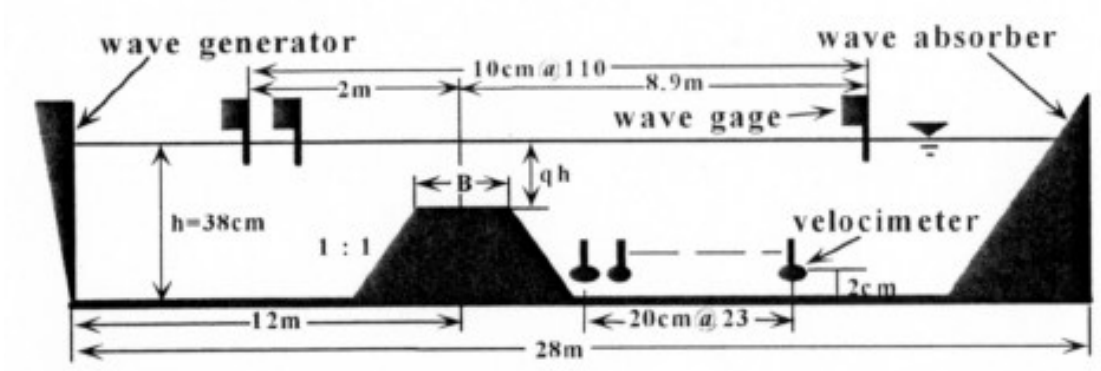


**Figure 3.3. – Experimental installation scheme used by Yamashiro et al. (1999)**

The Authors have used two different berm widths B (equal to 2h and 4h, with h=0.38 cm) and three different values of the freeboard above the crest f the barrier (equal to 0.1h, 0.2h and 0.3h). The barrier is trapezoidal with 1:1. slope. In some tests conditions waves break on the barrier.

In Fig. 3.4 are shown the energy spectra of the incident and transmitted wave, related to the test with wave of height H=4 cm, period T=1.43 s, width of the dike B=2h, freeboard of the structure 0.2h.

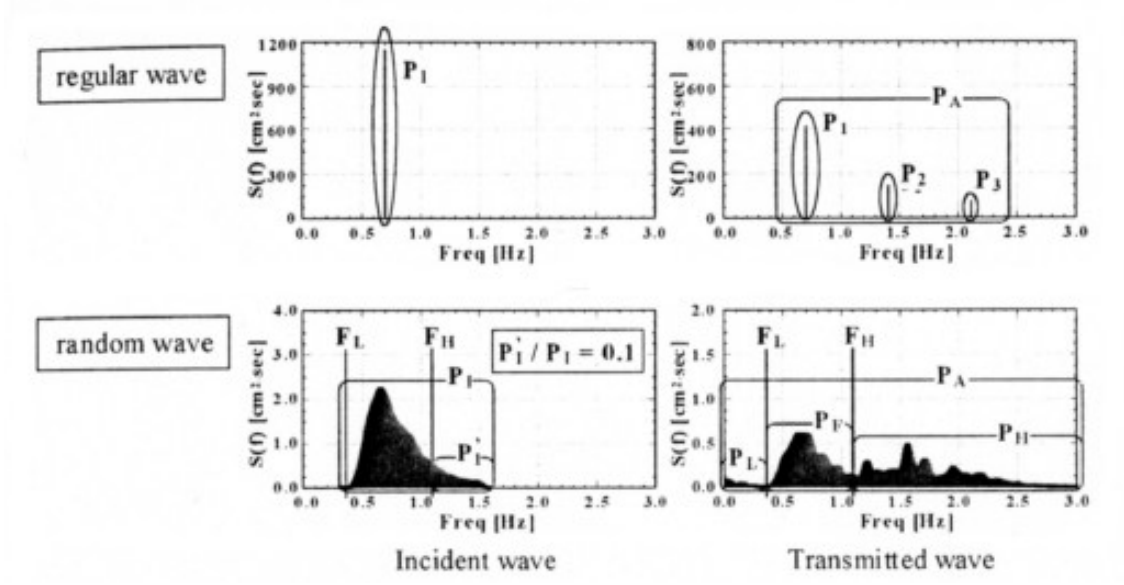


**Figure 3.4. – Energy spectra of incident and transmitted waves by Yamashiro et al. (1999)**

In the case of regular wave, pointing out with $P_A$ the energetic content of the spectra of transmitted wave, and with $P_1$, $P_2$, $P_3$ the energetic contents of the first , second and third harmonica, the modifications of the wave spectra result described by $P_1/P_A$, $P_2/P_A$, $P_3/P_A$, that expresses the relative power of the i-th harmonic.

In the case of the irregular waves, the Authors propose another variable, representative of the energetic contents of the lowest frequencies and of the highest frequencies. In particular, with reference to the Fig.xxx, "low frequency" $F_L$ is equal to the least value of frequency of the distribution incident spectrum, while the value of "high frequency" $F_H$ represent the frequency in which is distributed the 10% of the energy of the incidental wave. The value $P_L$, $P_F$, $P_H$ are obtained integrating energy spectra, respectively, in the interval [0, $F_L$], [$F_L$, $F_H$], and for f> $F_H$ and

they represent, respectively, the energetic content of the spectra "in low frequency", in the range of the incidental spectra and in "high frequency."

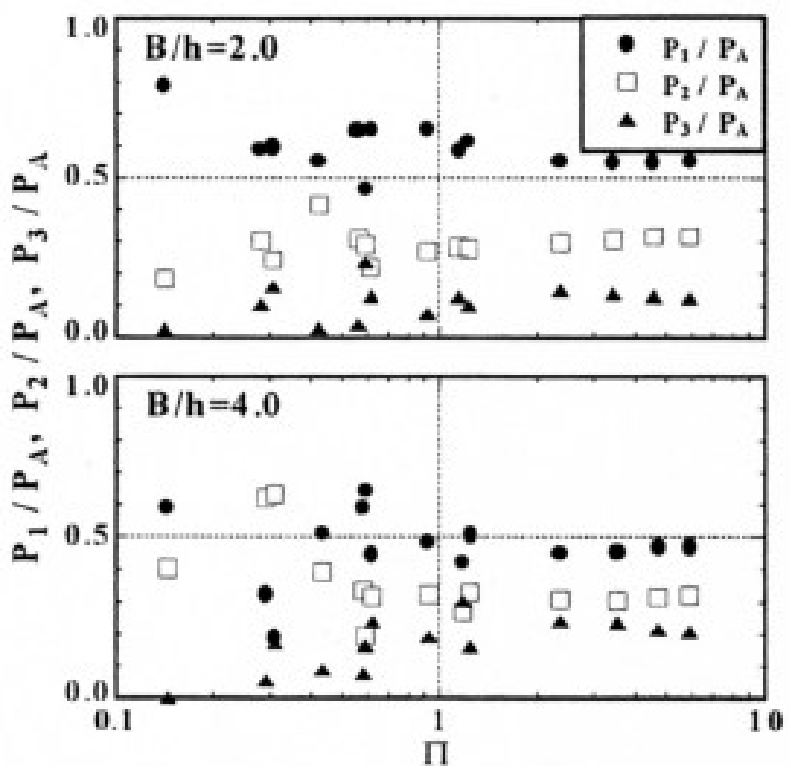


**Figure 3.5. – Values of relative power of harmonics by Yamashiro et al. (1999)**

In the Fig. 3.5, with reference at two different widths of the dike, are represented the relative powers of the hermonics in same wave conditions described through the following parameter of non linearity:

$$\Pi = \frac{H}{L_q}\coth^3(k_q h_q) \qquad [3.29]$$

in which H is the height of incidental wave, $h_q$ the depth above the barrier and $L_q$, $k_q$, respectively, length and the wavenumber above the barrier.

The Authors observe that, for the waves of lower height, characterized by the absence of breaking, the course of the relative powers is irregular, and characterized by a progressive growth of the energetic content of the superarmonics, particularly of the second. Increasing □, the relative powers seem to extend to a constant value. Such result can be attributed by the the effect of the breaking, that seems therefore to limit the growth and the propagation of the harmonics of superior order.

Van der Meer et al (2000) have investigated the modifications of the wave spectra to back of a submerged structure, through experimental tests in

channel with irregular waves. Authors have adopted a scale factor for the lengths of 1:15. The tests are been performed for different values of the water depth, between 4.5 m and 7.0 m, and significant wave height between 1.3 m and 2.2 m, and for two different values of the peak period Tp, equal to 5.0 sec and 7.0 sec. During the tests, various typologies of submerged structure are been used, as shown in the Fig. 3.6.

The relation between the freeboard ($R_c$) above the crest structure and the significant wave height vary between 0 (correspondent to the case of barrier with crest on the s.w.l.) and 1.0. The comparison among the characteristics of the wave motion offshore and back to the structure shows a general reduction of the energetic content of the wave and a change of the form of the spectra, characterized, for the transmitted wave, from a greater distribution of energy on the more elevated frequencies in comparison to the incidental wave, as already underlined by the studies previously examined. Such considerations are express in effective way comparing the moments of the spectral distributions. Pointing out with E(f) the function that defines the spectral density, the n-order moment is defined :

$$m_n = \int_0^\infty f^n E\left(f\right) df \qquad [3.30]$$

In particular, the significant spectral wave height is function of zero order moment through this relation:

$$H_{m0} = 4\sqrt{m_0} \qquad [3.31]$$

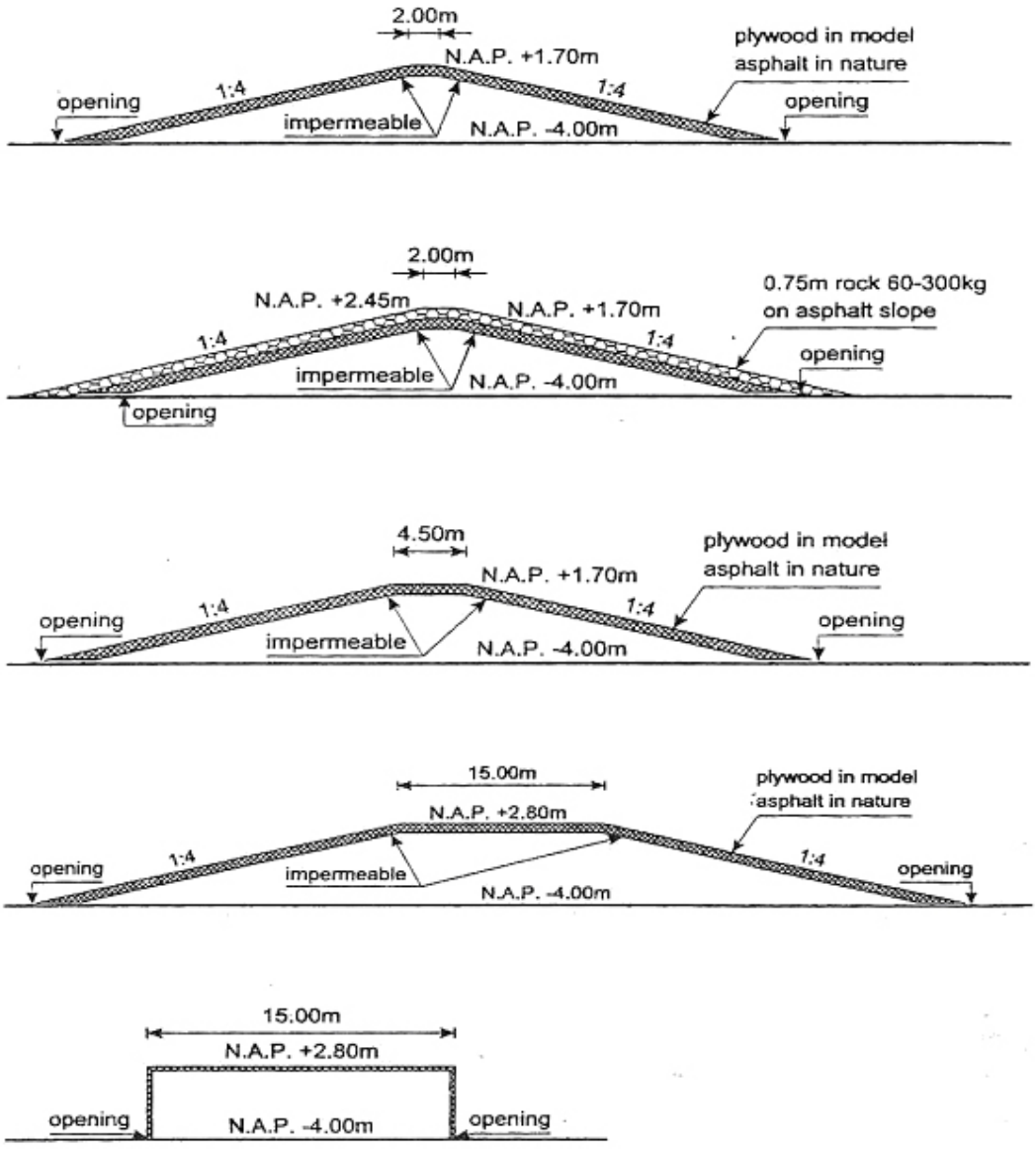


**Figure 3.6. – Experimental installation scheme used by van der Meer et al. (2000)**

while, for the mean spectral period, the Authors propose to use the following relationship:

$$T_m = T_{02} = \left(\frac{m_0}{m_2}\right)^{0.5} = \left(\frac{\int_0^\infty E(f)\,df}{\int_0^\infty f^2 E(f)\,df}\right)^{0.5} \qquad [3.32]$$

The relationship among the transmitted wave heights and incident wave height (coefficient of transmission) is expressed, in terms of spectral moments as:

$$k_t = \sqrt{\frac{\left(m_0\right)_t}{\left(m_0\right)_i}} \qquad [3.33]$$

In the Fig. 3.7 and 3.8 are shown the relationships among the peak period of the transmitted wave to back of the barrier and the incident wave, in function of the coefficient of transmission. Is is evident that the interaction wave-barrier doesn't involve a substantial alteration of the peak period, for all the types of structure examined.

The, contrarily, is modified in the interaction with the barrier, and, in particular, because of the distribution of energy on the high frequency, at the back of the structure, takes smaller values. For coefficients of transmission greater than 0.15 the relationship among the mean spectral period to back and to front of the structure seems to reach a constant value around 0.62.

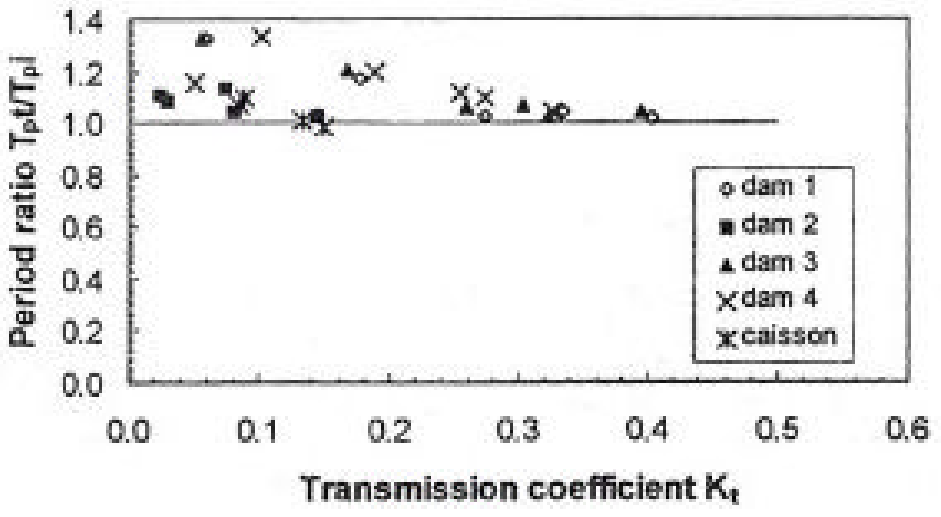


**Figure 3.7. – Relationship between peak period of incident and transmitted wave by Van der Meer et al (2000)**

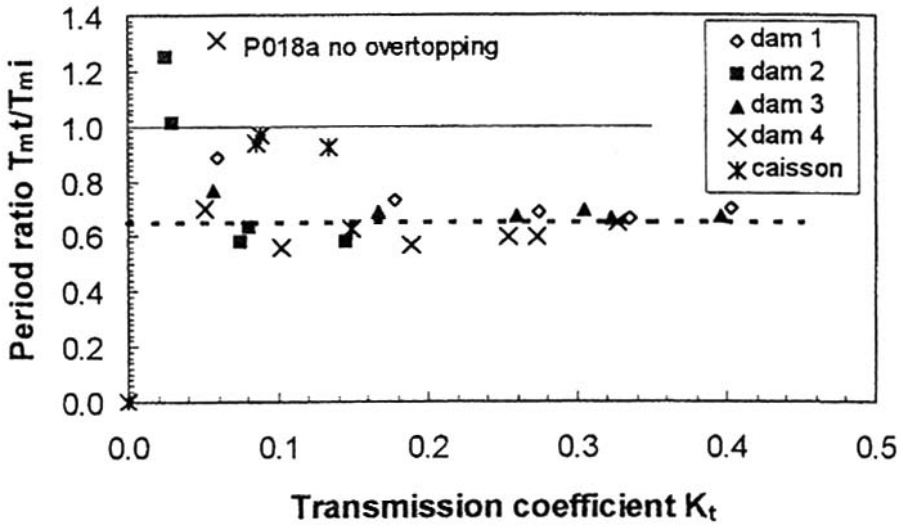


**Figure 3.8. – Relationship between mean spectral period of incident and transmitted wave by Van der Meer et al (2000)**

On the base of the effected observations, the Authors propose a method to represent the transmitted spectra, based on the form of the incident spectra and on the coefficient of transmission $k_t$. The method is based on the observation that, pointing out with $f_p$ the peak frequency, the spectra measured to back of the structure, shows, generally, a constant contents of energy in the interval [1.5 $f_p$, 3.5 $f_p$] in which is distributed about 40% of the total wave energy. Generalizing the result, and assuming the value 1.5 $f_p$ as representative of the limit between "high" and "low" frequency, the spectra proposed by the Authors for the transmitted wave introduces same form of the incident spectra for smaller frequencies to 1.5$f_p$ and a constant density for frequencies between 1.5$f_p$ and 3.5$f_p$; the energetic content of this last part of the spectra, that contains the contribution of the most elevated frequencies, is equal to the 40% of the total energy of the transmitted wave, valued on the base of the coefficient of transmission.

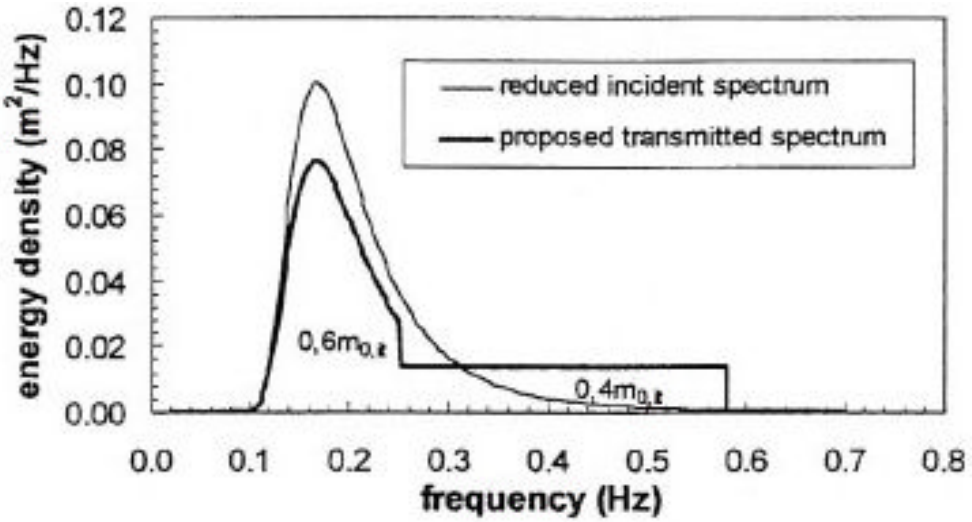


**Figure 3.9. – Spectral shape of transmitted wav proposed by Van der Meer et al (2000)**

The experimental work of Black & Oumeraci, 2001 , likewise to that examined in the previous paragraph, is based on the modifications of the spectral characteristics of the wave motion induced by the presence of a submerged barrier. The tests have been conducted in presence of impermeable rectangular obstacle with different values of height (h=0.40 m, 0.50 m, 0.60 m) and width (B=0.5 m, 1.0 m); the depth of the channel has been maintained constant, and equal to 0.70 m.

The scheme of the experimental installation is illustrated in Fig. 3.10. During the tests have been reproduced regular and irregular wave conditions, with JONSWAP type spectra. Significant wave height and peak period are reported in tab. 3.1.

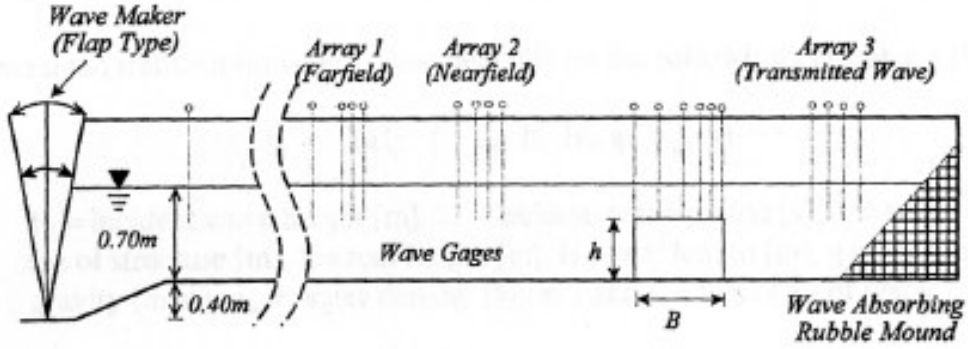


**Figure 3.10. – Experimental installation scheme used by Bleck & Oumeraci (1999)**

| | $T_p$ (s) | | | | | | | | |
|---|---|---|---|---|---|---|---|---|---|
| $H_s$ (cm) | 1.1 | 1.5 | 2.0 | 2.5 | 3.0 | 3.5 | 4.0 | 4.5 | 6.0 |
| 8.0 | x | x | x | x | x | x | x | x | x |
| 12.0 | x | x | x | x | x | x | x | x | |
| 16.0 | x | x | x | x | x | x | | | |
| 20.0 | x | x | x | x | x | | | | |

**Tab 3.1. – Wave conditions used by Bleck & Oumeraci (1999)**

For the computation of the mean spectral period the Authors have used the following relationships:

$$T_{01} = \frac{m_0}{m_1} = \frac{\int_0^\infty E(f)\,df}{\int_0^\infty fE(f)\,df}$$
$$T_{-10} = \frac{m_{-1}}{m_0} = \frac{\int_0^\infty f^{-1}E(f)\,df}{\int_0^\infty E(f)\,df} \qquad [3.34]$$

Both the periods are calculated by the average of the frequencies of the spectral distribution, weighted for the respective density of energy; the period $T_{01}$ mainly take in count the effect of the higher frequencies, while the period $T_{-10}$ mostly take in count the contributions of the lower frequencies. As previously observed, the transmitted spectra has, in comparison to the spectra of the incident wave, a lower energetic content and a different

shape, because of the transfer of energy to the higher harmonics (Fig. 3.11). The analysis of the experimental results has conducted to the proposal of the following regression formula, that ties the value of the coefficient of transmission to the relationship among her depth above the obstacle ($d_r$) and the height of the incident wave.

$$k_t = 1.0 - 0.83e^{\left(-0.72\frac{d_r}{H_i}\right)} \qquad [3.35]$$

The formula [3.35] show a good correlation with the experimental data, despite not takes in count the width of the obstacle, that also influence, transmission of the wave motion in the protected area.

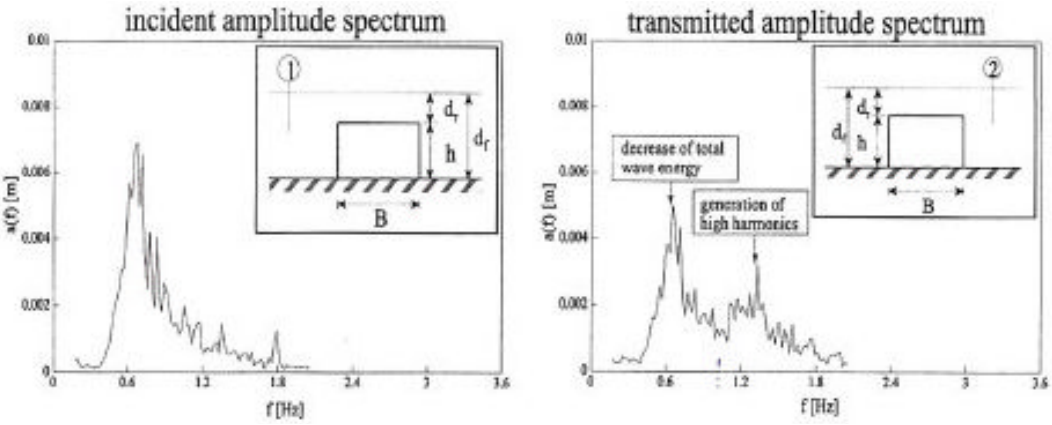


**Figure 3.11. – Comparison between incident and transmitted amplitude spectra by Bleck & Oumeraci (1999)**

# CHAPTER 4

## 4.1 2D Large WaveFlume Experiment At GWK

Within the European Community funded program "Access to Research Infrastructures action of the Human Potential" attention has been given to low crested/submerged breakwaters located on shallow foreshores. This because despite these kind of structures are frequently placed in the nearshore, very little studies are until now available about their performances under pre-breaking to post-breaking wave conditions. The large scale tests were carried out at LARGE WAVE CHANNEL (GWK) of the Coastal Research Centre (FZK), Hannover, Germany.

**Test facility**

The model tests were carried out at the "Grosser WellenKanal " of Hannover, Germany. The wave flume has a lenght of 300 m, a width of 5 m and a depth of 7 m. The facility is equipped with a piston type paddle for generating regualr and random waves. The installed power of the piston type wave generator combined with an upper flap is about 900 kW. The gearwheel driven carrier gives a maximum stroke of ± 2.10 m to the wave paddle. The stroke can be superimposed by upper flap movements of ± 10 degree in order to simulate natural water wave kinematics most accurately. A large cylinder integrated in the carrier compensates the water force in front of the paddle (rear is free of water). The wave generation is controlled by an online absorption system. This special system works with all kinds of regular and irregular wave trains. Thus, the tests are unaffected by re-reflections at the wave generator and can be carried out over nearly unlimited duration (Fig. 4.1).

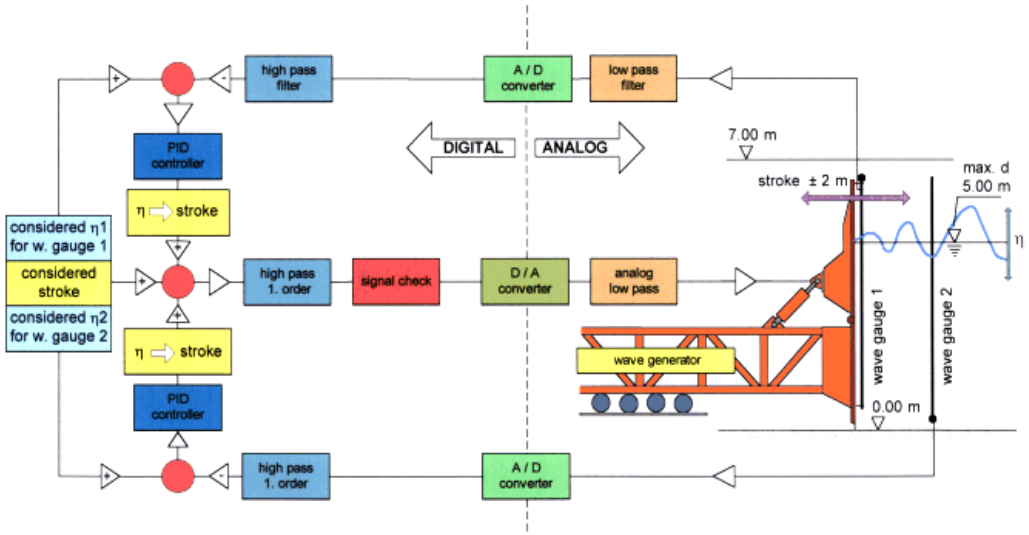


**Figure 4.1. Online Absorption Control System for the Wave Generator of the Large Wave Channel**

## Model set-up and instrumentation

The bathymetry in the flume was formed by moulding sand over fill in the channel to the required shape. From deep water near the paddle, the seabed was flat for 105.3 m than it sloped initially at 1:20 for 20 m to change for a more gentle slope of 1:50, and terminated in a 15 m horizontal section. The bed level at the test structure was + 3 m relative to the flume floor at the wave paddle. To minimize effects of any reflection from the end of the flume, an absorbing sand beach with 1:18 slope was built (Fig. 4.2 and 4.3).

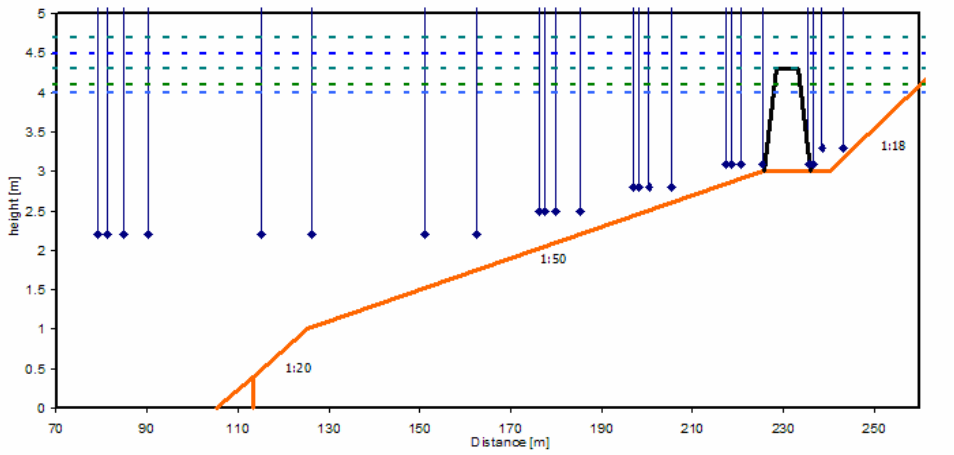


**Figure 4.2. Seabed profile, wave probes position and five different tested s.w.l.**

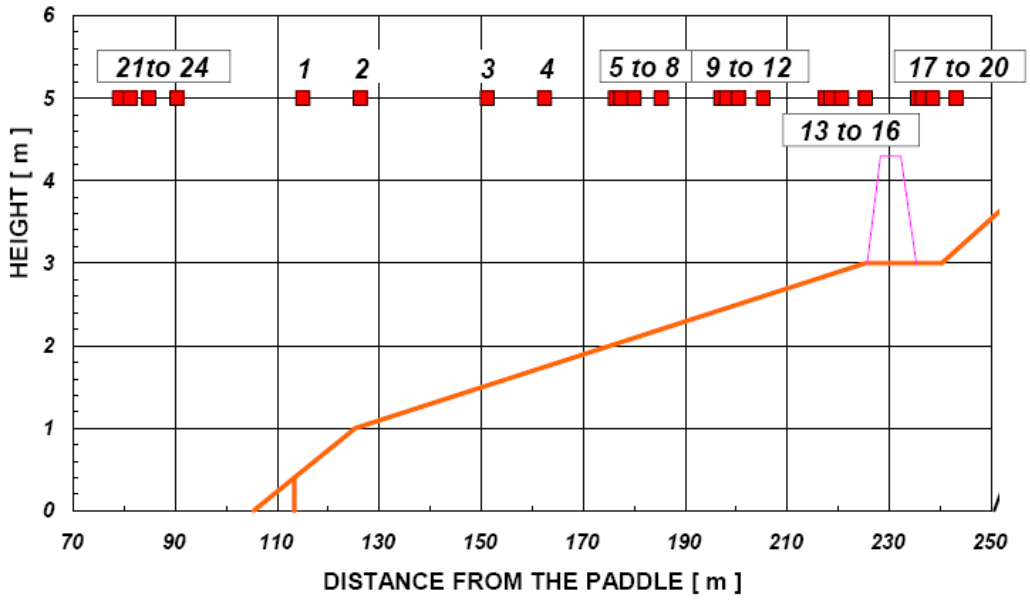


**Figure 4.3. Wave probes position.**

A 1.3 m high rubble mound breakwater was installed on a flat area at the end of 1:50 sand beach.

Three different cross sections were tested (Fig. 4.4):

1. 1 m berm width, with an impermeable sheet in the middle of the structure;
2. 1 m berm width, without impermeable sheet in the middle of the structure;
3. 4 m berm width, without impermeable sheet in the middle of the structure.

The impermeable sheet was located during the installation of cross section a) for a better understanding of permeability effects on hydraulic performance of low crested and no freeboard breakwater (Fig. 4.5). Afterward the cross section b) was obtained removing the sheet by lifting it up. In this way there was no modification of the cross section shape (Fig. 4.6).

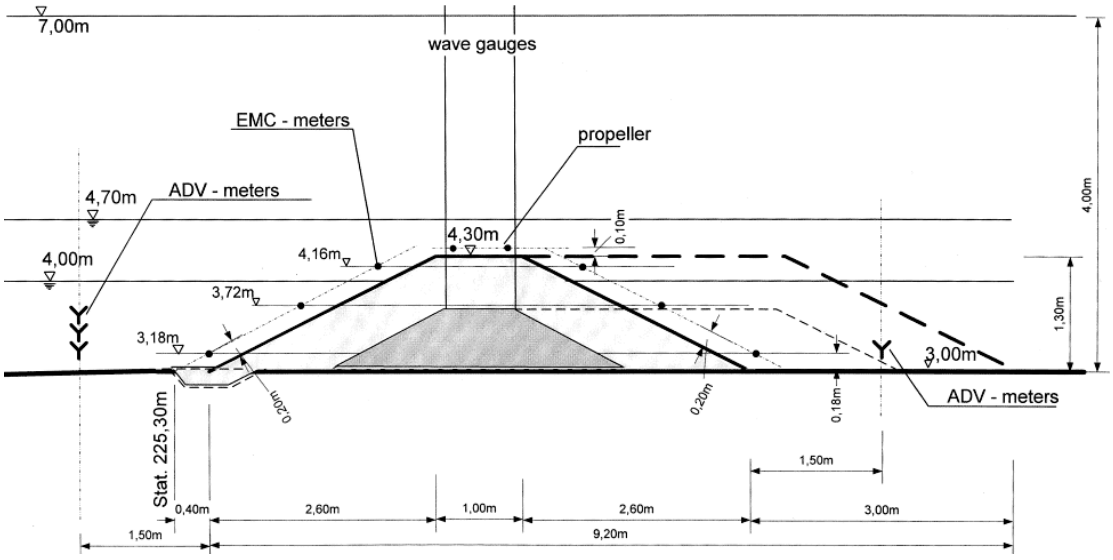


**Figure 4.4. Structure configurations and instruments**

**Figure 4.5. Structure installation with an impermeable sheet in the middle**

**Figure 4.6. Removal of impermeable sheet from middle of structure**

Two different type of armour rock were used as material for the rubble mound model, Normal Density Rock (armour layer) and High Density Rock (core). Both types were supplied by NCC Industries Norway. The High Density Rock came from NCC quarry at Valberg, Kragerø Norway, the Normal Density Rock came from NCC quarry at Skien, Norway. For both rock types two samples from the breakwater model were weighed and measured to determine statistical data for each type. The following Table 1 and 2 summarises technical data for the Normal Density Rock (NDR) and High Density Rock (HDR) and it was performed by Einar Helgason (Hydraulic and Coastal Engineering Laboratory Aalborg University).

| Description of quarry | Skien Quarry, Skien, 100 km south of Oslo, Norway | | |
|---|---|---|---|
| Rock type | Granitites Gneiss | | |
| Properties | Standard testing | Value | Note |
| Particle density | prEN 1097-6, B | - | |
| Rock density | | app. 2.65 | |
| Water absorption | prEN 1097-6, B | - | Not measured |
| Shape | CIRIA A1.5 | - | Thickness : Length |
| Block integrity | CIRIA A2.11 | - | Drop test breakage |

| | | | |
|---|---|---|---|
| Compressive strength | prEN 1926, A | - | No data available |
| Resistance to freezing and | prEN 1367-1, B | 0,2 % | Estimated |
| Resistance to salt crystallisation | prEN 1367-2 | - | Not measured |

**Table 4.1. Technical data for the Normal Density Rock (NDR).**

| Description of quarry | Valberg Quarry, Kragerø, 200 km south of Oslo, Norway | | |
|---|---|---|---|
| Rock type | Gabbro | | |
| Properties | Standard testing | Value | Note |
| Particle density | prEN 1097-6, B | 3.05 ±0.05 | |
| Rock density | | 2.98 – 3.02 | |
| Water absorption | prEN 1097-6, B | 0.12 ±0.05 % | |
| Shape | CIRIA A1.5 | < 5 % | Thickness : Length |
| Block integrity | CIRIA A2.11 | < 5 % | Drop test breakage |
| Compressive strength | prEN 1926, A | 150 ±50 MPa | |
| Resistance to freezing and | prEN 1367-1, B | 0,5 % | |
| Resistance to salt crystallisation | prEN 1367-2 | 1.0 ±0.2 % | |

**Table 4.2. Technical data for the High Density Rock (HDR).**

Weight distribution was obtained using two samples from the breakwater model in GWK of 1.5 x 1.5m where weighted and measured.

The grading is calculated as the ratio between the 85 percent and 15 percent value as:

$$\frac{D_{85}}{D_{15}} = 1.51 \quad \text{(NDR)}$$

$$\frac{D_{85}}{D_{15}} = 1.59 \quad \text{(HDR)}$$

From the measured weight the nominal diameter is calculated as:

$$D_n = \left( \frac{W}{\rho_a} \right)^{1/3} \quad [4.1]$$

where W is the weight and $\rho a$ denotes the density. Statistics for weighing is reported in Figure 4.7 and 4.8 it gave the following results:

*Armour layer*

- $W_{50}$ = 30.4 kg, $W_{15}$ = 16.2 kg, $W_{85}$ = 55.7 kg (NDR)
- $D_{50}$ = 22.5 cm, $D_{15}$ = 18.3 cm, $D_{85}$ = 27.6 cm (NDR)

*Core*

- $W_{50}$ = 19.0 kg, $W_{15}$ = 11.0 kg, $W_{85}$ = 42.0 kg (HDR)
- $D_{50}$ = 18.4 cm, $D_{15}$ = 15.3 cm, $D_{85}$ = 24.5 cm (HDR)

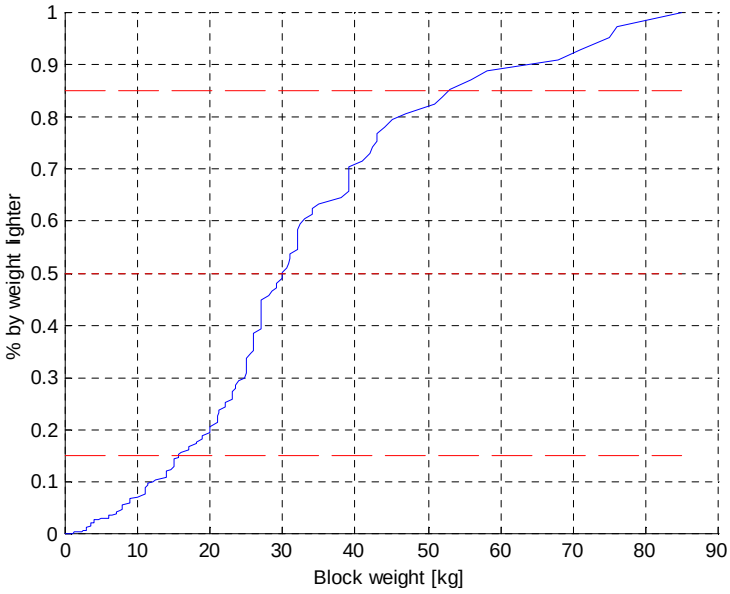


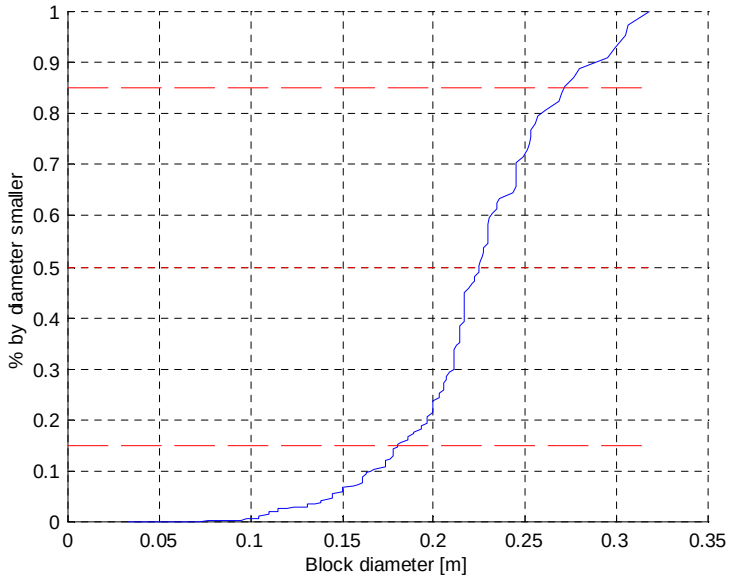


**Figure 4.7. Statistics for weighing for NDR**

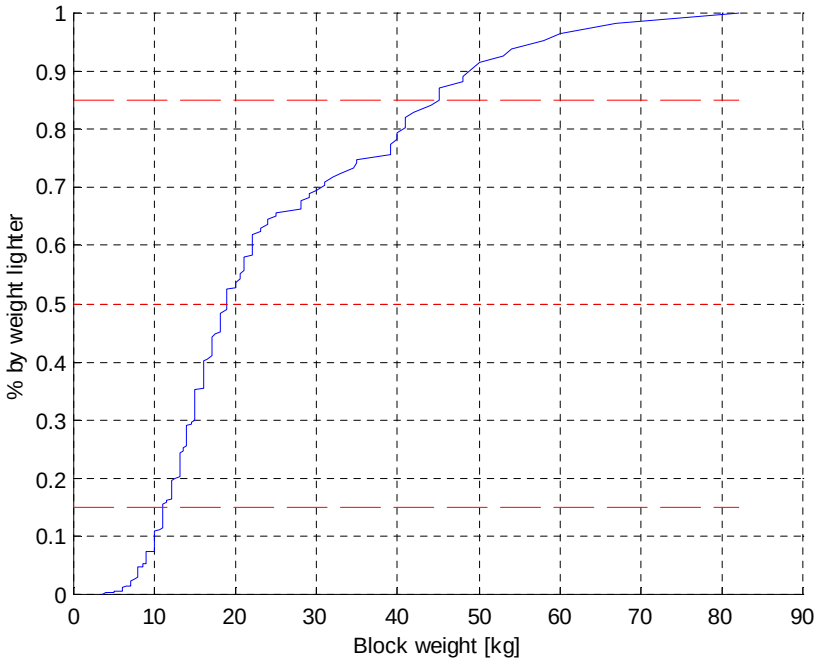


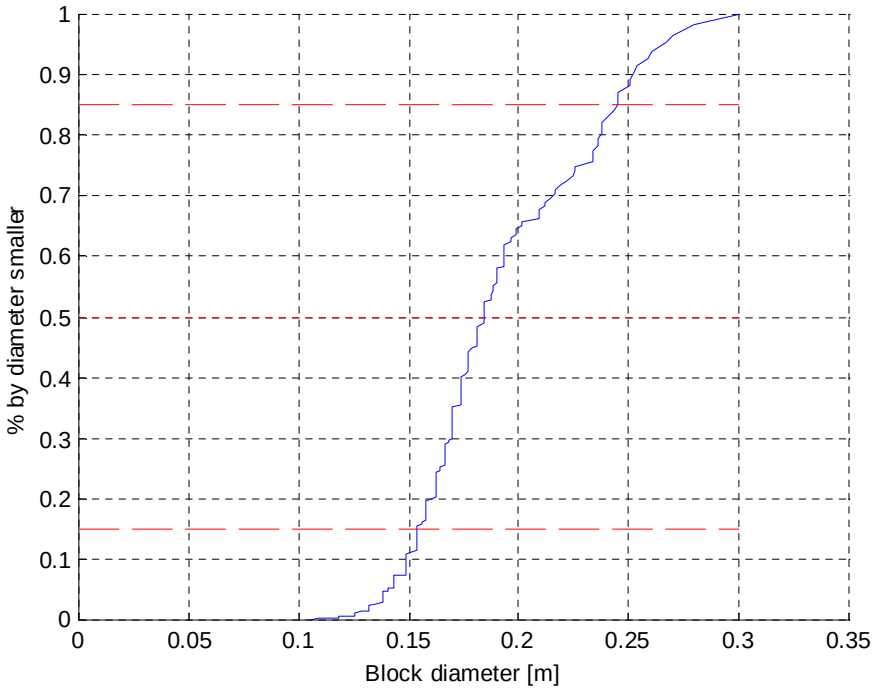


**Figure 4.8. Statistics for weighing for HDR**

Rubble mound front and rear slopes were kept constant, equal to 1:2. Five s.w.l. have been changed in order to obtain different configurations ranging from low crested to submerged.

To measure the wave characteristics, a set of 27 probes was sampled at 50 Hz (Figure 4.2). Wave velocities were measured using the following instruments supported by Coastal Research Centre:

- a set of 4 ADV (Acoustic Doppler Velocity-meter), 3 placed 1.5 m in the front and 1 located 1.5 m at the rear side of the structure, only for the cross section c) there was an extra ADV supported by UoB;
- a set of 6 EMC (Electro Magnetic Currentmeter), 3 placed on the front slope and 3 on the back slope of the structure;
- 2 propellers were placed on the top of the berm;
- 1 seabed profiler mounted on a movable carriage.

All the velocimeters were sampled at 50 Hz with the exclusion of UoB's ADV that it sampled at 100Hz.

## Calibration and model test programm

*TMA* spectra were run giving wave conditions at the structure variable from shoaling to post-breaking (Tab.4.3). Each test was preliminary run (at least for 500 waves) without the structure, in order to achieve reliable estimates of incident wave parameters, $H_{moi}$ and $T_{pi}$.

| Test | $h$ (m) | $H_{mo}$ (m) | $T_p$ (s) | $R_c$ (m) | $B$ (m) | Test | $h$ (m) | $H_{mo}$ (m) | $T_p$ (s) | $R_c$ (m) | $B$ (m) |
|---|---|---|---|---|---|---|---|---|---|---|---|
| 1 | 1 | 0.6 | 3.5 | 0.3 | 1 | 25 | 1.3 | 0.6 | 3.5 | 0 | 4 |
| 2 | 1 | 0.8 | 4.5 | 0.3 | 1 | 26 | 1.3 | 0.8 | 4.5 | 0 | 4 |
| 3 | 1 | 0.9 | 4.5 | 0.3 | 1 | 27 | 1.3 | 1 | 4.5 | 0 | 4 |
| 4 | 1 | 1 | 4.5 | 0.3 | 1 | 28 | 1.3 | 1 | 6.5 | 0 | 4 |
| 5 | 1 | 1 | 6.5 | 0.3 | 1 | 29 | 1.5 | 0.6 | 3.5 | -0.2 | 1 |
| 6* | 1 | 0.6 | 3.5 | 0.3 | 1 | 30 | 1.5 | 0.8 | 4.5 | -0.2 | 1 |
| 7* | 1 | 0.8 | 4.5 | 0.3 | 1 | 31 | 1.5 | 1 | 4.5 | -0.2 | 1 |
| 8 | 1.1 | 0.6 | 3.5 | 0.2 | 1 | 32 | 1.5 | 1 | 6.5 | -0.2 | 1 |
| 9 | 1.1 | 0.8 | 4.5 | 0.2 | 1 | 33 | 1.5 | 1.1 | 6.5 | -0.2 | 1 |
| 10 | 1.1 | 1 | 4.5 | 0.2 | 1 | 34 | 1.5 | 0.6 | 3.5 | -0.2 | 4 |
| 11 | 1.1 | 1 | 6.5 | 0.2 | 1 | 35 | 1.5 | 0.8 | 4.5 | -0.2 | 4 |
| 12* | 1.1 | 0.6 | 3.5 | 0.2 | 1 | 36 | 1.5 | 1 | 4.5 | -0.2 | 4 |
| 13* | 1.1 | 0.7 | 4.5 | 0.2 | 1 | 37 | 1.5 | 1 | 6.5 | -0.2 | 4 |
| 14* | 1.1 | 0.8 | 4.5 | 0.2 | 1 | 38 | 1.5 | 1.1 | 6.5 | -0.2 | 4 |
| 15* | 1.1 | 0.9 | 4.5 | 0.2 | 1 | 39 | 1.7 | 0.6 | 3.5 | -0.4 | 1 |
| 16 | 1.3 | 0.6 | 3.5 | 0 | 1 | 40 | 1.7 | 0.8 | 4.5 | -0.4 | 1 |
| 17 | 1.3 | 0.8 | 4.5 | 0 | 1 | 41 | 1.7 | 1 | 4.5 | -0.4 | 1 |
| 18 | 1.3 | 0.9 | 4.5 | 0 | 1 | 42 | 1.7 | 1 | 6.5 | -0.4 | 1 |
| 19 | 1.3 | 1 | 4.5 | 0 | 1 | 43 | 1.7 | 1.1 | 6.5 | -0.4 | 1 |
| 20 | 1.3 | 1 | 6.5 | 0 | 1 | 44 | 1.7 | 0.6 | 3.5 | -0.4 | 4 |
| 21* | 1.3 | 0.6 | 3.5 | 0 | 1 | 45 | 1.7 | 0.8 | 4.5 | -0.4 | 4 |
| 22* | 1.3 | 0.7 | 4.5 | 0 | 1 | 46 | 1.7 | 1 | 4.5 | -0.4 | 4 |
| 23* | 1.3 | 0.8 | 4.5 | 0 | 1 | 47 | 1.7 | 1 | 6.5 | -0.4 | 4 |
| 24* | 1.3 | 0.9 | 4.5 | 0 | 1 | 48 | 1.7 | 1.1 | 6.5 | -0.4 | 4 |

* Tests with an impermeable sheet in the middle of the cross section.

# CHAPTER 5

# Data analysis and results

## 5.1 Linear and nonlinear transformations

As ocean surface gravity waves propagate toward the shore in shoaling waters, they undergo substantial evolution from their deep-water state. In the shoaling waters, linear and nonlinear processes act simultaneously to transform the wave characteristics. Changing bottom topography causes refraction and shoaling of the wavefield, which result in spatial variations in the amplitudes and directions. Although linear theory predicts the observed increasing wave amplitudes and narrowing directional distributions of swell and sea waves in a qualitative sense, nonlinear effects are important. Nonlinear evolution can alter the spectral (frequency-direction) characteristics of the wavefield as well as the wave profiles. Initially symmetric wave profiles and oscillatory velocities become asymmetric and skewed. In addition, phase speeds substantially differ from those predicted by the linear dispersion relationship.

As waves travel from deep to shallow water, the dispersion characteristics of the wavefield play an important role in the mechanism of the nonlinear wave interactions. Three regions of different dispersion characteristics can be distinguished. In deep water (relative depth $kh >> 0(1)$, where k is a characteristic wavenumber and h the water depth), the wavefield undergoes strong frequency dispersion. Strong frequency dispersion is the dependency of phase speed c on frequency w (deep-water waves $c=g/w$, where g is the gravitational acceleration). In this region, the dispersion characteristics permit resonant interactions among quartets of waves to occur, resulting in slow cross-spectral energy transfers. Although energy exchanges due to these cubic nonlinearities are very small on wavelength scales, the wave spectrum is substantially modified over hundreds of wavelengths (Hasselmann, 1962).

In very shallow water (kh 1, a condition approximately satisfied by wind waves within the surf zone), waves are almost nondispersive (shallow-water waves c=/gh). Near-resonant interactions among triads of waves occur, resulting in rapid spectral evolution.

In intermediate depths (kh= 0(1)), between the deep-water region with strongly dispersive waves and the shallow-water region with nondispersive waves, waves are weakly dispersive (c= $(g/c_o)$tanh kh) and undergo substantial changes caused by the off-resonant energetic triad interactions. Triad interactions drive rapid spectral evolution over several (rather than hundreds of) wavelengths.

### 5.1.1 Non linear triad wave interaction

In the shoaling region, the short evolution distance and moderate dispersion suggest that second-order (quadratic) nonlinearities involving triads of waves are important. triad interactions occur among waves with frequencies and wavenumbers such that:

$$f_1 \pm f_2 = f_3 \qquad [5.1]$$

$$k_1 \pm k_2 = k_3 \qquad [5.2]$$

where f and k are the scalar frequency and vector wavenumber, respectively.

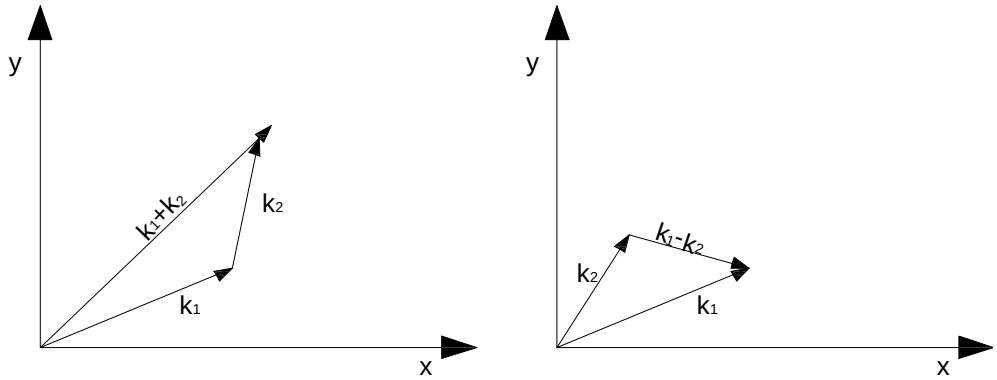


**Figure 5.1. – Wavenumber vectors of triad interactions (a): sum interaction, (b): difference interaction**

The wave components ($f_1$,$k_1$) and ($f_2$,$k_2$) each satisfy the linear dispersion relation:

$$\omega^2 = gk \tanh\left(kh\right) \qquad [5.3]$$

in which k is the wavenumber magnitude. The physical meaning of [5.1] and [5.2] is that the sum (or difference) interaction between wave components 1 and 2 forces motions with the scalar-sum (or difference) frequency and the vector-sum (or difference) wavenumber (Fig. 5.1). If component 3 satisfies the linear dispersion relation [5.3] then the interaction is resonant (Armstrong et al., 1962) implying a continued one-way transfer of energy to component 3. Note that for gravity surface waves this is only possible in very shallow water where the waves are non dispersive. In fact theories for weakly nonlinear wind-generated surface gravity waves show that the nonlinear triad interactions do not support resonances (e.g. Phillips, 1960; Hasselman, 1962). If component 3 does not satisfy the linear dispersion relation [5.3] then the interaction is non-resonant (in intermediate depths where waves are weakly dispersive) and the transfer is back-and-forth because of the mismatch in the phase speed.

The intensity of the triad interactions is mainly controlled by the phase mismatch. The difference between the so-called bound wavenumber given by $k_1 \pm k_2$ and the free wavenumber obtained from the linear dispersion relation $k(f_3)$ represents the wavenumber mismatch:

$$\Delta_k = \left|k_1 \pm k_2\right| - \left|k\left(f_3\right)\right| \qquad [5.4]$$

The normalized wavenumber mismatch:

$$\delta_k = \Delta_k \Big/ \left|k\left(f_3\right)\right| \qquad [5.5]$$

is a measure of the departure from exact resonance. Its magnitude determines the intensity of energy exchanges between the interacting waves. Zero mismatch (nondispersive shallow-water waves) represents the limiting case in the interaction process, in which the interacting waves remain intact and in phase (resonant interaction) during evolution. Thus, the magnitude of energy transfer is maximum and a continued one-way transfer takes place to the harmonics over relatively short evolution distance. When the mismatch $\delta_k << 1$ (weakly dispersive shoaling waves), phase relations

between the interacting waves vary slightly over a wavelength. Consequently the magnitudes and the sign of energy transfers between the interacting waves vary slowly over a wavelength, allowing significant net energy transfers over several wavelengths. Large values of the mismatch (strongly dispersive deep-water waves), imply that phase relations between interacting waves vary rapidly over a wavelength, not allowing for significant energy transfers.

It is common practice to distinguish between the sum and difference interactions. In shallow water, the sum interactions between the primary waves at the energetic part of the spectrum (with peak frequency $f_p$) lead to the generation of harmonics around a frequency 2f (first harmonic of the primary). Eventually, the sum interactions between the primary waves near $f_p$ and the first harmonics at $2f_p$ give rise to harmonics near $3f_p$. The difference interactions between primary waves within the energetic part of the spectrum lead to the generation of bound long waves.

## 5.2 Bispectral analysis of water waves

In this section, aspects of nonlinear dynamics of waves propagating in shallow water and aver obstacle are investigated using the bispectral analysis. Since its introduction, the bispectrum has been used extensively to examine nonlinearity in shoaling surface gravity waves. The purpose of this chapter is to gain more understanding and physical insight in the nonlinear transformation of wave spectra in shallow water and aver obstacle with aid of the bispectral analysis.

### 5.2.1 The bispectrum

The bispectrum was introduced by Hasselmann et al. (1963) to examine wave nonlinearity in intermediate water depths. Since its introduction, bispectral analysis has been used to study nonlinear phenomena in a wide variety of fields such as seismic action (Haubrich, 1965), fluid turbulence (Yeh and Van Atta, 1973), plasma fluctuations (Kim and Powers, 1979) and deep-water surface gravity waves (Masudo and Kuo, 1981b). Recently, it has been used extensively to examine nonlinearity in shoaling surface gravity waves (Elgar and Guza, 1985b; Herbers and Guza, 1992).

The sea surface elevation can be represented using spatially varying Fourier components, in which the time variation can be factored out (assuming time periodicity) as follows:

$$\varsigma\left(x,t\right) = \sum_{p=-\infty}^{\infty} C_p\left(x\right)\exp\left[-i\left(\omega_P t\right)\right] \qquad [5.6]$$

where $\omega_p$ is the radian frequency (=$2\pi$f), p is the rank of the harmonic, $C_p$ is the complex Fourier amplitude varying with position x.

For a Gaussian sea, the sea surface can be represented as a superposition of statistically independent waves in which the phases are random. Consequently the sea surface can be fully described by the continuous energy spectrum, which is defined as the Fourier transform of the second-order correlation function R($\tau$) of the time series,

$$E\left(\omega\right) = \frac{1}{2\pi}\int_{-\infty}^{\infty} R\left(\tau\right)\exp\left(-i\omega\tau\right)d\tau \qquad [5.7]$$

where R($\tau$) is given by

$$R\left(\tau\right) = \left\langle \zeta\left(t\right)\zeta\left(t+\tau\right)\right\rangle \qquad [5.8]$$

in which $\tau$ is a time lag, and < > denotes the expected-value, or average, operator. Note that the spectral energy density function E($\omega$) is defined for positive and negative frequencies.

For discretely sampled data, the discrete energy spectrum $E_p$ can be represented in terms of Fourier amplitudes,

$$E_p = \left\langle C_p \; C_p^* \right\rangle \qquad [5.9]$$

where C is the complex conjugate amplitude of $C^*$. The discrete energy spectrum $E_p$ is related to the continuous one by $E_p = E\left(\omega\right)\Delta\omega \quad \text{for} \quad \omega \cong \omega_p$, in which $\Delta\omega = 2\pi\Delta f$ is the angular frequency v band. The energy spectrum [5.9] is independent of the phases. If the phases of Fourier components are not random and statistically correlated, the sea surface is not Gaussian (Hasselmann et al., 1963). Departure from a Gaussian form cannot be detected by the energy spectrum. Higher-order spectra such as the bispectrum can be used to investigate nonlinearity in shallow-water waves. It is a complex quantity, formally defined as the Fourier transform of the third-order correlation function of the time series:

$$B\left(\omega_1, \omega_2\right) = \left(\frac{1}{2\pi}\right)^2 \int_{-\infty}^{\infty} \int R\left(\tau_1, \tau_2\right) \exp\left[-i\left(\omega_1\tau_1 + \omega_2\tau_2\right)\right] d\tau_1 d\tau_2 \qquad [5.10]$$

In which

$$R(\tau_1, \tau_2) = \left\langle \eta\left(t\right)\eta\left(t+\tau_1\right)\eta\left(t+\tau_2\right)\right\rangle \qquad [5.11]$$

The digital (discrete) bispectrum, for discretely sampled data, is (Haubrich, 1965; Kim and Powers, 1979)

$$B_{l,m} = \left\langle C_l C_m C_{l+m} \right\rangle \qquad [5.12]$$

in which l and m are the frequency indices. The digital bispectrum for discretely sampled data can be estimated from [5.12] by ensemble averaging. It relates to a triad of waves with frequency indices 1, m and l+ m.

The bispectrum $B_{l,m}$ vanishes if:

1. There is no energy present at frequencies l or m or l+m (i.e., zero Fourier amplitude of any component participating in the triad interactions);

2. There is no phase relation (coherence) between the waves forming the triad (i.e., statistically independent free waves).

On the other hand, if the wave at (n=l+m) is generated through the interaction between l and m, then a phase coherence will exist and the expected value of the bispectrum will be nonzero.

The bispectrum can be efficiently computed using symmetry properties, in which it can be uniquely described by its values in a bi-frequency octant. For a digital time series with Nyquist frequency $f_N$, the bispectrum is uniquely defined within a triangle in ($f_1$, $f_2$) space (bi-frequency plan) with vertices at (1=0, m=0), (1=$f_N$, m=0), and (l=$f_{N/2}$, m=$f_{N/2}$).

The bispectrum can be used to identify coupled modes, however it does not give a qualitative measure of the intensity of nonlinear interactions cince its value depends on the amplitudes of the three waves involved in the interaction. It is convenient to cast the bispectrum into its normalized magnitude and phase, the so-called bicoherence and biphase.

### 5.2.2 Skewness and asymmetry

The so-called skewness and asymmetry of the sea surface are profile distortions caused by the presence of bound harmonics due to nonlinear interactions. The so-called skewness is the lack of symmetry with respect to the horizontal. Skewed profiles of gravity water waves are characterized by sharp crests and flat troughs (Stokes-type wave), in which the harmonics are phase-locked and in phase with the primary. The name derives from the fact that the probability density function of these profile is skewed. On the other hand, the asymmetry is the lack of symmetry with respect to the vertical. Asymmetric profiles are usually characterized by steep forward fronts and mild rear faces (nearly saw-toothed shape), in which the harmonics are phase-locked and leading the primary. The skewness of a random variable (a) is conventionally defined as its normalized third central moment:

$$S = \frac{\left\langle \underline{x} - \mu_x \right\rangle}{\sigma_x^3} \qquad [5.13]$$

The mean square, or the variance of the surface elevation can be recovered from the integral of the energy spectrum, i.e. (using the discrete form)

$$\left\langle \eta^2(t) \right\rangle = \sum_{p=-\infty}^{\infty} E_p \qquad [5.14]$$

Hasselmann et al. (1963) showed that the integral over the real part of the bispectrum recovers the mean cube, or third-order moment of the surface elevation:

$$\left\langle \eta^3(t) \right\rangle = \sum_{l=-\infty}^{\infty} \sum_{m=-\infty}^{\infty} \mathrm{Re}\left\{ B_{l,m} \right\} \qquad [5.15]$$

The skewness or the nondimensional mean cube of the surface elevation can be obtained by normalizing [5.15] by the variance to the power 3/2:

$$S = \frac{\left\langle \eta^3(t) \right\rangle}{\left\langle \eta^2(t) \right\rangle^{3/2}} \qquad [5.16]$$

Similarly, the asymmetry of the surface elevation can be obtained from the integral over the imaginary part of the bispectrum after normalization with the variance to the power 3/2:

$$A = \frac{\sum_{l=-\infty}^{\infty} \sum_{m=-\infty}^{\infty} \mathrm{Im}\left\{ B_{l,m} \right\}}{\left\langle \eta^2(t) \right\rangle^{3/2}} \qquad [5.17]$$

The skewness and asymmetry represent overall measures of nonlinearity and indicate the departure of the wave profile statistics from the Gaussian

distribution. These parameters are used in the analysis of data presented in the following sections.

**Bispectral evolution of waves**

Observations of shoaling waves are analyzed to elucidate the phenomenon of harmonic generation in the region back to submerged breakwater. The objectives of these analyses are to determine the significant interactions that lead to harmonic generation and the influence of wave breaking on the intensity of nonlinear couplings.

## 5.3 Analysis and results

For the purpose of this work only submerged barrier conditions have been take in count. Referring to Tab. 4.3 only tests from 25 to 34, from 43 to 46 and from 51 to 56 will be used. The surface elevation spectra are shown in Fig. 3.2. In the breakwaters regions, strong energy transfers occur from the primary to the higher harmonics. In shallow water over the obstacle, wave breaking takes place leading to reduction of the total energy.

The bispectra are computed according to equation [5.10], in which the complex Fourier amplitudes $A_p$ were determined from the time records with a standard FFT-algorithm. The data were processed by dividing the record into equal segments, each of 20 seconds duration resulting in a frequency resolution for the raw data of 0.002 Hz. The bispectral estimates are obtained by ensemble averaging over all segments. Therefore the number of degrees of freedom in the estimates is variable.

Absolute values of the continuous bispectra (bicoherence computed using equation [5.10]) for gauge 18 are given from Figure. 5.2 to 5.21, where only the positive quadrants $f_2>0$) are shown. Note that the bispectra are symmetric around the diagonal $f_1 = f_2$.

The bicoherence is shown in panel (b) of Figure 5.2 in which a bispectral peak exists at (0.28 Hz, 0.28 Hz). This peak indicates the self-interaction of the primary at 0.28 Hz with itself leading to the first harmonic at 0.56 Hz, according with power spectra shown in panel (a). In Figure 5.3 are shown three bispectral peak; the first at $f_1=f_2=0.22$ Hz that indicates the self-interaction of the primary at 0.22 Hz with itself leading to the first harmonic at 0.44 Hz; the second one at $f_1=f_2=0.44$Hz that indicates the self-interaction of the second harmonic at 0.44 Hz with itself leading to the forth harmonic at 0.88 Hz. The third peak indicates a phase coupling between first harmonic at 0.22 Hz and third harmonic at 0.66 Hz. In Figure 5.4 are shown a self interacting bispectral peak at $f_1=f_2=0.22$ Hz; it is also shown a peak at $f_1=0.22$ Hz and $f_2=0$.

All bispectral panels indicate a phase coupling at $(f_p,f_p)$ and at $(f_p,2f_p)$. Intensity of phase coupling depends on wave and breakwater characteristics. To summarize the effect of barrier in Figure 5.22 and 5.23 are reported the values of bicoherence for all data sets at $(f_p,f_p)$ and $(f_p,2f_p)$ against B/L ratio. Note that the self interaction at fp depends on crest width, in fact for large width (B=4.0m) bicoherence tends to be constant; instead for smaller crest width (B=1.0 m) bicoherence tends to increase rapidly.

This seems to be due to non linearity as can be noted comparing Figure 5.22 and 5.23 with Figure 5.28. Results are summarized in table 5.1

| Gauge | 2 | 16 | 17 | 18 | 19 | 20 |
|---|---|---|---|---|---|---|
| Test | $f_p$(Hz) | $B(f_p,f_p)$ | | | | |
| 25 | 0.18 | 0.5273 | 0.8067 | 0.7260 | 0.6534 | 0.5881 |
| 26 | 0.22 | 0.4801 | 0.7467 | 0.6720 | 0.6048 | 0.5443 |
| 27 | 0.19 | 0.4970 | 0.7000 | 0.6300 | 0.5670 | 0.5103 |
| 28 | 0.14 | 0.3787 | 0.5333 | 0.4853 | 0.4368 | 0.3931 |
| 29 | 0.19 | 0.2935 | 0.4133 | 0.3699 | 0.3329 | 0.2996 |
| 30 | 0.21 | 0.5349 | 0.7533 | 0.6780 | 0.6102 | 0.5492 |
| 31 | 0.16 | 0.5112 | 0.7200 | 0.6480 | 0.5832 | 0.5249 |
| 32 | 0.17 | 0.4591 | 0.6467 | 0.5691 | 0.5122 | 0.4609 |
| 33 | 0.19 | 0.4023 | 0.5667 | 0.5100 | 0.4590 | 0.4131 |
| 34 | 0.23 | 0.3692 | 0.5200 | 0.4680 | 0.4212 | 0.3791 |
| 43 | 0.20 | 0.6153 | 0.8667 | 0.8407 | 0.7986 | 0.7906 |
| 44 | 0.18 | 0.4260 | 0.6000 | 0.5820 | 0.5529 | 0.5474 |
| 45 | 0.17 | 0.4497 | 0.6333 | 0.6112 | 0.5806 | 0.5748 |
| 46 | 0.19 | 0.4118 | 0.5800 | 0.5643 | 0.5361 | 0.5308 |
| 51 | 0.14 | 0.3313 | 0.4667 | 0.4527 | 0.4300 | 0.4257 |
| 52 | 0.23 | 0.5451 | 0.7467 | 0.7243 | 0.6881 | 0.6812 |
| 53 | 0.16 | 0.5065 | 0.7133 | 0.6898 | 0.6553 | 0.6619 |
| 54 | 0.1 | 0.4970 | 0.7000 | 0.6790 | 0.6451 | 0.6386 |
| 55 | 0.22 | 0.3692 | 0.5200 | 0.5044 | 0.4792 | 0.4744 |
| 56 | 0.16 | 0.4023 | 0.5667 | 0.5497 | 0.5222 | 0.5170 |

**Table 5.1. Summary of bispectral analysis**

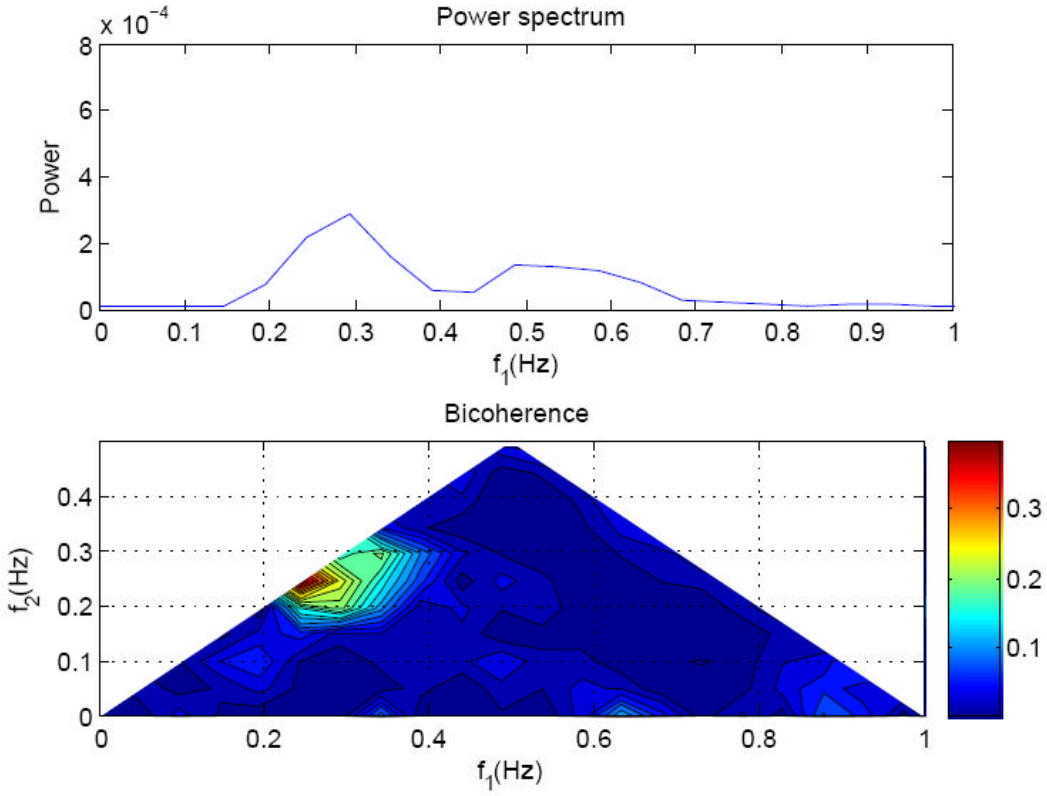

**Figure 5.2. – Bicoherence test 25 gauge 18**

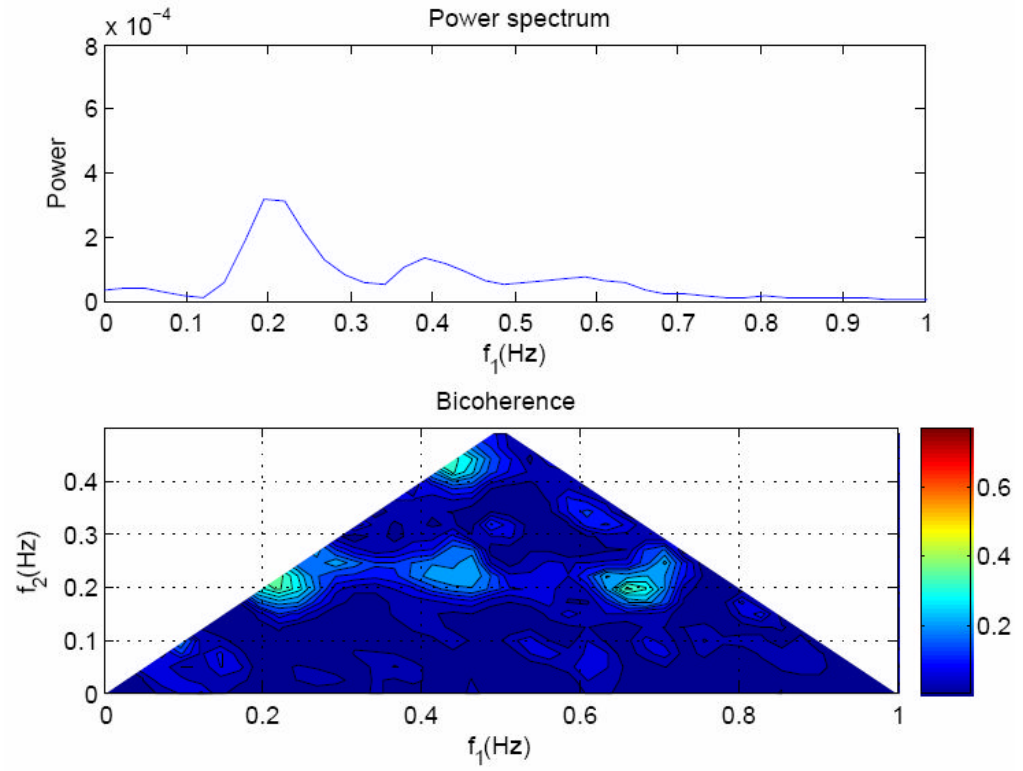


**Figure 5.3. – Bicoherence test 26 gauge 18**

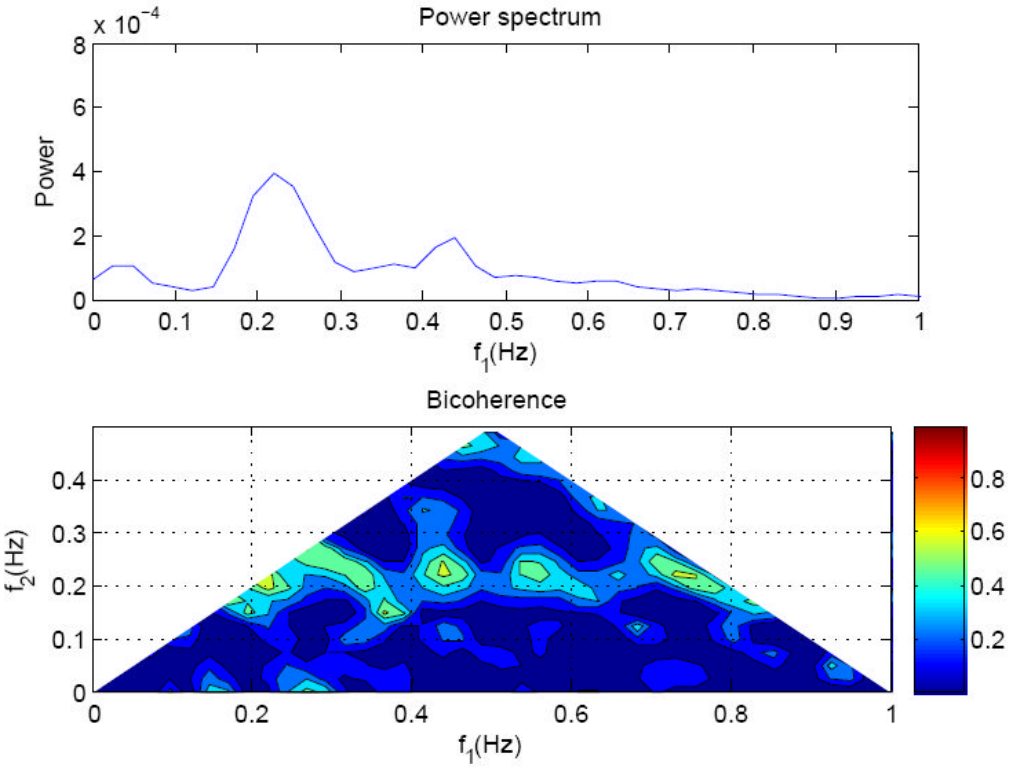


**Figure 5.4. – Bicoherence test 27 gauge 18**

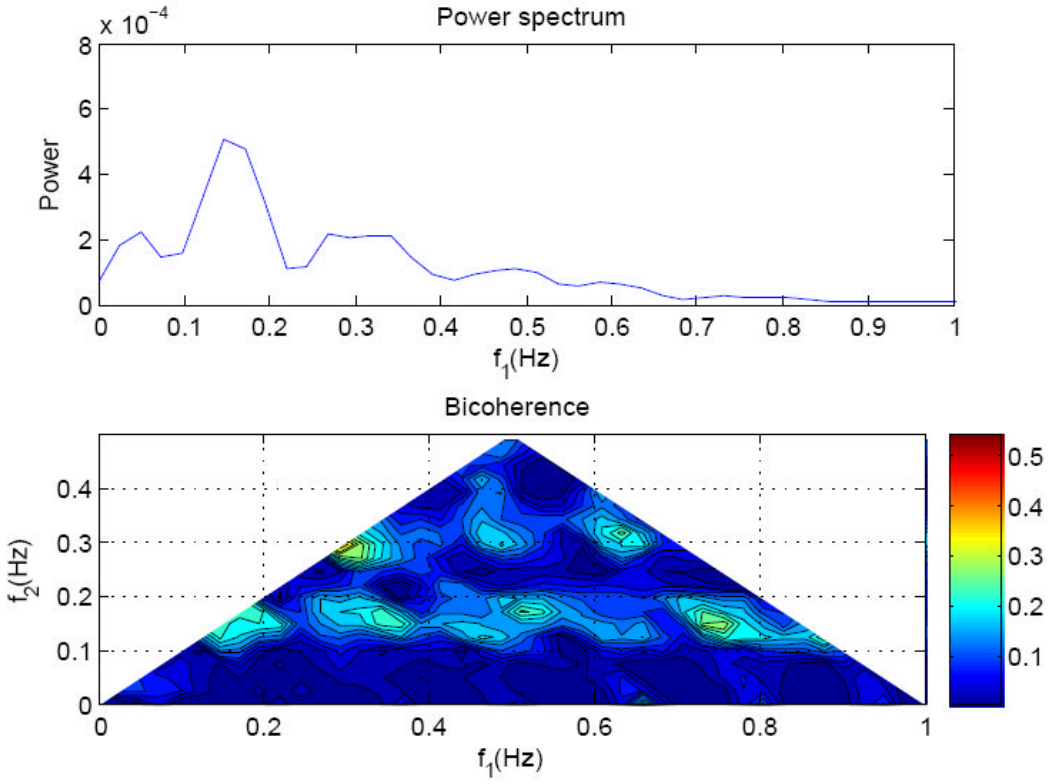


**Figure 5.5. – Bicoherence test 28 gauge 18**

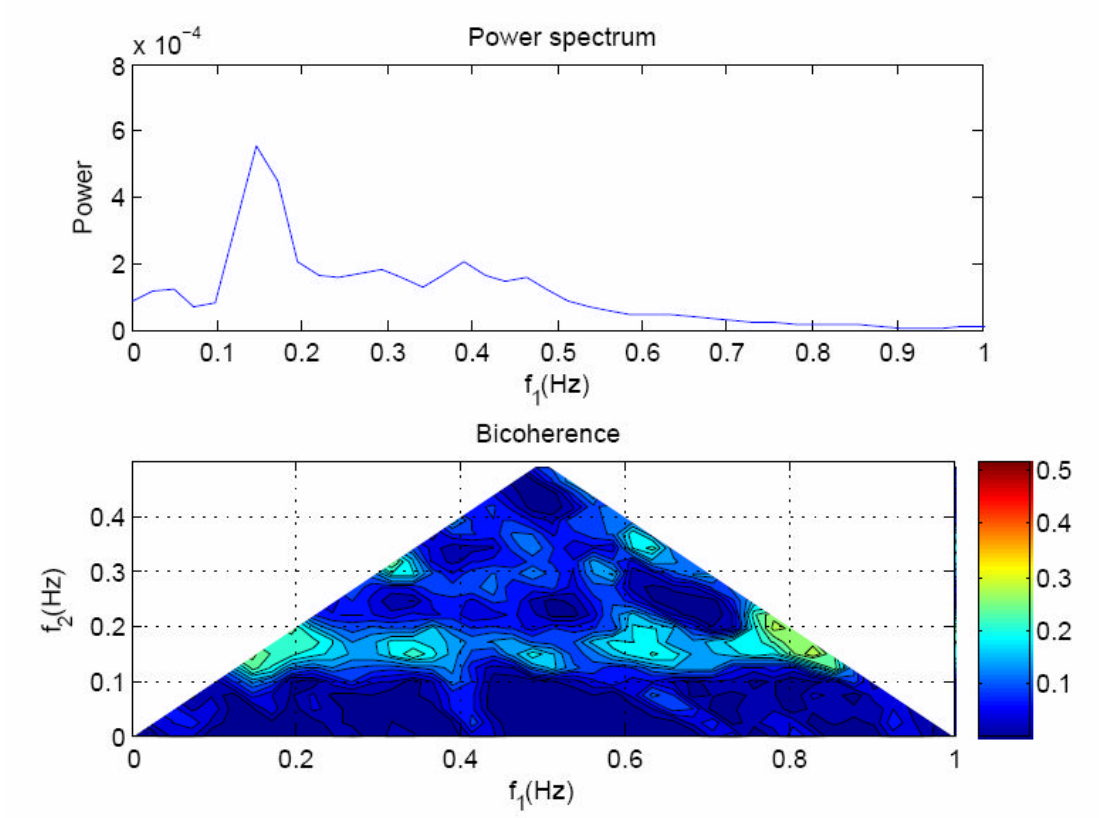


**Figure 5.6. – Bicoherence test 29 gauge 18**

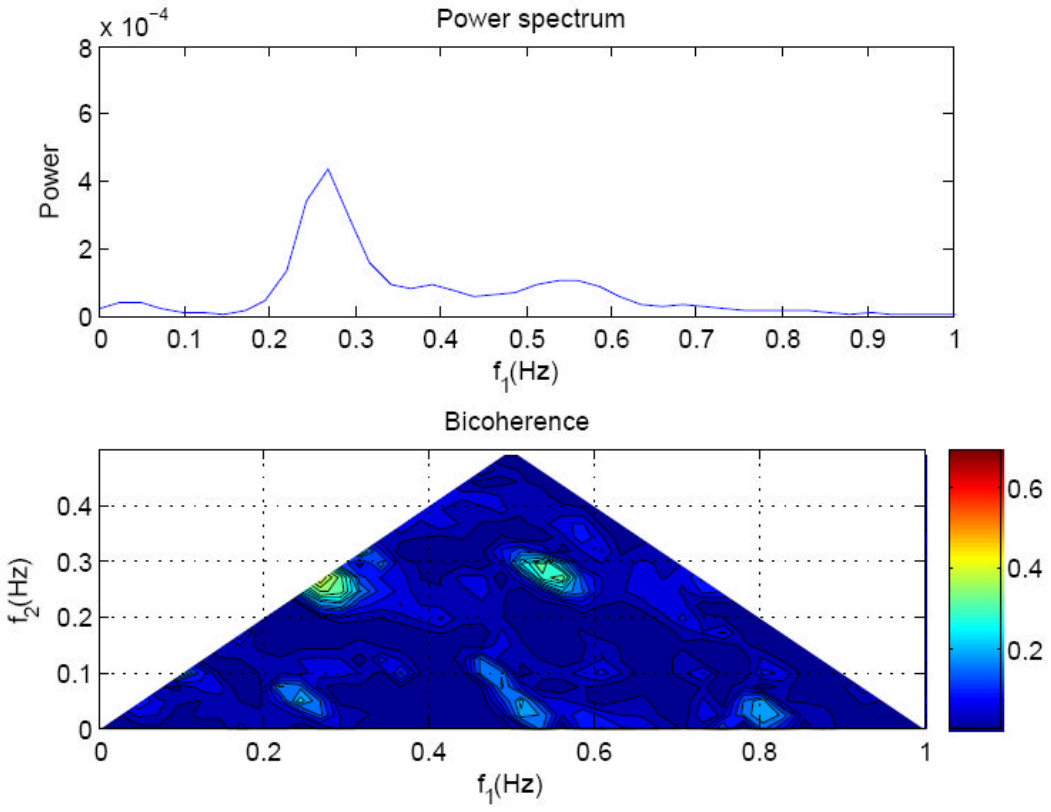


**Figure 5.7. – Bicoherence test 30 gauge 18**

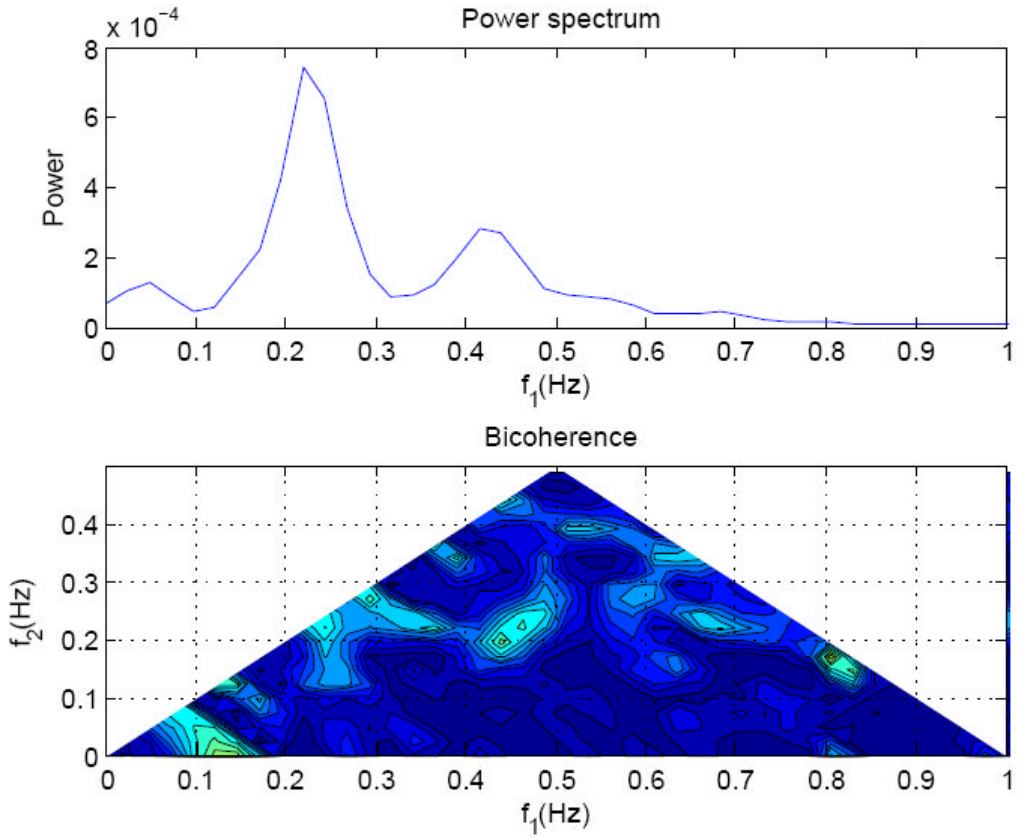

**Figure 5.8. – Bicoherence test 31 gauge 18**

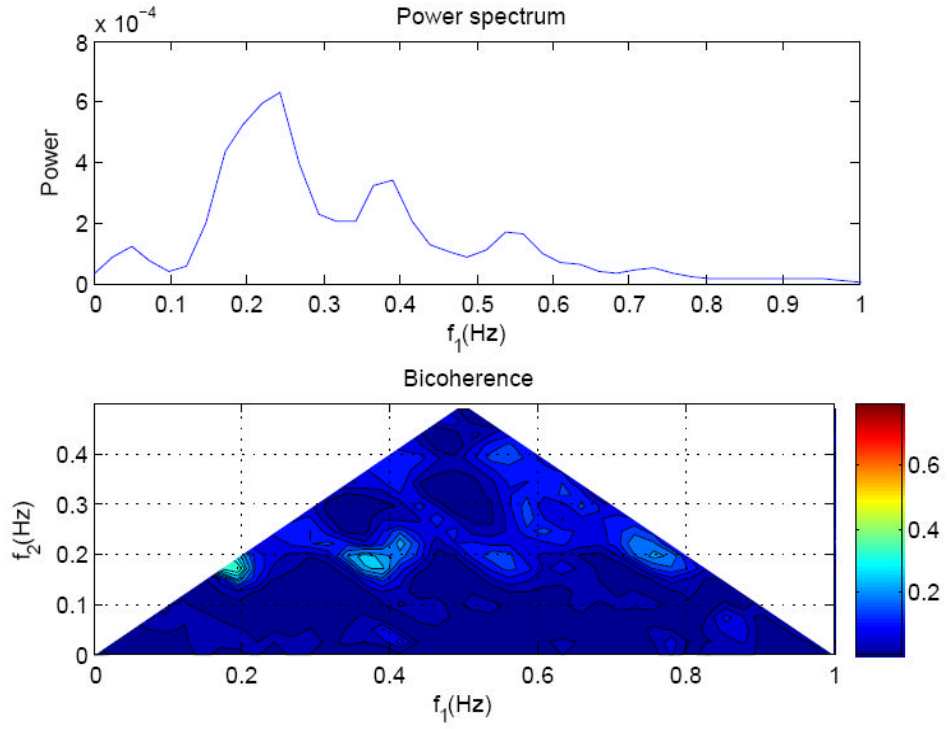


**Figure 5.9. – Bicoherence test 32 gauge 18**

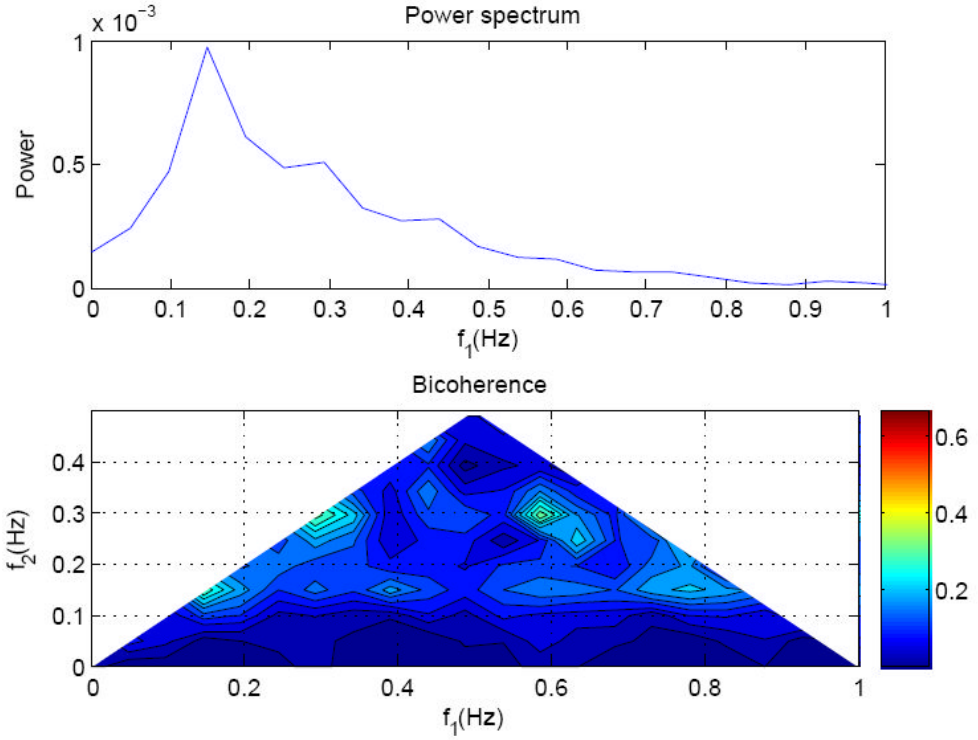


**Figure 5.10. – Bicoherence test 33 gauge 18**

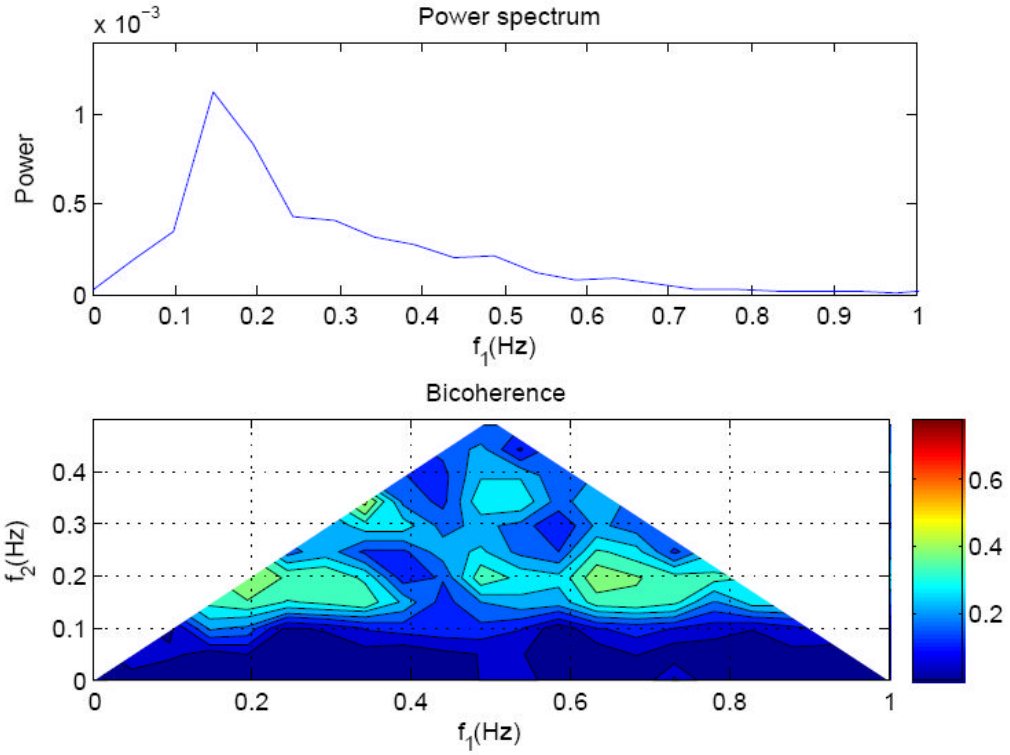


**Figure 5.11. – Bicoherence test 34 gauge 18**

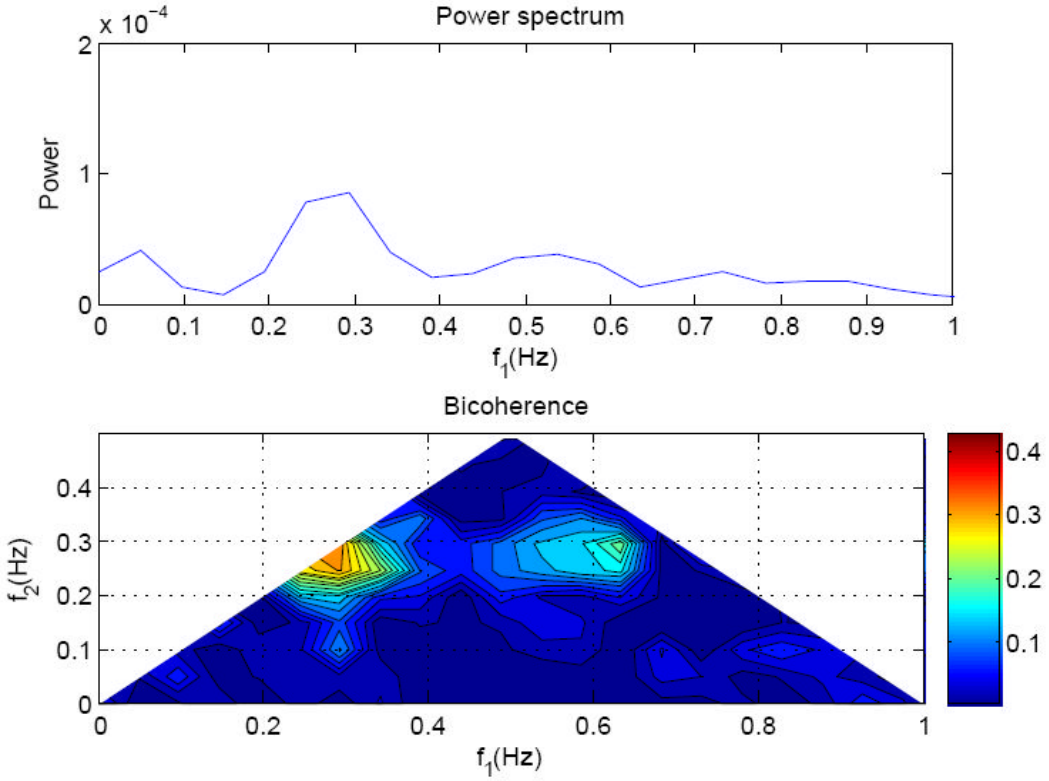


**Figure 5.12. – Bicoherence test 43 gauge 18**

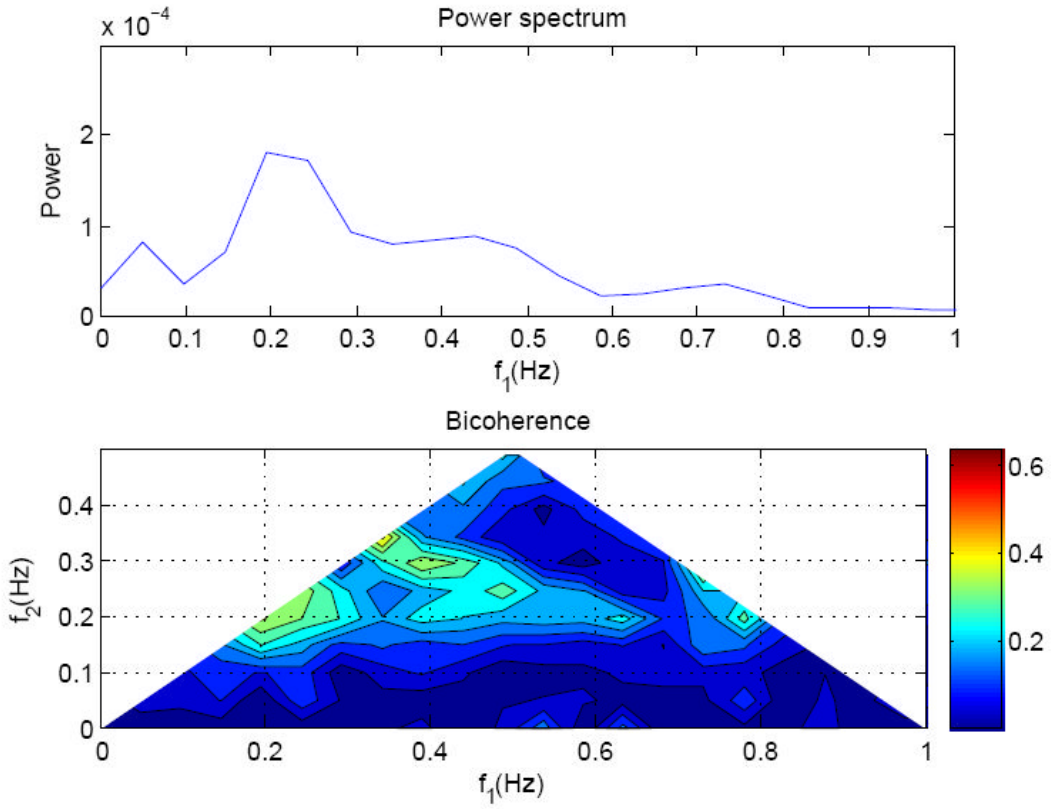


**Figure 5.13. – Bicoherence test 44 gauge 18**

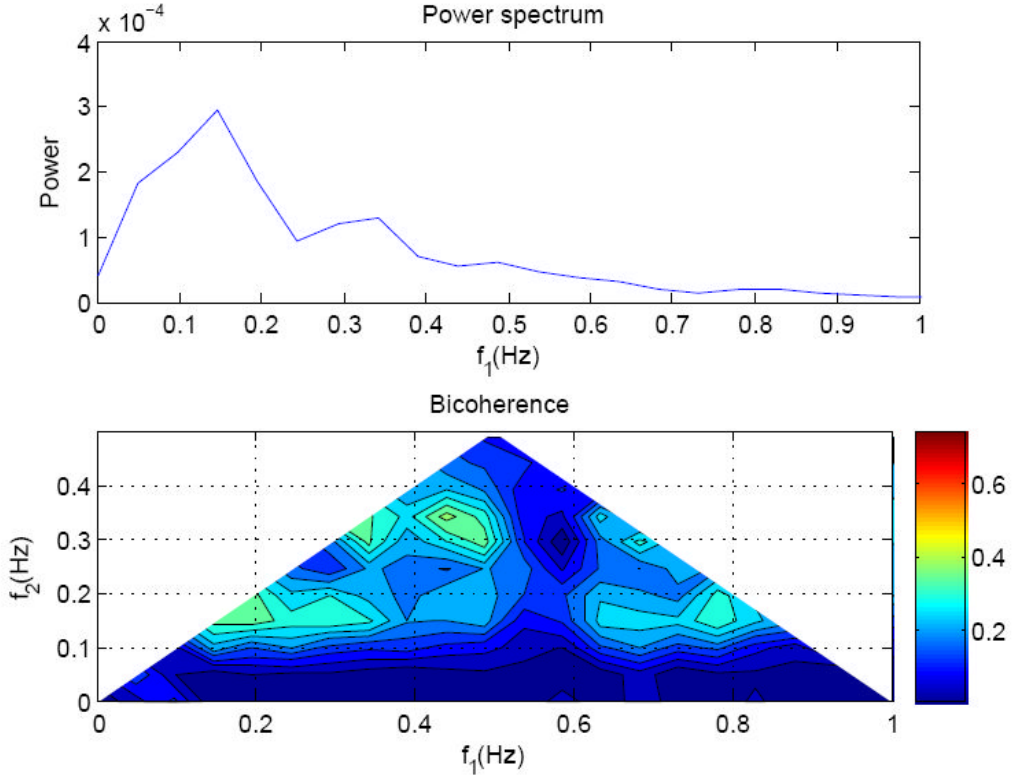


**Figure 5.14. – Bicoherence test 45 gauge 18**

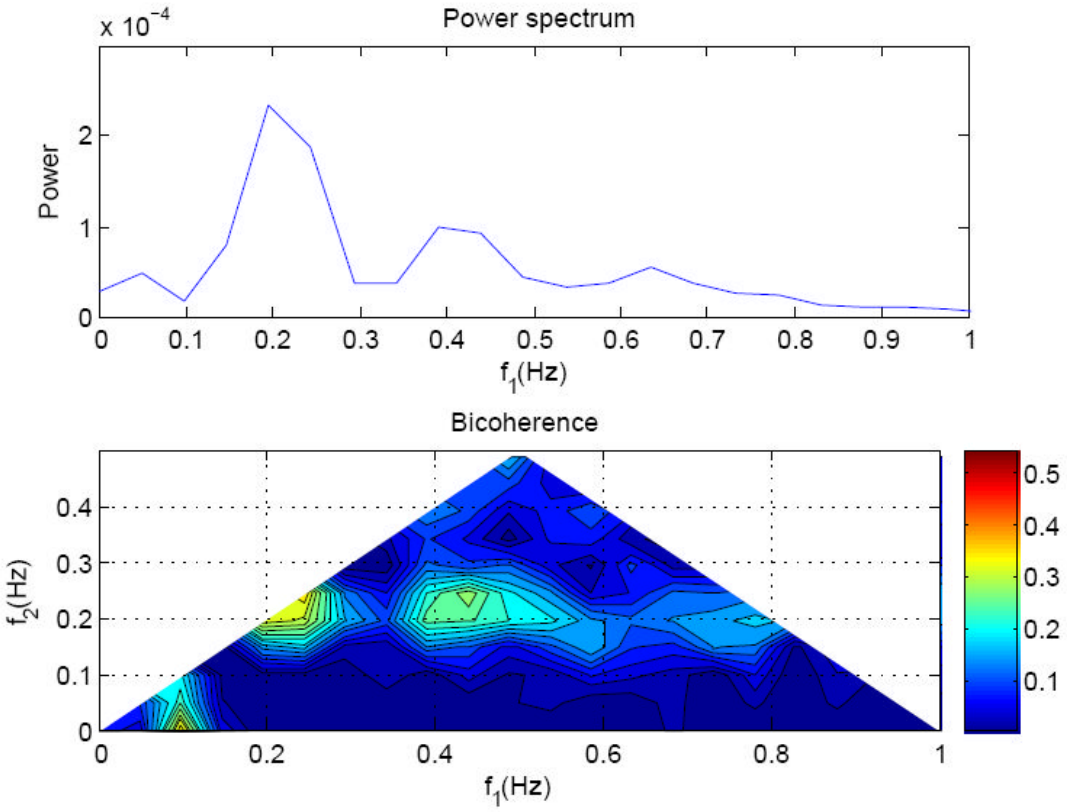


**Figure 5.15. – Bicoherence test 46 gauge 18**

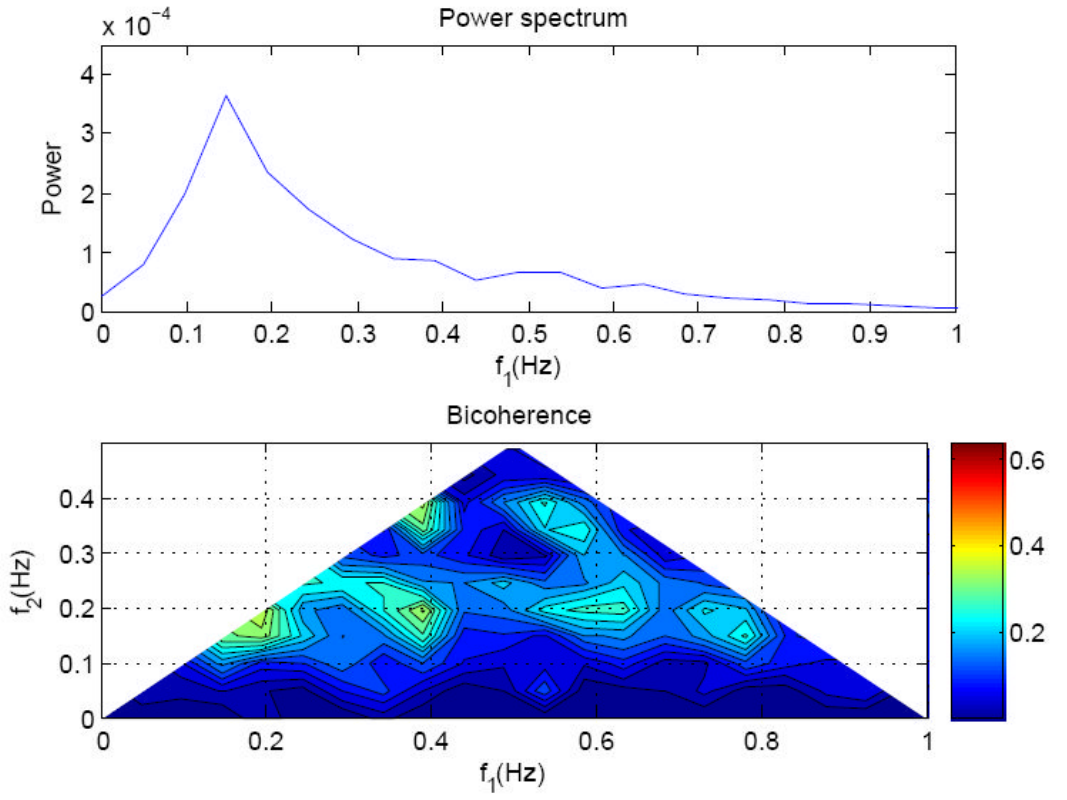


**Figure 5.16. – Bicoherence test 51 gauge 18**

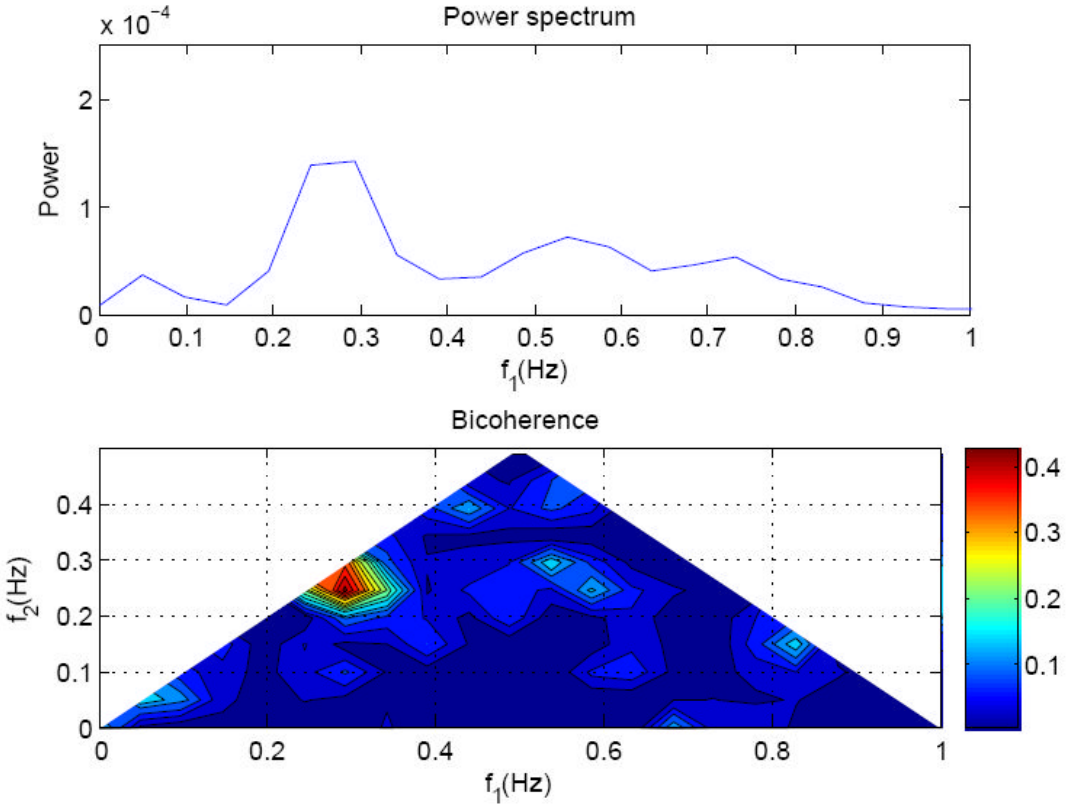


**Figure 5.17. – Bicoherence test 52 gauge 18**

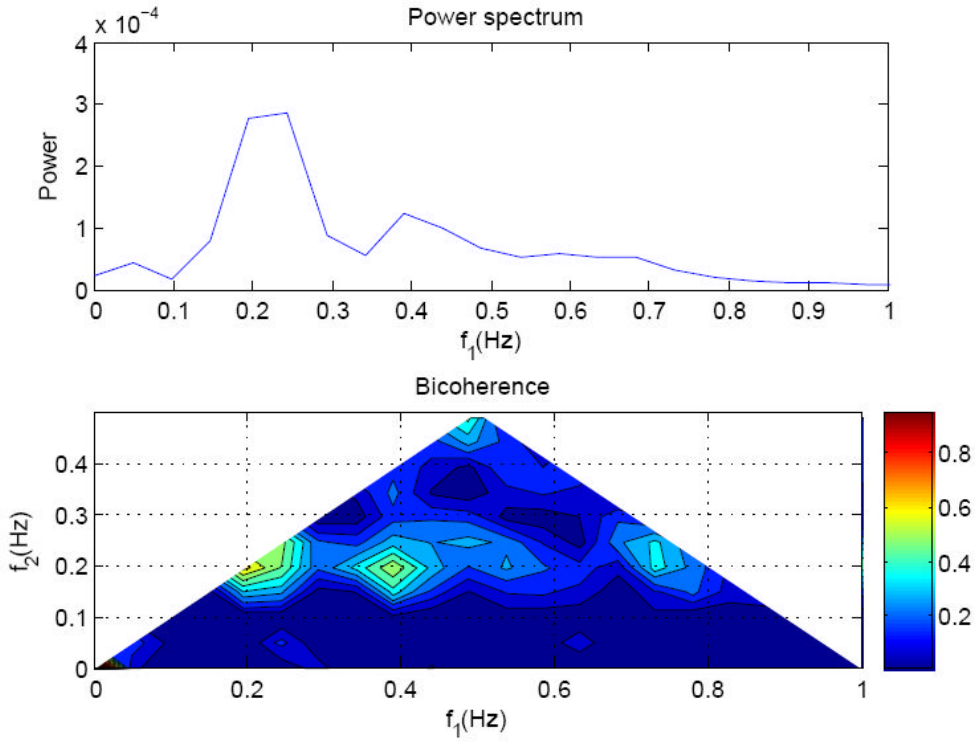


**Figure 5.18. – Bicoherence test 53 gauge 18**

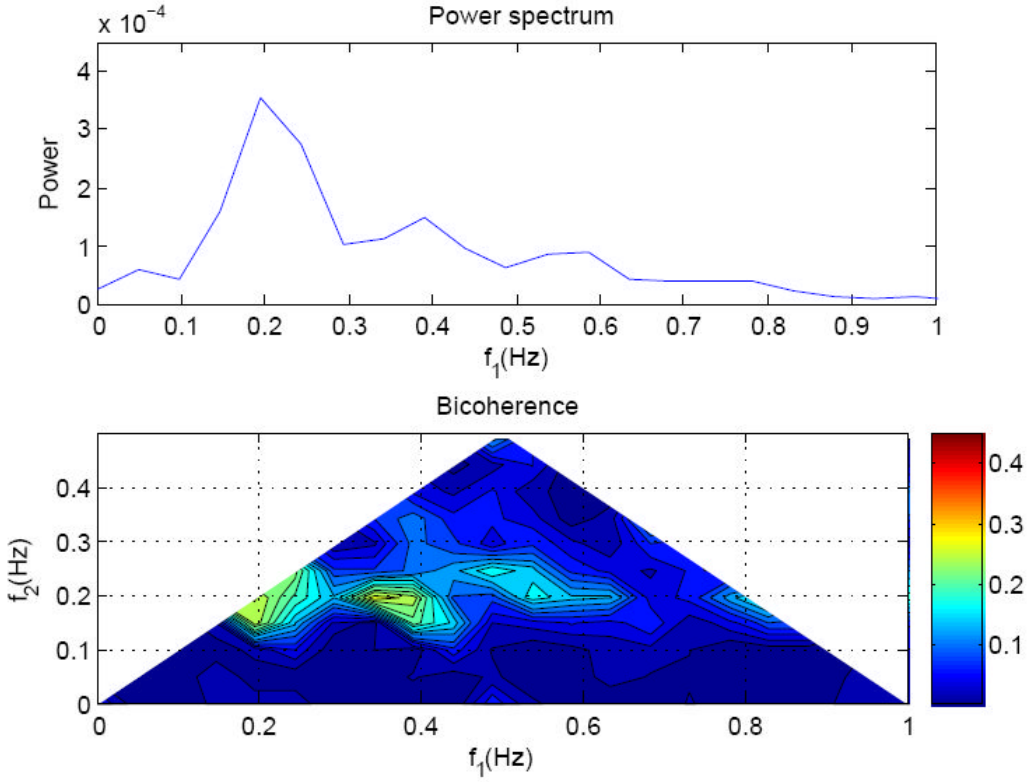


**Figure 5.19. – Bicoherence test 54 gauge 18**

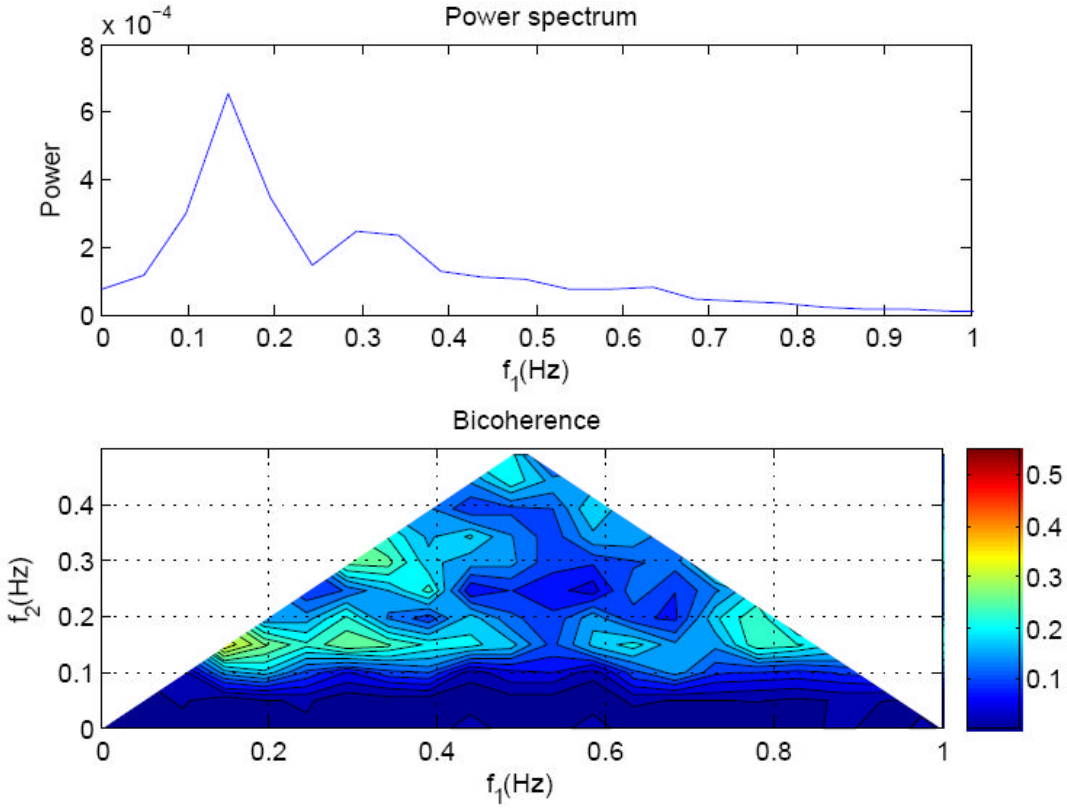


**Figure 5.20. – Bicoherence test 55 gauge 18**

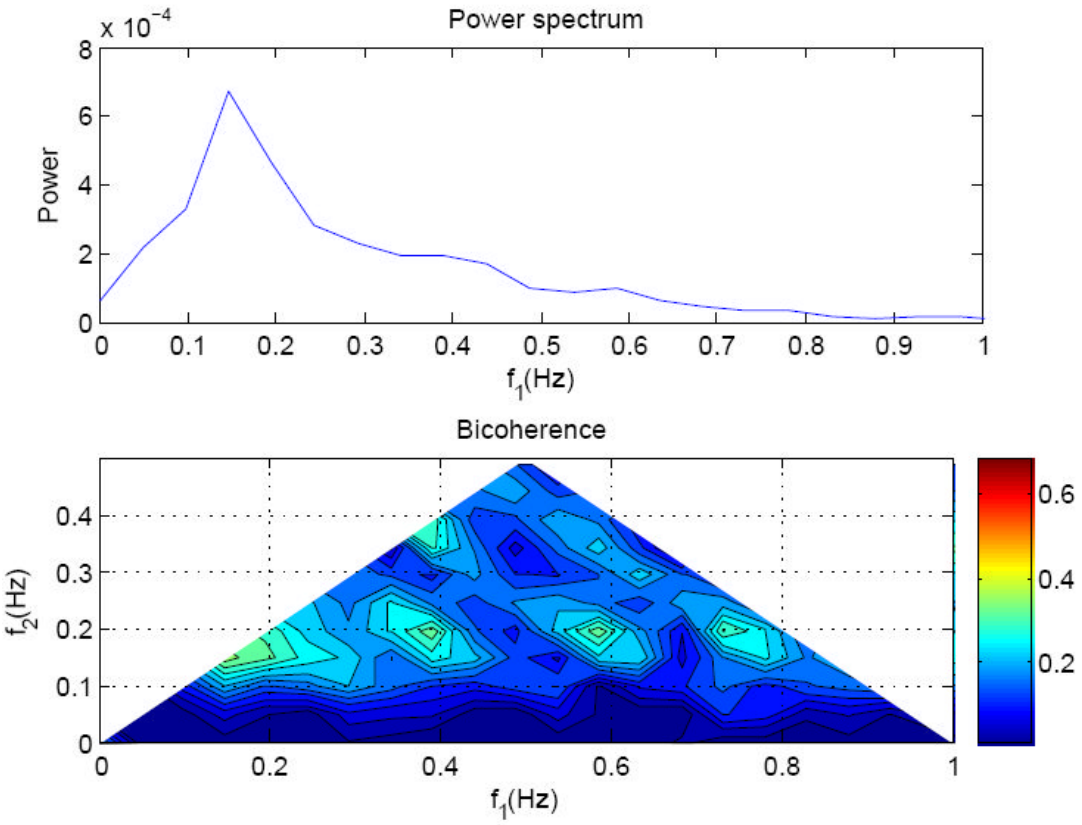


**Figure 5.21. – Bicoherence test 56 gauge 18**

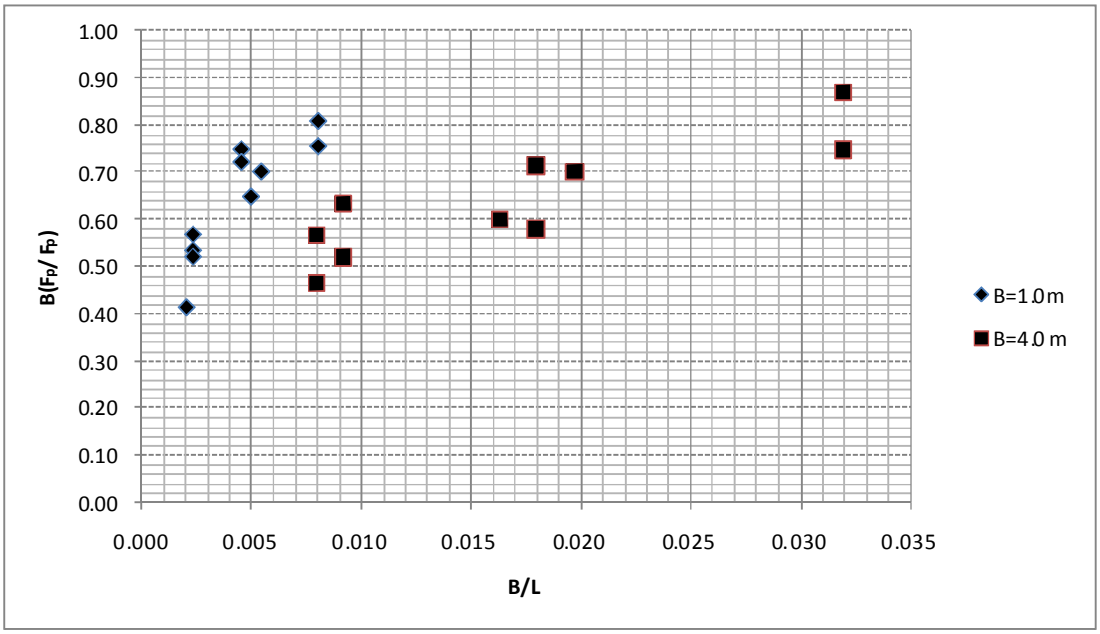


**Figure 5.22. – Bicoherence value at (fp,fp) against B/L at gauge 18**

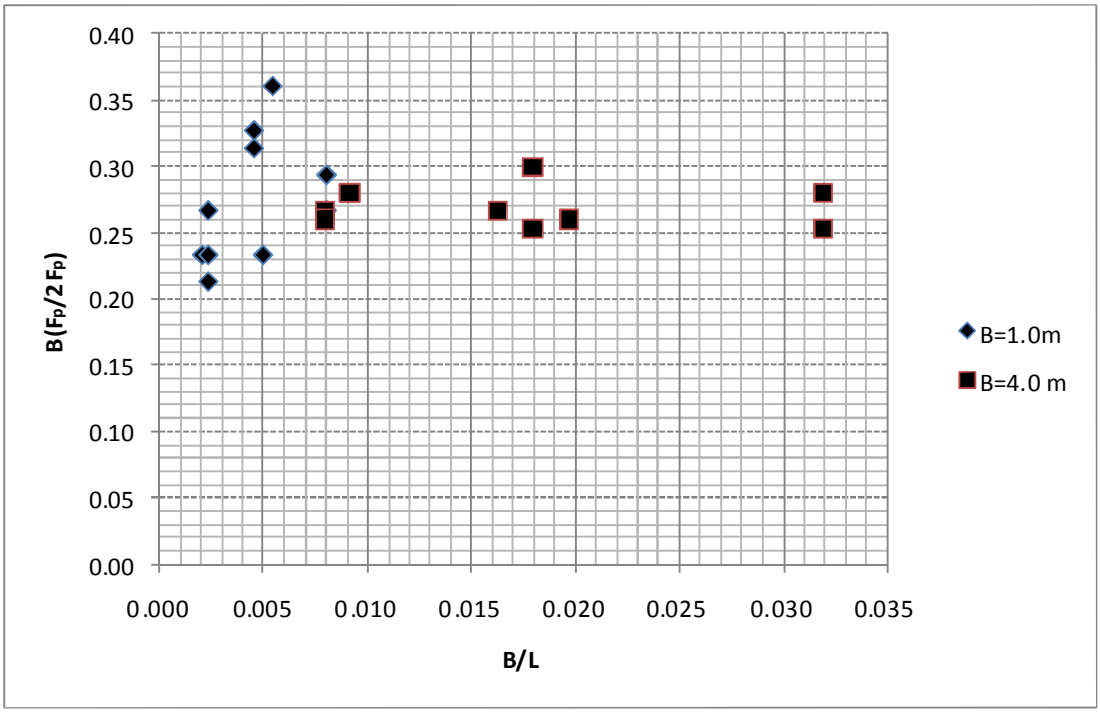


**Figure 5.23. – Bicoherence value at (fp,2fp) against B/L at gauge 18**

The overall nonlinearity parameters, skewness and asymmetry, have been calculated at gauge 18 using equations [5.16] and [5.17]. Their variations against $f_p$, $K_t$, $M_{0low}/M_{0high}$ ratio, Ursell number, and B/L ratio are shown in Figure from 5.24 to 5.29. The asymmetry increases linearly increasing $f_p$ and $K_t$, $M_{0low}/M_{0high}$ ratio and decrease increasing Ursell number . Regarding asymmetry variations in function of B/L ratio (Figure 5.28), its value shows a different tendency for short crest width. The variation of the skewness shows a different trend than the variation of the asymmetry (Figure 5.29). In most of the shoaling region, the values of the asymmetry remain rather low. They increase rapidly over the barrier. For B=1.0m asymmetry and skewness rapidly decrease (Figure 5.30 and 5.31), instead for large crest width (B=4.0 m) non linear parameters seem to continue to increase (Figure 5.31 and 5.32).

A question which deserves attention in this context relates the possibility of a "memory" in the wavefield on the downwave side of the barrier, of what happened over the bar. Such "memory" is equivalent to a persistent phase lock between harmonics. This in turn imply spatial nonhomogeneity. This possibility is well established for interaction between a discrete, finite set of wave components, in particular monochromatic wave and its harmonics, where a recurrent pattern of cross spectral energy transfer back and forth occurs, resulting in spatially periodic amplitude variations. However these effects are expected to cancel out in case of continuous spectrum. Analyzing spatial variation of bicoherence (Figure 5.24) can be noted the different behaviour of large crest width (B=4.0 m, tests 52 and 53) and short crest width (B=1.0 m, tests 25 and 26). Bicoherence variations indicate a significant increase on the upslope, to a maximum at guage 17 near the top of the barrier, bicoherence decrease rapidly for short crest width to values between 0.5 at gauge 20. These values are similar to those at gauge 16 before the barrier. This implies that there is no memory of bar location. For large crest width bicoherence decrease on the downslope less rapidly than the case of B=1.0 m and seem to became constant after gauge 19 with values higher than the values at gauge 16. This implies that for large crest width there is a sort of "memory" of bar location. Can be noted that the length of zone after barrier that retain the memory of bar can be longer than the zone covered by wave gauge.

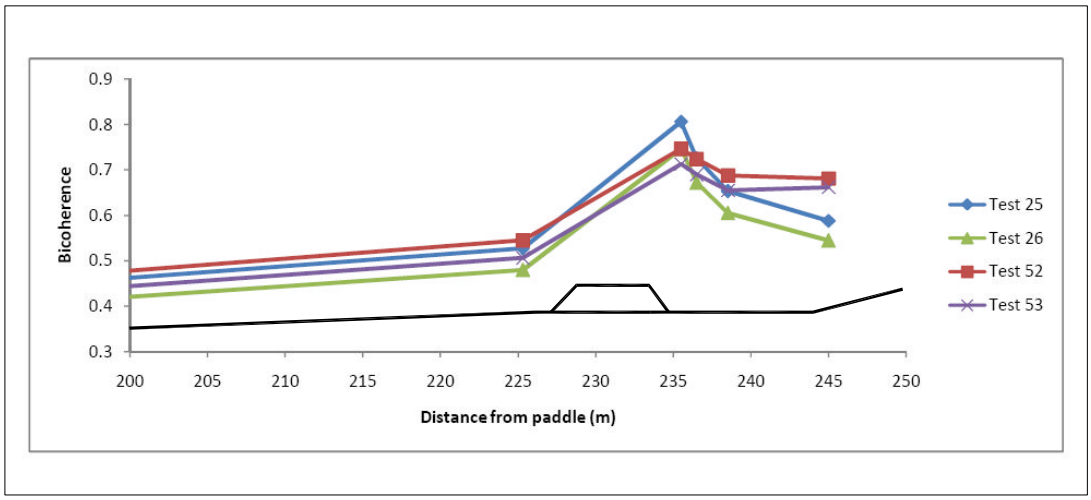


**Figure 5.24. – Spatial variation of bicoherence at guage 16, 17, 18, 19 and 20 for tests 25, 26, 52 and 53**

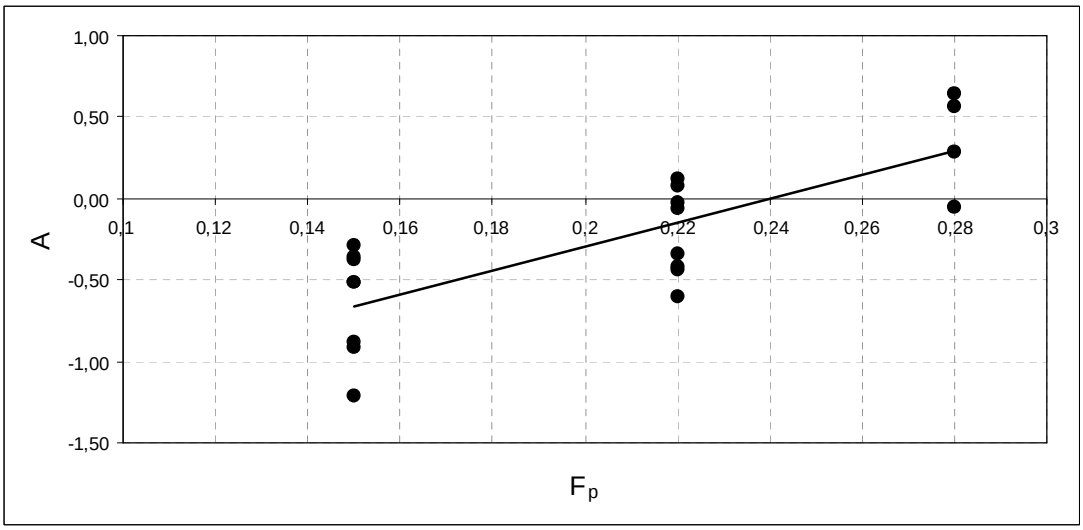


**Figure 5.25. – Asymmetry value at against $f_p$ at gauge 18**

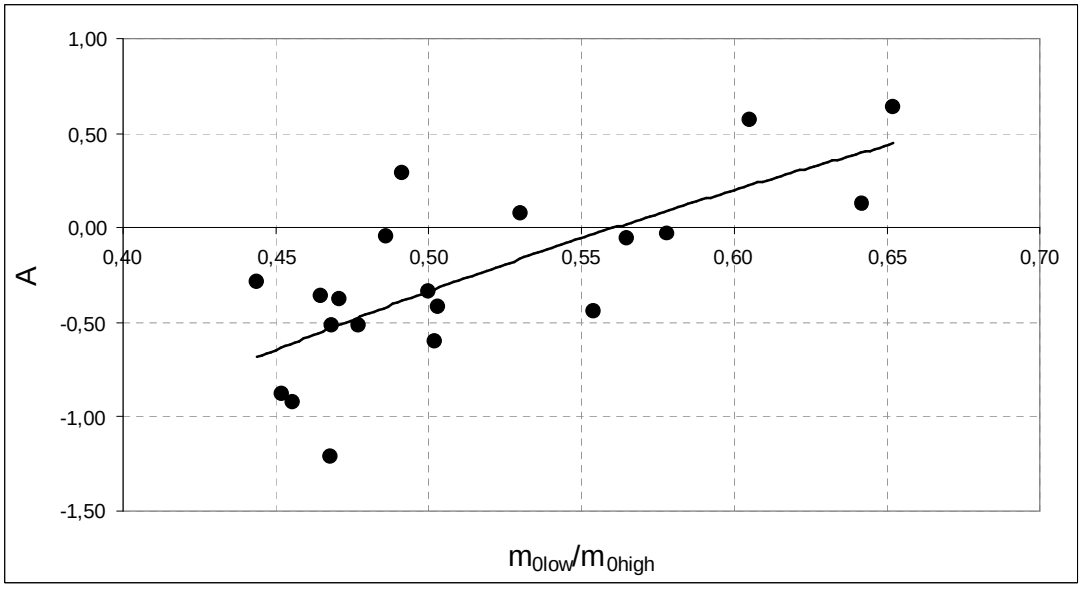


**Figure 5.26. – Asymmetry value at against $M_{0low}/M_{0high}$ ratio at gauge 18**

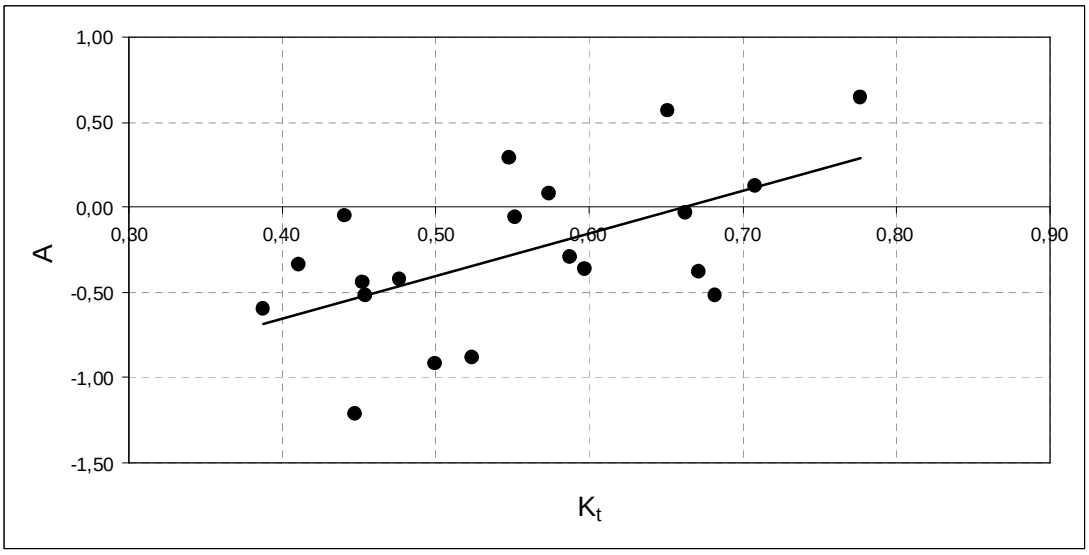


**Figure 5.27. – Asymmetry value at against transmission coefficient ratio at gauge 18**

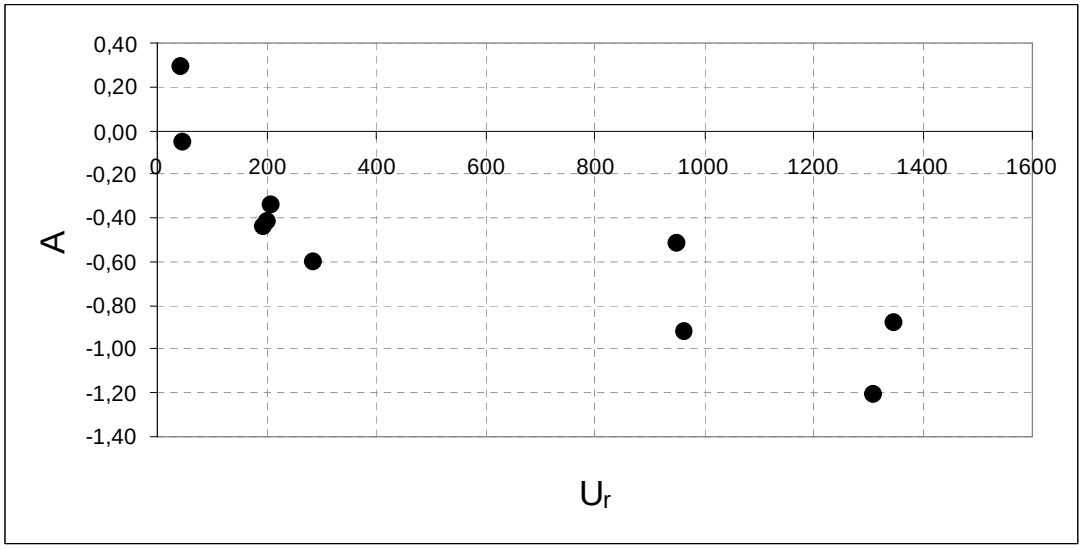


**Figure 5.28. – Asymmetry value at against Ursell number at gauge 18**

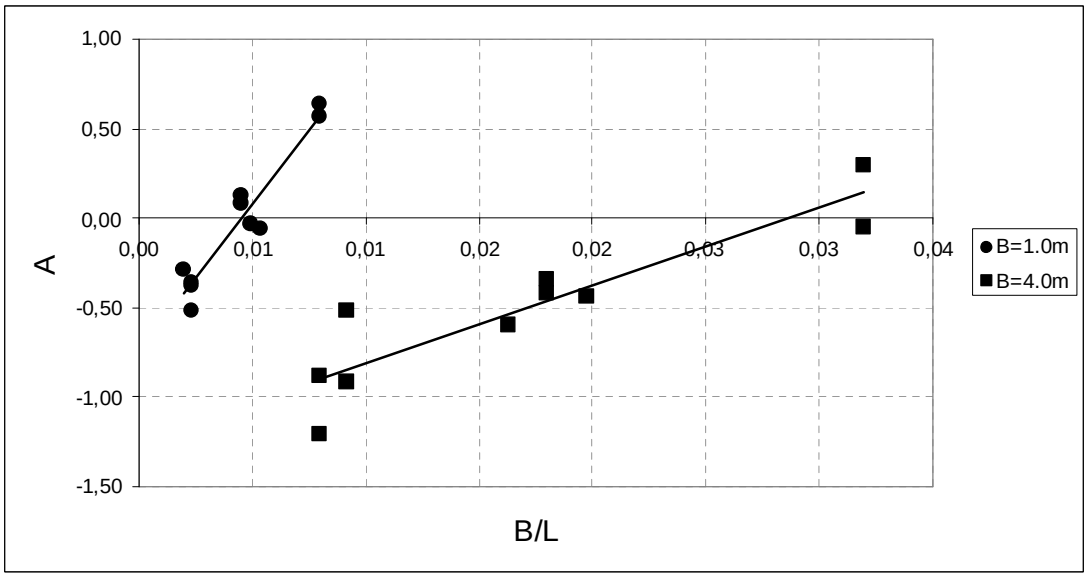


**Figure 5.29. – Asymmetry value at against B/L ratio at gauge 18**

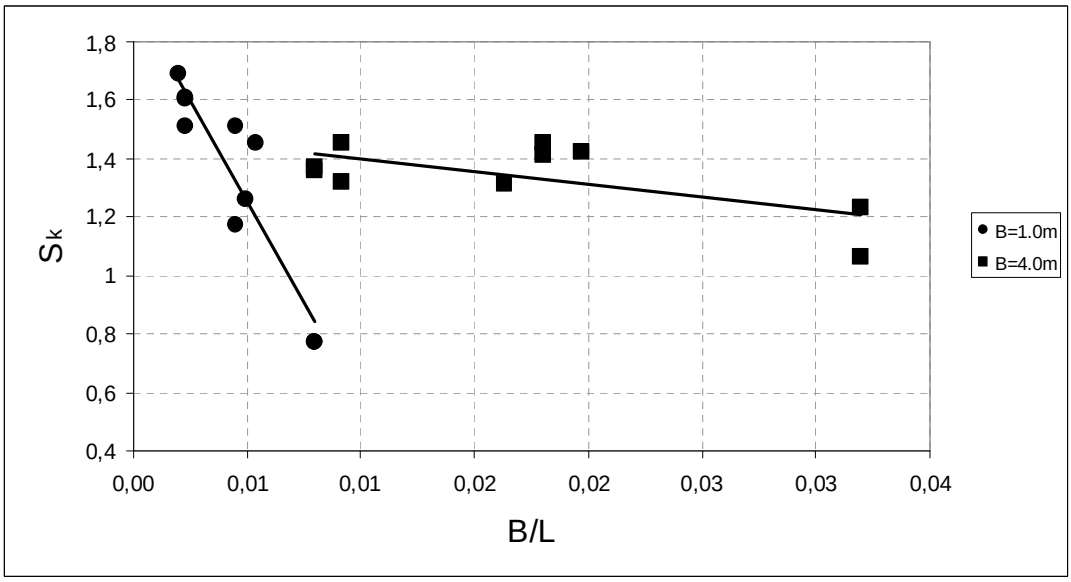


**Figure 5.30. – Skewness value at against B/L ratio at gauge 18**

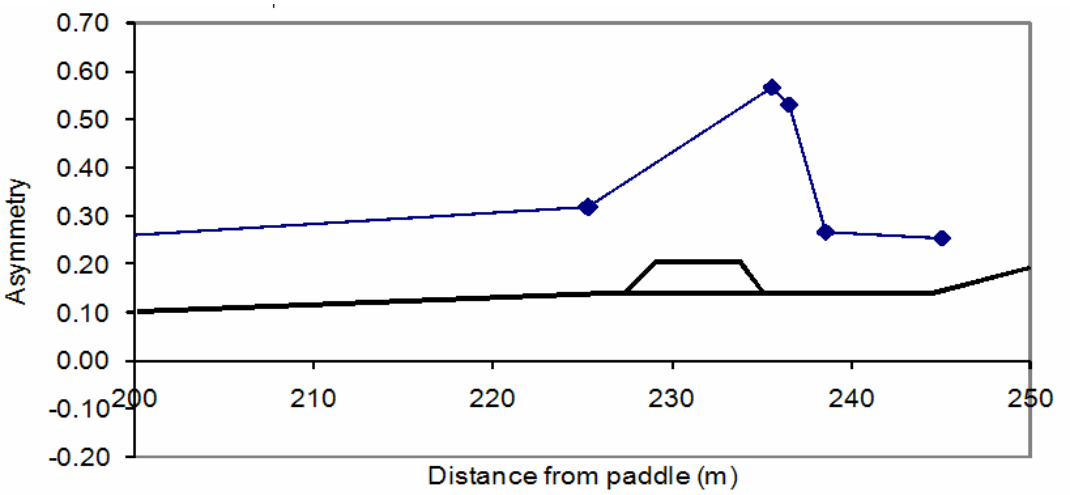


**Figure 5.31. –Spatial variation of asymmetry for test 25**

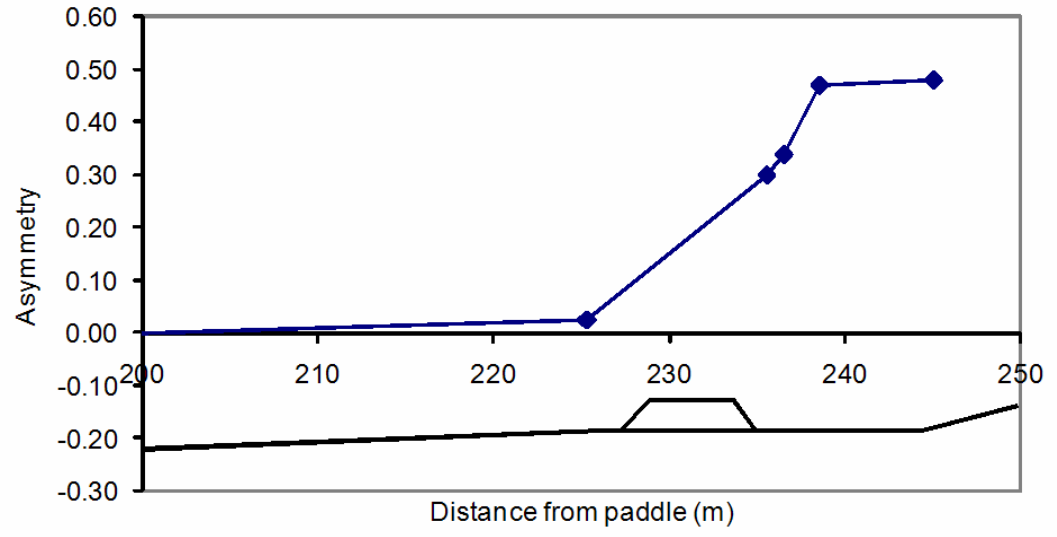


**Figure 5.32. –Spatial variation of asymmetry for test 52**

## 5.4 Hilbert Huang transform

Fourier-based spectral analysis methods have been widely used for studying random waves. One major weakness of these methods is the assumption of linear superposition of wave components. As a result, the energy of a nonlinear wave spreads into many harmonics, which are phase-coupled via the nonlinear dynamics inherent in ocean waves. In addition to the nonlinearity issue, Fourier spectral analysis should, strictly speaking, be used for periodic and stationary processes only, but wave propagation in the ocean is certainly neither stationary nor periodic. Recently, Huang and his colleagues developed a new analysis technique, the HHT. Through analytical examples, they demonstrated the superior frequency and temporal resolutions of the HHT for analyzing non stationary and nonlinear signals ( Huang et al. 1998, 1999). Using this analysis, the physical interpretation of nonlinearity is frequency modulation, which is fundamentally different from the commonly accepted concept associating nonlinearity with harmonic generation. Huang et al. argued that harmonic generation is caused by the perturbation method used in solving the nonlinear equation governing the physical processes; thus, the harmonics are produced by the mathematical tools used for the solution rather than being a true physical phenomenon.

HHT consists of two phase, the first step is to preprocess the data by the empirical mode decomposition method, with which the data are decomposed into a number of intrinsic mode function components. Thus, we will expand the data in a basis derived from the data. The second step is to apply the Hilbert transform to the decomposed IMFs and construct the energy-frequency-time distribution, designated as the Hilbert spectrum, from which the time localities of events will be preserved. In other words, we need the instantaneous frequency and energy rather than the global frequency and energy defined by the Fourier spectral analysis. Therefore, before going any further, we have to clarify the definition of the instantaneous frequency.

### 5.4.1 Instantaneous frequency

In the traditional Fourier analysis, the frequency is definedfor the sine or cosine function spanning the whole data length with constant amplitude. As an extension of this definition, the instantaneous frequencies also have to relate to either a sine or a cosine function. Thus, we need at least one full oscillation of a sine or a cosine wave to define the local frequency value. According to this logic, nothing shorter than a full wave will do. Such a definition would not make sense for non-stationary data for which the frequency has to change values from time to time. For an arbitrary time series, X(t), we can always have its Hilbert Transform, Y (t), as

$$Y\left(t\right) = \frac{1}{\pi} P \int_{-\infty}^{\infty} \frac{X\left(t'\right)}{t - t'} dt' \qquad [5.18]$$

where P indicates the Cauchy principal value. This transform exists for all functions of class $L_p$ (see, for example, Titchmarsh 1948). With this definition, X(t) and Y (t) form the complex conjugate pair, so we can have an analytic signal, Z(t), as

$$Z\left(t\right) = X\left(t\right) + iY\left(t\right) = a\left(t\right) e^{i\theta t} \qquad [5.19]$$

in which

$$a\left(t\right) = \left[X^2\left(t\right) + Y^2\left(t\right)\right]^{1/2}, \quad \theta\left(t\right) = \arctan\left(\frac{X\left(t\right)}{Y\left(t\right)}\right) \qquad [5.20]$$

Theoretically, there are infinitely many ways of defining the imaginary part, but the Hilbert transform provides a unique way of defining the imaginary part so that the result is an analytic function. A brief tutorial on the Hilbert transform with the emphasis on its physical interpretation can be found in Bendat & Piersol (1986). Essentially equation [5.18] defines the Hilbert transform as the convolution of X(t) with 1/t; therefore, it emphasizes the local properties of X(t). In equation [5.19], the polar coordinate expression further clarifies the local nature of this representation: it is the best local fit of an amplitude and phase varying trigonometric function to X(t). Even with

the Hilbert transform, there is still considerable controversy in defining the instantaneous frequency as:

$$\omega = \frac{d\theta\left(t\right)}{dt} \qquad [5.21]$$

### 5.4.2 Intrinsic mode function

An intrinsic mode function (IMF) is a function that satisfies two conditions: (1) in the whole data set, the number of extrema and the number of zero crossings must either equal or differ at most by one; and (2) at any point, the mean value of the envelope defined by the local maxima and the envelope defined by the local minima is zero. The first condition is obvious; it is similar to the traditional narrow band requirements for a stationary Gaussian process. The second condition is a new idea; it modifies the classical global requirement to a local one; it is necessary so that the instantaneous frequency will not have the unwanted fluctuations induced by asymmetric wave forms. Ideally, the requirement should be "the local mean of the data being zero". For non-stationary data, the "local mean" involves a "local time scale" to compute the mean, which is impossible to define. As a surrogate, we use the local mean of the envelopes defined by the local maxima and the local minima to force the local symmetry instead. This is a necessary approximation to avoid the definition of a local averaging time scale. Although it will introduce an alias in the instantaneous frequency for nonlinearly deformed waves, the effects of nonlinearity are much weaker in comparison with non-stationarity. With the physical approach the method does not always guarantee a perfect instantaneous frequency under all conditions. Nevertheless even under the worst conditions, the instantaneous frequency so defined mis still consistent with the physics of the system studied. The name "intrinsic mode function" is adopted because it represents the oscillation mode imbedded in the data. With this definition, the IMF in each cycle, defined by the zero crossings, involves only one mode of oscillation, no complex riding waves are allowed. With this definition, an IMF

is not restricted to a narrow band signal, and it can be both amplitude and frequency modulated. In fact, it can be non-stationary.

The details of both Empirical Mode Decomposition (EMD) and the Hilbert Spectral Analysis (HSA) are given in Huang et al. (1996, 1998 and 1999). The following summary is based on a simplified version given in Huang (2005). The EMD method is necessary to reduce any data from non-stationary and nonlinear processes into simple oscillatory function that will yield meaningful instantaneous frequency through the Hilbert transform. Contrary to almost all the previousdecomposing methods, EMD is empirical, intuitive, direct, and adaptive, with the a posteriori defined basis derived from the data. The decomposition is designed to seek the different simple intrinsic modes of oscillations in any data based on the principle of scale separation. The data, depending on it complexity, may have many different coexisting modes of oscillation at the same time. Each of these oscillatory modes is represented by an Intrinsic Mode Function (IMF) with the following definitions: (a) in the whole data set, the number of extrema and the number of zero-crossings must either equal or differ at most by one, and (b) at any point, the mean value of the envelope defined by the local maxima and the envelope defined by the local minima is zero. The IMF is a counter part to the simple harmonic function, but it is much more general: instead of constant amplitude and frequency, IMF can have both variable amplitude and frequency as functions of time. This definition is inspired by the simple example of constant plus sinusoidal function given above. The total number of the IMF components is limited to *ln2N*, where N is the total number of data points. It satisfies all the requirements for a meaningful instantaneous frequency through Hilbert transform. Pursuant to the above definition for IMF, one can implement the needed decomposition of any function, known as sifting, as follows: Take the test data; identify all the local extrema; divide the extrema into two sets: the maxima and the minima. Then connect all the local maxima by a cubic spline line to form an upper envelope. Repeat the procedure for the local minima to form a lower envelope. The upper and

lower envelopes should encompass all the data between them. Their mean is designated as m1, and the difference between the data and m1 is designated as, h1, a proto-IMF:

$$X\left(t\right) - m_1 = h_1 \qquad [5.22]$$

Ideally, $h_1$ should satisfy the definition of an IMF by construction of $h_1$ described above, which should have made it symmetric and having all maxima positive and all minima negative. Yet, in changing the local zero from a rectangular to a curvilinear coordinate system some inflection points could become additional extrema. New extrema generated this way actually reveal the hidden modes missed in the initial treatment. The sifting process sometimes can recover signals representing low amplitude riding waves with repeated siftings. The sifting process serves two purposes: to eliminate riding waves and to make the wave profiles more symmetric. While the first condition is absolute necessary for Hilbert transform to give a meaningful instantaneous frequency, the second condition is also necessary in case the neighboring wave amplitudes having too large a disparity. As a result, the sifting process has to be repeated many times to reduce the extracted signal an IMF. In the subsequent sifting process, $h_1$ is treated as the data for the next round of sifting; therefore,

$$h_1 - m_{11} = h_{11} \qquad [5.23]$$

After repeated sifting, up to k times, $h_{1k}$:

$$h_{1(k-1)} - m_{1k} = h_{1k} \qquad [5.24]$$

If $h_{1k}$ becomes an IMF, it is designated as $c_1$:

$$c_1 = h_{1k} \qquad [5.25]$$

the first IMF component from the data. Here one has a critical decision to make: when to stop. Too many rounds of sifting will reduce the IMF to FM page criterion; too few rounds of sifting will not have a valid IMF. In the past, different criteria have been used, including Cauchy type criterion (Huang et al. 1998), S-number criterion (Huang et al. 2003), fixed-number

criterion (Wu and Huang 2004), and etc. With any stoppage criterion, the, $c_1$ should contain the finest scale or the shortest period component of the signal. one can, then, remove $c_1$ from the rest of the data by

$$X(t) - c_1 = r_1 \qquad [5.26]$$

Since the residue, $r_1$, contains all longer period variations in the data, it is treated as the new data and subjected to the same sifting process as described above. This procedure can be repeated to all the subsequent rj's, and the result is

$$\begin{aligned} & r_1 - c_2 = r_2, \\ & \ldots \\ & r_{n-1} - c_n = r_n \end{aligned} \qquad [5.27]$$

The sifting process should stop when the residue, $r_n$, becomes a constant, a monotonic function, or a function contains only a single extrema, from which no more IMF can be extracted. By summing up Equations [5.26] and [5.27] we finally obtain

$$X(t) = \sum_{j=1}^{n} c_j + r_n \qquad [5.28]$$

Thus, sifting process produces a decomposition of the data into n-intrinsic modes, and a residue, $r_n$. When apply the EMD method, a mean or zero reference is not required; EMD needs only the locations of the local extrema. The sifting process generates the zero reference for each component. Without the need of the zero reference, EMD avoids the troublesome step of removing the mean values for the large non-zero mean.

### 5.4.4 Data analysis

The data of surface elevation used in this chapter is the same data used for bispectral analysis in previous section. In order to show the results of data analysis only tests 25, 26, 52 and 53 are reported.

In figure 5.33, 5.34, 5.35 and 5.36 are reported respectively Fourier power spectra for tests 25, 26, 52 and 53 at gauge 2 and 18.

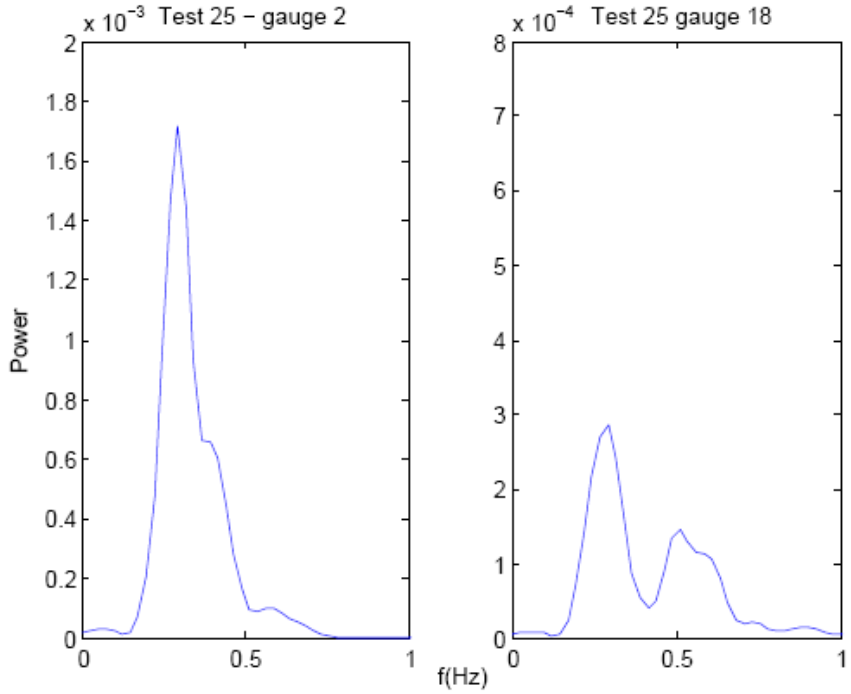


**Figure 5.33. –Fourier power spectra for test 25 at gauge 2 and 18**

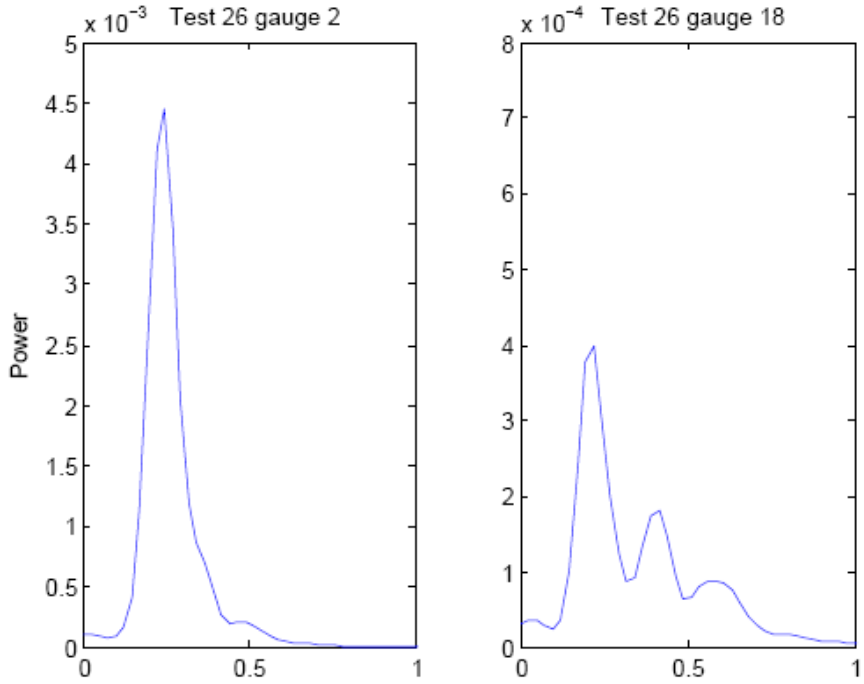


**Figure 5.34. –Fourier power spectra for test 26 at gauge 2 and 18**

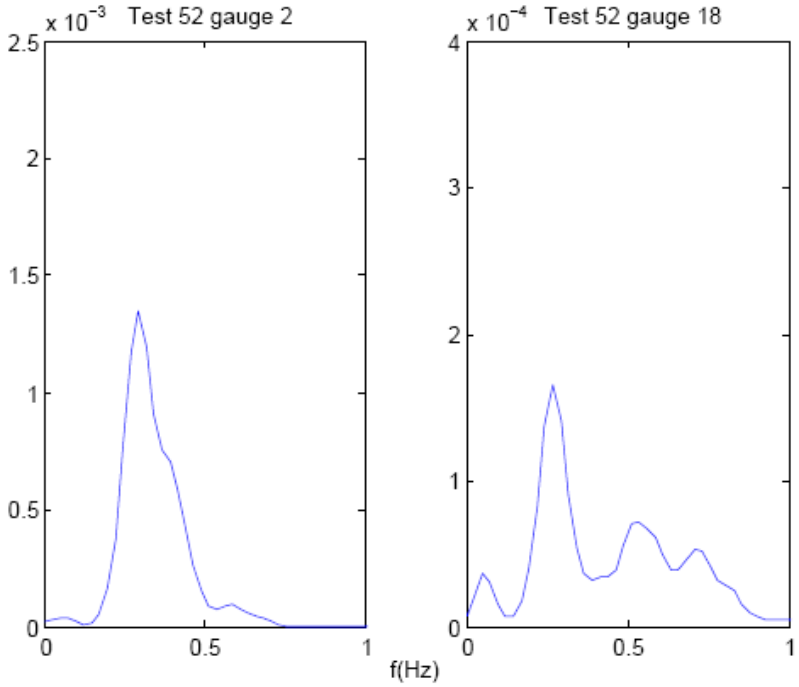


**Figure 5.35. –Fourier power spectra for test 52 at gauge 2 and 18**

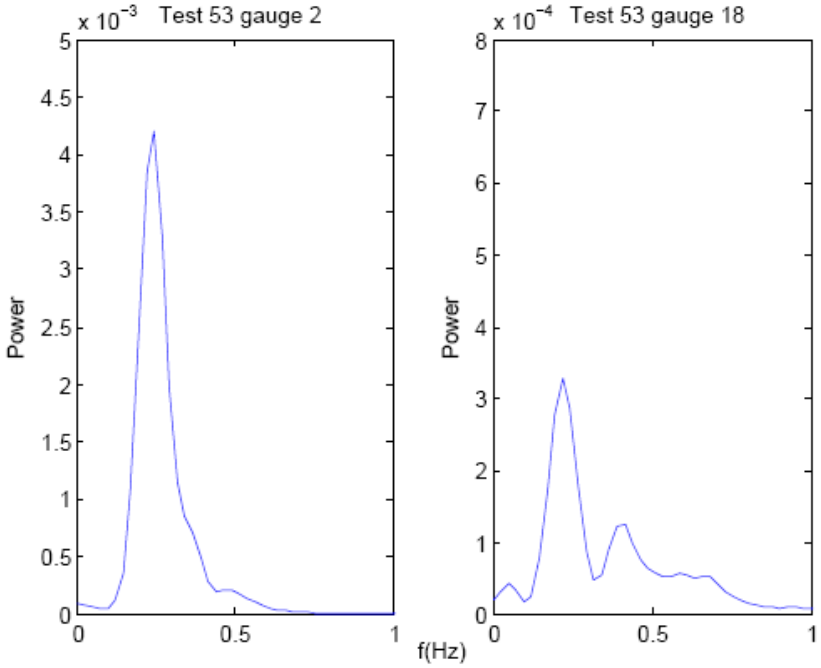


**Figure 5.36. –Fourier power spectra for test 53 at gauge 2 and 18**

The wave characteristics are first estimated by Fourier spectrum. The mean spectral wave height $H_{m0}$, mean period $T_p$, and first spectral moment $m_0$ are shown in Tab. 1.

| | Test 25 | | | Test 26 | | | Test 52 | | | Test 53 | | |
|---|---|---|---|---|---|---|---|---|---|---|---|---|
| Gauge | 2 | 16 | 18 | 2 | 16 | 18 | 2 | 16 | 18 | 2 | 16 | 18 |
| $H_{m0}$ (m) | 0.69 | 0.6 | 0.34 | 0.94 | 0.835 | 0.419 | 0.66 | 0.62 | 0.285 | 0.94 | 0.87 | 0.375 |
| $T_p$ (s) | 3.45 | 3.45 | 3.45 | 4.5 | 4.5 | 4.5 | 3.5 | 3.5 | 3.55 | 4.55 | 4.55 | 4.55 |
| $m_0(m^2)$ | 0.0296 | 0.0226 | 0.0072 | 0.054 | 0.0436 | 0.011 | 0.0273 | 0.0243 | 0.0051 | 0.0553 | 0.048 | 0.0088 |

**Table 1 – Spectral characteristics for tests 25, 26, 52 and 53**

| | $m_0(m^2)$ | $m_{0h}(m^2)$ | $m_{0l}(m^2)$ | $m_{0h}/m_0$ | $K_t$ |
|---|---|---|---|---|---|
| 25 | 0.0072 | 0.0027 | 0.0045 | 0.38 | 0.566666667 |
| 26 | 0.0110 | 0.0049 | 0.0061 | 0.44 | 0.501796407 |
| 52 | 0.0051 | 0.0025 | 0.0026 | 0.50 | 0.459677419 |
| 53 | 0.0088 | 0.0035 | 0.0053 | 0.40 | 0.431034483 |

**Table 2 – Spectral moments of total spectrum and spectral moments of high and low part of spectra, according to van der Meer et al. (2000)**

In Tab. 2 are reported values of spectral moments of total spectra and of high and low part of spectra according to methodology proposed by van der Meer et al. (2000) as reported in chapter 3.

Next, the data are analyzed by HHT non-linear and non-stationary time series analysis method. Sets of Intrinsic Mode Functions were obtained applying the Empirical Mode Decomposition method to each wave record.

The detailed results of the decomposition of test 25 gauge 18 into four IMF are presented in Fig. 5.37 and the sea surface elevation data are shown in Fig. 5.37 (a). Since the time scales are identified as the intervals between the successive alternations of local maxima and minima, IMF represents oscillation modes, embedded in the data analyzed. The different IMFs correspond to the different physical time scales, which characterize the various dynamical oscillations in the time series. A wave component with nearly constant time scale exists and dominates in each IMF, representing the carrier wave constituent at the specific time scale. These oscillations have not only different time scales, but also have a different range of energy. The limits of the vertical axis in Fig. 5.37 are different for the different IMF. The most energetic IMF in the decomposition is the second (c), and third (d) components, which have a close range of amplitude variation. The shortest oscillations in the decomposition, represented by the first IMF (b) have smaller amplitudes than the ones of (c) and (d). Physically these high frequency oscillations, extracted in the first constituent, may represent short period waves generated by interaction between wave and submerged breakwater. The complete representation of the sea surface elevation recorded in this data can be considered as a composition of three dominant wave oscillations, extracted in the first (b), second (c) and third (d) IMF and a several, but finite number of components with smaller amplitudes.

The contribution of different IMF to the energy and frequency contents of wave data is investigated. The spectra of wave records are compared with spectra of its IMF in Fig. 5.38, 5.39, 5.40

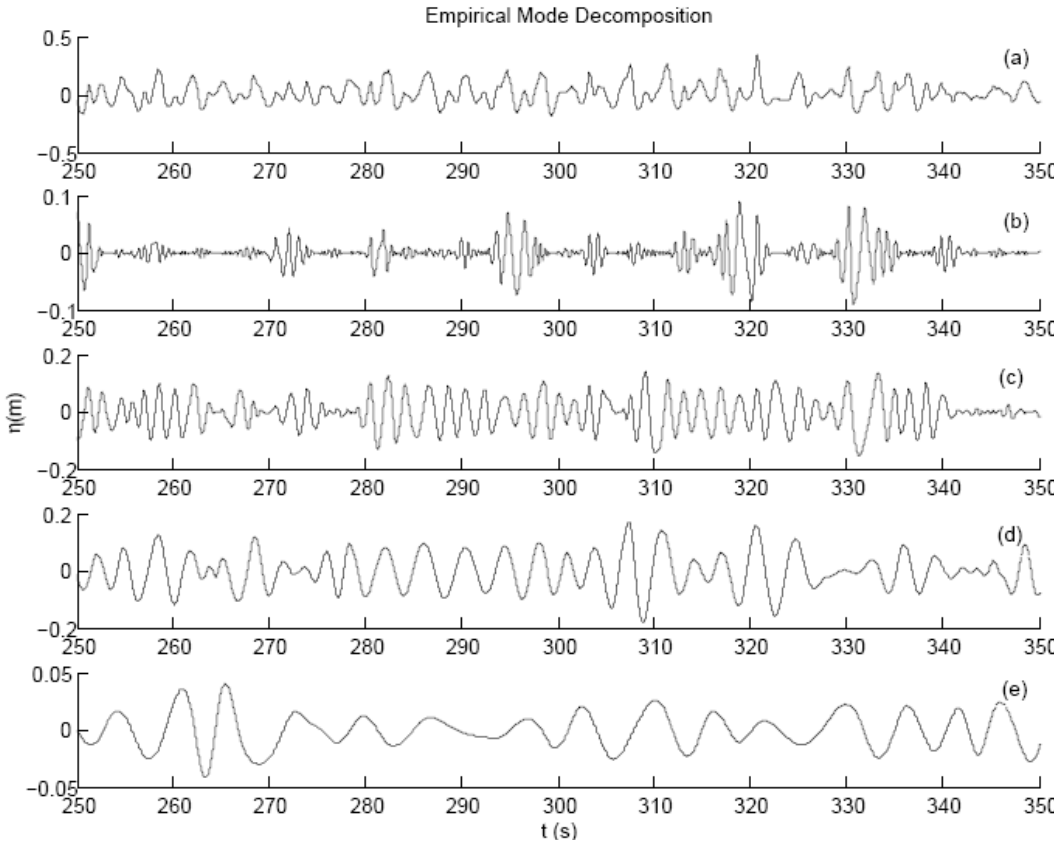


**Figure 5.37. – Empirical Mode Decomposition for test 25 at gauge 18**

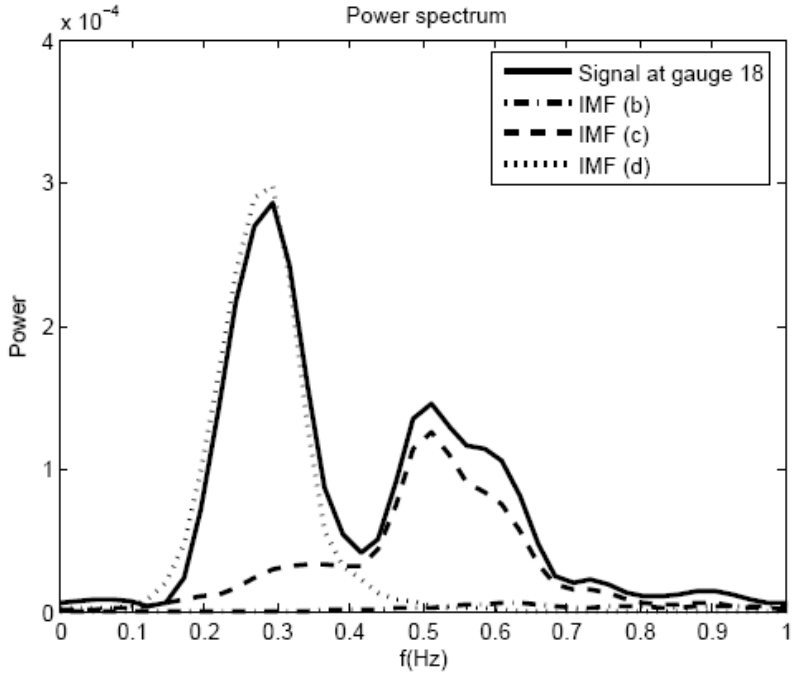


**Figure 5.38. – Spectrum of wave data and its IMFs for test 25 at gauge 18**

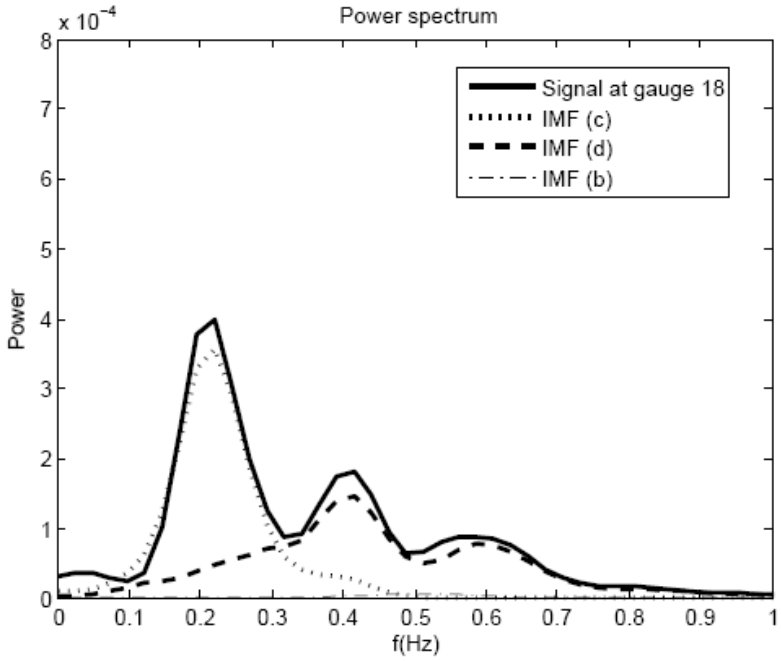


**Figure 5.39. – Spectrum of wave data and its IMFs for test 26 at gauge 18**

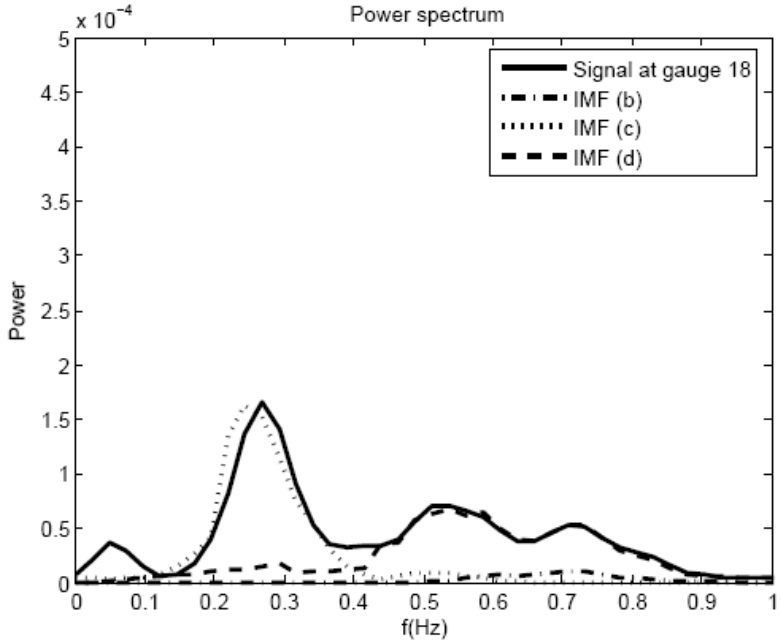


**Figure 5.40. – Spectrum of wave data and its IMFs for test 52 at gauge 18**

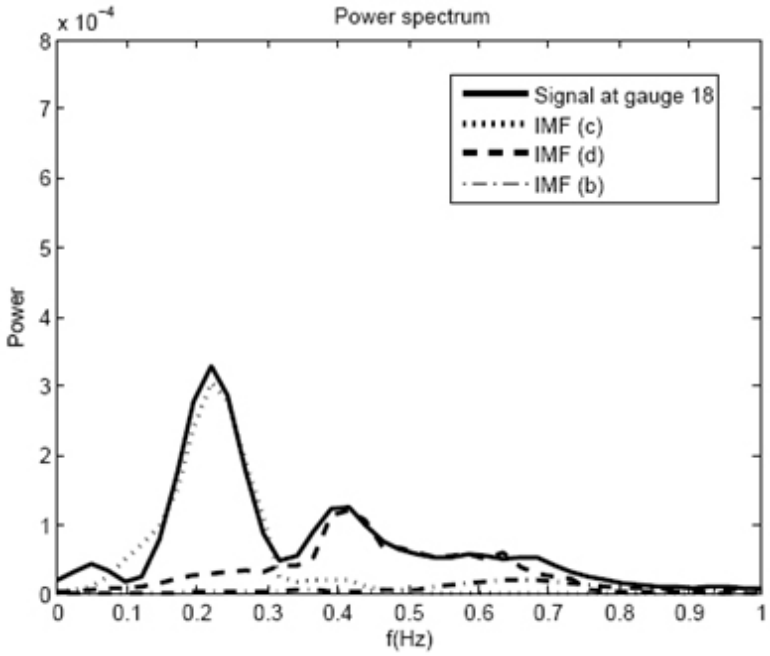


**Figure 5.41. – Spectrum of wave data and its IMFs for test 53 at gauge 18**

A mixture of three wave systems is registered, whose Fourier spectrum is correspondingly two-peaked with first peak frequency $fp_1$ = 0.28 Hz and second one $fp_2$ = 0.54 Hz. These two dominant wave oscillations are well separated by the EMD method into two different IMF (c), and (d) whose spectra are shown by dashed line and dotted line, respectively.

The energy and time characteristics of individual IMF are estimated and compared with wave characteristics in order to estimate quantitatively the contribution of different IMF to the wave data. The zero-th moment $m_0$ is proposed as a measure of integrally determined energy of IMFs while pectral peak frequency $f_p$ is utilized as the representative frequency.

The characteristics are presented in Tab. 3. The second and third IMF have the highest energy in the decomposition and their peak frequencies agree with the major two peaks of wave spectrum.

| IMF | $H_{m0}$ (m) | $f_p$ (Hz) | $m_0(m^2)$ |
|---|---|---|---|
| (b) | 0.079 | 0.78 | 0.0040 |
| (c) | 0.198 | 0.55 | 0.0025 |
| (d) | 0.228 | 0.27 | 0.0033 |

**Table 3 – Spectral characteristics of IMFs for test 25 at gauge 18**

The results of application of EMD presented here are also valid for other wave records. The energy hierarchy of IMF in decomposition of a wave record reflects clearly the specific peculiarity of particular wave data.

The peculiarities in the variations of the IMF are reflected in the frequency-time distribution of the energy. The Hilbert spectrum H(□,t) of record are shown in Fig. 5.38.

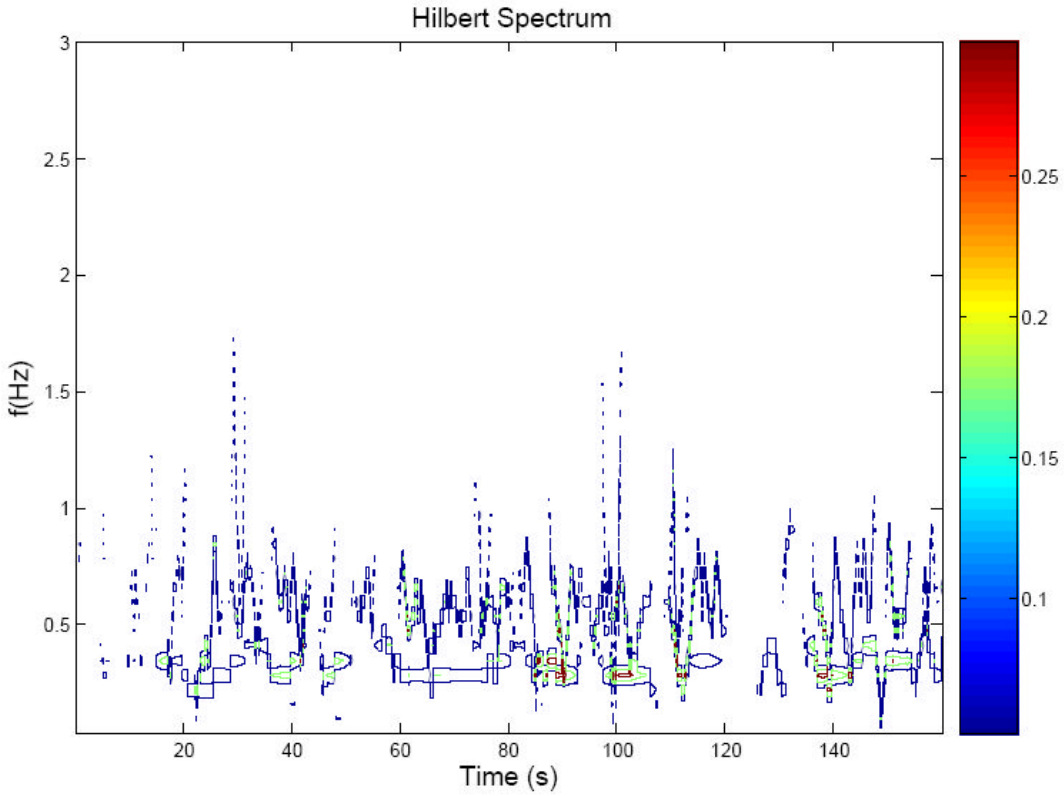


**Figure 5.38. – Hilbert spectrum of IMFs for test 25 at gauge 18**

The Hilbert spectrum in Fig. 5.38 shows high wave energy in the higher frequency range around 0.55 Hz, where the spectral peak of the second IMF is located, as well as in the lower frequency range around 0.27 Hz, the location of the peak of the third, IMF in Fig. 5.37.

At this point, in analogy to the methodology used by van der Meer et al. (1999), the spectrum is divided not by an arbitrary criterion imposing the high frequencies confined between $1.5f_p$ and $3.5f_p$, and low frequency between $0.5f_p$ and $1.5\ f_p$. In order to evaluate the amount of energy transferred behind breakwater at high and low frequency, will be used IMFs obtained by EMD, representing embedded mode at high and low frequency. Results are reported in Tab. 4

| | $m_0(m^2)$ gauge 16 | $m_{0h}(m^2)$ IMF (b) | $m_{0l}(m^2)$IMF (c) | $m_{0h}/m_0$ |
|---|---|---|---|---|
| 25 | 0.0072 | 0.0027 | 0.0045 | 0.38 |
| 26 | 0.0110 | 0.0053 | 0.0056 | 0.48 |
| 52 | 0.0051 | 0.0017 | 0.0035 | 0.32 |
| 53 | 0.0088 | 0.0019 | 0.0070 | 0.21 |

**Table 4– Spectral moments of total spectrum and spectral moments of high and low part of spectra, according decomposition.**

Comparing Tab. 2 and Tab. 4 it can be noticed that for short crest width (tests 25 and 26) results are in substantial agreement with those obtained applying van der Meer technique. In contrast for large crest width van der Meer's technique overstates the amount of energy transferred at high frequencies. In fact ratios between $m_{0h}/m_0$ computed using van der Meer criteria are about 30% higher than those calculated using IMFs as representative of high and low frequencies.

## CONCLUSION

This study was undertaken with the aim of increasing the knowledge of the nonlinear dynamics in the transformation of wave spectra in passing over submerged breakwater.

With the purpose to study the spectral evolution of the wave motion in the rear side of submerged barriers have been used an extensive data set in 2D large scale wave flume carried out at GWK of Hannover (Germany). This data set represents a unique set for the purposes of this thesis. In fact having to analyze the connected non linear phenomena to the transformation of the wave motion is essential that the data are not affections from scale effects.

In fact the effects induced by the model scale on the evolution of the non linear phenomena are not quantifiable because of nonlinear nature of the phenomena.

Bispectral analysis is used to elucidate aspects of nonlinear dynamics of shallow-water waves acting with submerge barrier. Analyses of laboratory observations of nonlinear wave field have yielded the following conclusions:

- Harmonic generation in shallow water after barriers is ascribed to nonlinear triad wave interactions. The generation of the second spectral peak results from the sum interactions between pairs of waves at the primary spectral peak. On the other hand the generation of the low-frequency waves is due to the difference interactions between pairs of waves at the primary spectral peak.

- In the initial shoaling region, weak nonlinearity leads to increase in the skewness values only but not in those of the asymmetry, whereas strong nonlinearity in the region just before wave breaking leads to a significant increase in the asymmetry values.

- Nonlinear couplings induced by a bar region in a random wave field shows a different behavior for short and large crest width. For short crest vanish in the deepening region beyond the bar due to decreasing nonlinearity. There is no memory of phase locks which existed over the barrier. The wave field on the rear side is statistically homogeneous and can be fully described by the energy density spectrum, without the need for additional, site-dependent phase information. For large crest width wave field show a sort of "memory" of barrier location due to nonlinearity, in fact values of asymmetry are constant after the obstacle.

The importance of the analyzing technique for the correct understanding of the wind wave phenomenon is discussed. Widely used methods for wave analysis assume linear and stationary sea waves.

The Hilbert-Huang Transform method is proposed as alternative one for the investigation of non-linear and non-stationary wave field.
The specific peculiarities of wave process are well captured by EMD and reproduced by IMF.

- Easy separation of the different time and energy associated with the oscillations in the data is well achieved by EMD.

- The energy hierarchy of IMF in decomposition of wave records, observed during different wave and breakwater conditions, reflects the specific peculiarities of the particular wave data.

- The EMD method with its great ability to extract different oscillation modes embedded in the data can facilitate the investigation of sea waves. The attention can be concentrated on a finite number of

IMF, each of them characterizing much simply, than the original one, the dynamical system.

- HHT has been used to quantify the amount of energy that is transferred to the highest frequencies. Results have been compared to van der Meer (2000) results. It is shown a substantial agreement for short crest width, although for large crest width van der Meer technique shows an overstatement of the amount of energy transferred at high frequencies.

High order spectral analysis constitute an useful tool to show the t non linear nature of the phenomena that occur in of interaction between the wave motion and the submerged barriers. On the base of these results has been possible to define the behaviour of the barriers to vary of their geometry. The following step of the research in this field could be represented by laboratory tests performed in presence of sand with the purpose to appraise the influence of the non linearity on the sand transport.

## REFERENCES


**Adams, CB and Sonu, C.J.** "*Wave Transmission Across Submerged Near Suface Breakwater*". Coastal Engineering '86, American Society of Civil Engineer, New York 1986, pp. 1729 - 1737.

**Ahrens, J.P**. "*Characteristics of Reef Breakwaters*". CERC Technical Report pp. 87- 17, 1987.

**Ahrens, J.P.** "*Reef Breakwater Response to Wave Attack*", Berm Breakwaters: Inconventional Rubble-Mound. American Society of Civil Engineers, 1988, pp 21-40.

**Battjes, J.A., and J.P.F.M. Janssen**, "*Energy loss and set-up due to breaking of random waves*", Proc. Coastal Eng. Conf., 16th, pp. 569-587, 1978.

**Battjes, J.A., and S. Beji**, "*Breaking waves propagating over a shoal*", 15579-15589, 1992. 23 Proc. Coastal Eng. Conf., , pp. 42-50, 1992.

**Beji, S. and Battjes, J.k** "*Experimental Investigation of Wave Propagation over a Bar*", Coastal Engineering, 19: 1-2, 1993, pp. 15 1 - 162.

**Beji, S. and Battjes. J.A.** "*Numerical Simulation of Nonlinear Wave Propagation Over a Bar*", Coastal Engineering, 23: 1-2, 1994, pp. 1-16.

**Beji, S., and Battjes, J.A.**, "*Experimental investigation of wave propagation over a bar*", Coastal Eng., 19, pp. 151-162, 1993.

**Cooker, M. and Peregrine, H.** "Solitary Waves Passing Over Submerged Breakwaters", 21 International Conference on Coastal Engineering, American Society of Civil Engineers, New York, 1989, pp. 624-631.

**Cornett, A., Mansard, E. and Funke, E.** "*Wave Transformation and Load Reduction Using a Small Tandem Reef Rreakwater - Physical Model Tests*", Ocean Wave Measurement and Analysis, American Society of Civil Engineers, New York, 1 994, pp. 1008-1023.

**Cruz, E.C., Isobe, M. and Watanabe, A.** "*Nonlinear Wave Transformation Over a Submerged Permeable Breakwater*", 23 International Conference on Coastal Engineering, American Society of Civil Engineers , New York, Vol. 1, 1993, pp. 1101- 1114.

**Darlymple, R.A.** "*Physical Modelling in Coastal Engineering*", AA. Balkema, Rotterdam. 1985, pp. 3 - 9.

**Dattari, J., Raman, H. and Shankar, N.J.** "*Performance Characteristics of Submerged Breakwaters*", 16 International Conference on Coastal Engineering, American Society of Civil Engineers, New York, 1979, pp. 2152 2171.

**Dick, T.M. and Brebner, A.** "*Solid and Permeable Submerged Breakwaters*", 11 International Conference on Coastal Engineering, American Society of Civil Engineers, New York, 1969.
*directional wave spectra in shallow water*", J. Geophys. Res., 97, pp.
*dissipation model for random breaking waves*", J. Geophys. Res., 90(C5),

**Driscoll, A.M., Dalrymple, R.A. and Grilli, S.T.** "*Harmonic Generation and Transmission Past a Submerged Rectangular Obstacle*", 23 International Conference in Coastal Engineering, American Society of Civil Engineers, New York, Vol. 1, 1 993, pp. 1142- 1160.

**Fulford, E.T.** "*Reef Type Breakwaters for Shore Stabilization*", Coastal Zone '85, American Society of Civil Engineers, New York, 1985.

**Gimenez, M.H., Sanchez-Carratala, C.R. and Medina, J.R.** "Analysis of false waves in numericaL sea simulations", Ocean Engineering, 21-8, 1994, pp. 751-764.

**Goda, Y.** "*Re-analysis of Laboratory Data on Wave Transmission over Breakwaters*", Report of the Port and Harbour Research Institute, Vol. 1 8, No. 3, 1969.

**Goda, Y. and Suzuki, Y.** "*Estimation of Incident and Reflected Waves in Random Wave Experiments*", 15 Intemational Conference on Coastal Engineering, American Society of Civil Engineers, New York, 1977, pp. 828-845.
**Goda, Y., Takada, N. And Monya, Y.** "*Laboratory Investigation of Wave Transmission over Breakwaters*", Report of the Port and Harbour Research Institute, No. 13, 1967.

**Grilli, S.T., Losada, M.A. and Martin, F.** "*Characteristics of Solitary Wave Breaking Induced by Breakwaters*", Journal of Waterway, Port and Coastal Engineering, American Society of Civil Engineers, New York, 1994, pp. 74 - 92.
**Grilli. S.T. and Svendsen, I.A.** "*Long Wave Interaction with Steeply Sloping Structures*", 22 International Conference on Coastal Engineering, American Society of Civil Engineers, New York, Vol. 2, 199 1, pp. 1200- 12 13.

**Horikawa, K. and Kuo, C.T.** "*A Study on Wave Transformation Inside Surf Zone*", 10 International Conference on Coastal Engineering, American Society of Civil Engineers, New York, Vol. 1, 1966, pp217 - 233.

**Huang, N.E., Shen, Z. and Long, S.R.** "*A new view of nonlinear water waves: The Hilbert spectrum*", Ann. Rev. Fluid Mech. 31, pp. 417-457.,1999.

**Huang, N.E., Shen, Z., Long, R., Wu, C., Shin, S., Zheng, Q., Yuen, Y., Tung, C. and Liu, H.** "*The empirical mode decomposition and Hilbert spectrum for nonlinear and non-stationary time series analysis*", Proc. R. Soc.

**Kamphuis, J.W**. "Advanced Lectures in Coastal Engineering", Lecture Notes in Civil Engineering 853, Queen's University, 1995.

**Kamphuis, J.W.** "Incipient Wave Breaking", Coastal Engineering, Vol. 15, No. 3, 199 1, pp. 185- 203.

**Kobayashi, N. and Wurjanto, A.** "Wave Transmission Over Submerged Breakwaters", Journal of Waterway, Port and Coastal Engineering, American Society of Civil Engineers, New York, 1155, 1989, pp. 662-680.

**Lee, J.J., Chang, C.** "*Interaction of Nonlinear Waves and Coastal Structures*", 23 International Conference on Coastal Engineering, American Society of Civil Engineers ,New York, Vol. 2, 1993, pp. 2327-1340.

**Liberatore, G. and Petti, M.** "*Wave Transformations Over a Submerged Bar : Experiments and Theoretical interpretations*", 23" International Conference on Coastal Engineering, American Society of Civil Engineers , New York, Vol. 1, 1993. pp. 447-459.

**Liu, P.C.** "*Is the wind wave frequency spectrum outdated?*", Ocean Engineering 27, pp. 577-588.,2001.
London. 454: pp. 903-995, 1998.

**Losada, I.J., Silva, R. and Losada, M.A.** "*3-D Non-Breaking Regular Wave Interaction with Submerged Breakwaters*", Coastal Engineering, 28, 1996, pp. 229-248.

**Madsen, O. S. and White, S .M.** "Reflection and Transmission Carac teristics of Porous Rubblemound Breakwaters", MR-76-5, Coastal Engineering Research Centre, US Amy Corps of Engineers, Fort Belvoir, Va., 1976.

**Mansard, E.P.D., Funke, ER., Readshaw, J.S. and Girard, R. K.** "*On the Transfomation of Wave Statistics due to Shoaling*", 24 International

Conference on Coastal Engineering, American Society of Civil Engineers, New York, 1989, pp. 106-120.

**Mansard,E.P.D. and Funke, E.R.** "*On the Reflection Analysis of Irregular Waves*", Technical Report No. TR-HY-017, National Research Council of Canada, Ottawa, 1987.

**Massel, S.R** "*Harmonie Generation by Waves Ropagating over a Subrnerged Step*", Coastal Engineering, 7, 1983, pp. 357-380.

**Massel, S.R.** "*Wavelet analysis for processing of ocean surface wave records*", Ocean Engineering. 28, pp.957-987., 2001.

**Mizuguchi, M. 1982**. "Individual wave analysis of irregular wave deformation in the nearshore zone". Proc. of ICCE'82, pp.485-504.
**Ochi, M. K.** "*Ocean Waves - The stochastic approach*", Cambridge University Press., 1998.

**Ohyama, T. and Nadaoka, K.** "*Modelling the Transformation of Nonlinear Waves Passing over a Submerged Dyke*", 23" International Conference on Coastal Engineering, American Society of Civil Engmeers , New York, Vol. 1, 1993, pp. 526-539.

**Petti, M. and Ruol, P.** "*Expenmental Study on the Behaviour of Submerged Detached Breakwaters*", 3rd International Conference on Coastal and Port Engineering in Developing Countries, Vol. 1, 199 1, pp. 167 - 179.

**Petti, M. and Ruol, P.** "*Laboratory Tests on the Interaction Between Nonlinear Long Waves and Submerged Breakwaters*", 23 International Conference on Coartal Engineering, American Society of Civil Engineers , New York, Vol. 1, 1993, pp. 792-803.
pp. 9159-9167, 1985.

**Seelig, W.N.** "*Estimation of Wave Transmission Coefficients for overtopping of Impermeable Breakwaters*", CERC Coastal Engineering Technical Aid 80-7, 1980.
**Seelig, WN.** "*Effect of Breakwatm on Waves : Laboratory Tests of Wave Transmission by Overtopping*", Coastal Structures '79, American Society of Engineers, New York, 1979, pp. 941-961.

**Smith, E.R. and Kraus, N.C.** "*Laboratory Study on Macro-Features of Wave Breaking Over Bars and Artificial Reefs*", CERC Technical Report 90-12, 1990.

**Tanaka, N.** "*Effects of Submerged Rubblemound Breakwater on Wave Attenuation and Shoreline Stabilization*", Proceedings of 23" Japanese Coastal Engineering Conference, 1976.

**Ting, F.C.K. and Kim, Y.K.** "*Vortex Generation in Water Waves Propagating Over a Submerged Obstacle*", Journal of Coastal Engineering, American Society of Civil Engineers. New York, 24: 1-2,1994, pp. 23-49.

**U.S. Army Corps of Engineers.** " *Shore Protection Manual*", Coastal Engineering Research Centre, Vicksburg, Mississippi, 1984.

**van der Meer, J.W**. "*Rock Slopes and Gravel Beaches Under Wave Attack*", Delft Hydraulics Communication No. 396, 1988.

**van der Meer, J.W.** "*Stability and Transmission at Low-Crested Structures",* Delft Hydraulics Publication 453, 1991.

**van der Meer, J.W. and Pilarczyk, K.W.** "*Stability of Low-Crested and Reef Breakwaters*", Coastal Engineering '90, Arnerican Society of Civil Engineers, New York, 1990, pp. 1375- 13 88.

**van der Meer, J.W., and D'Angremond, K.** "*Wave Transmission at Low-Crested Structures*", Coastal Institution of Civil Engineers, London, 1992.

**van der Meer, J.W., and Daemen, F.R.** "*Stability and Wave Transmission at Low-Crested Rubblemound Structures*", Journal of Waterway, Port and Coastal Engineering, American Society of Civil Engineers, New York, 120: 1, 1994, pp. 1 - 19.

**Veltcheva, A. and Nakamura**, S. 2000. "*Wave groups and Low Frequency waves in the coastal zone*", Rep. of PHRI, 39,4: pp.75-94., 2004.

**Veltcheva, A. D. and Guedes Soares, C.** "*Identification of the components of wave spectra by the Hilbert Huang transform method*", Applied Ocean Research, 26, 1-12, 2004.

**Veltcheva, A.D.** "Wave *and group transformation by a Hilbert spectrum*",

**Vidal, C., Losada, M.A., Medina, R., Mansard, E.P.D. and Gomez-Pina, G.** "*Universal Analysis for the Stability of Both Low Crested and Submerged Breakwaters*", 23 International Conference on Coastal.